# Compression molding of chopped woven thermoplastic composite flakes

## A study on processing and performance

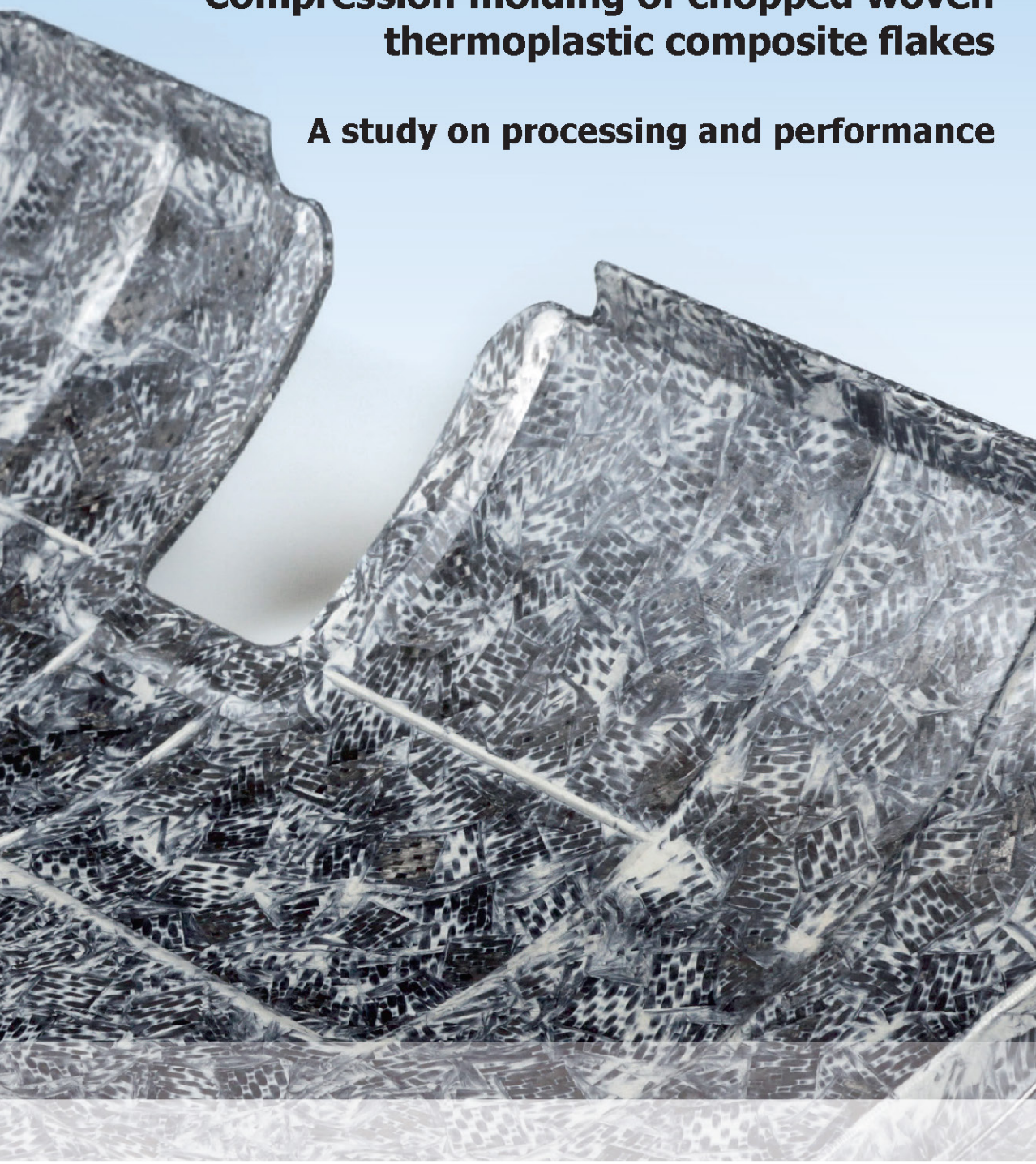

TPRC

M.I. Abdul Rasheed

# COMPRESSION MOLDING OF CHOPPED WOVEN THERMOPLASTIC COMPOSITE FLAKES

## A STUDY ON PROCESSING AND PERFORMANCE

Mohammed Iqbal

De promotiecommissie is als volgt samengesteld:

*Voorzitter en secretaris:*
prof.dr. G.P.M.R. Dewulf — Universiteit Twente

*Promotoren:*
prof.dr.ir. R. Akkerman — Universiteit Twente
prof.dr.ir. L.E. Govaert — Universiteit Twente

*Assistent promotor:*
dr.ir. H.A. Visser — Universiteit Twente

*Leden (in alfabetische volgorde):*
dr.ir. T.C. Bor — Universiteit Twente
prof.dr.ir. J. Degrieck — Universiteit Gent
prof.dr.ir. D.J. Schipper — Universiteit Twente
prof.dr. N. Warrior — University of Nottingham

This research project was financially supported by the ThermoPlastic composites Research Center (TPRC).

Compression molding of chopped woven thermoplastic composite flakes: a study on processing and performance
Abdul Rasheed, Mohammed Iqbal
PhD Thesis, University of Twente, Enschede, The Netherlands
July 2016

ISBN 978-90-365-4151-0
DOI 10.3990/1.9789036541510

Printed by Gildeprint Drukkerijen, Enschede, The Netherlands

*Cover: photograph of a compression molded flake reinforced composite panel, molded with the process developed in this research (Chapter 6). It demonstrates the capabilities of the material and the process.*

# COMPRESSION MOLDING OF CHOPPED WOVEN THERMOPLASTIC COMPOSITE FLAKES

PROEFSCHRIFT

ter verkrijging van
de graad van doctor aan de Universiteit Twente,
op gezag van de rector magnificus,
prof.dr. H. Brinksma,
volgens besluit van het College voor Promoties
in het openbaar te verdedigen
op vrijdag 15 juli 2016 om 14:45 uur

door

Mohammed Iqbal Abdul Rasheed

geboren op 3 juli 1987

te Thanjavur, India

Dit proefschrift is goedgekeurd door de promotoren:

prof.dr.ir. R. Akkerman
prof.dr.ir. L.E. Govaert

en door de assistent promotor:

dr.ir. H.A. Visser

# Summary

Continuous fiber reinforced composites with high-performance thermoplastic polymer matrices have an enormous potential in terms of performance, production rate, cost efficiency and recyclability. The use of this relatively new class of materials by the aerospace and automotive industry has been growing steadily during the last decade. However, the use of continuous reinforcements limit the complexity of the shape of the end products, as defects such as wrinkles can form during processing. Moreover, a significant amount of process waste is generated, which lowers the efficiency of the conventional production processes involving a prepreg cutting stage and/or final trimming stages.

The overall efficiency of the manufacturing value chain of composites can be improved by adjoining a complementary manufacturing process that utilizes the process waste incurred in the primary process. The discontinuous form of reinforcements in the reclaimed material will provide a means to manufacture complex 3D geometries with near-net edges and at the same time use the raw material efficiently. However, the discontinuities in the reinforcing phase lead to a reduced mechanical performance compared to continuous reinforcements. Suitable applications include semi-structural parts and non-load bearing structures.

This thesis focuses on the processing of planar discontinuous reinforcements and the associated mechanical performance. Chopped thermoplastic semi-preg with a woven fabric reinforcement, referred to as flakes, is considered as a standalone molding compound in this study. A compression molding process is chosen to manufacture parts, as it allows for complex geometries while retaining a long fiber length. Although processing of different types of discontinuous reinforcements has been studied in the past, the processing of the specific class of planar reinforcements with a woven architecture and high fiber content has not been explored so far.

The principal objective is to develop a strategy for manufacturing woven-flake reinforced parts with good quality and consistent mechanical properties. For achieving this goal, the flow behavior of chopped woven material, process induced jamming of the material and the mechanical properties of molded plates are experimentally investigated and are explained with theoretical models.

Experiments show that the rheological behavior of the chopped woven flakes evolves during the course of the compression molding process. Furthermore, the randomly positioned woven flakes, with local structural integrity, are found to agglomerate

and mechanically jam during the squeezing process. This effect is found to be a function of flake size and closing rate of the mold. The resulting jammed regions are detrimental to the mold as well as to the performance of the molded part, and hence, should be avoided. It is shown that the transition from a flowing state to a jammed state occurs due to the dominance of inter-flake frictional behavior and a diffusive flow of polymer over a lubricated advective flow of the flake reinforced polymer. The jamming of flakes cannot be completely eliminated, given the existence of the flake structure. However, it can be postponed by selecting suitable process settings, flake size and part thickness. Furthermore, the consolidation process in the presence of jammed regions is atypical compared to continuously reinforced composites due to the stochastic nature of the material, especially if the material is allowed to flash at the edges.

Manufacturing parts with integrated functional features, like stiffening ribs, is one of the attractive aspects of the material and the process under study. Therefore, the filling behavior of the chopped material in integrated ribs of different aspect ratios is analyzed with respect to the final consolidation quality. The study provides preliminary guidelines for detailing rib like features, in terms of processing.

The mechanical performance of flat laminates under a tensile load case is investigated experimentally and is found to have a considerable scatter. A simple phenomenological model is used to describe the failure of the flake reinforced composite. Further, a statistical framework is developed around the analytical model to capture the uncertainty in the tensile strength in terms of a material allowable. The trends in the experimentally observed scatter is satisfactorily reproduced, however, further investigation is required to validate the framework.

The work presented in the thesis shows the multidisciplinary nature of the problem, with strong correlations between the material, process and the design of the part leading to the final part performance. Therefore, a processing strategy is proposed which takes into consideration the aforementioned three basic blocks to manufacture consistent parts. Finally, the proposed strategy is validated by manufacturing a full-scale part with typical design features, which successfully demonstrates the processing capabilities of the material and the developed process.

# Samenvatting

Continu-vezelversterkte composieten op basis van hoogwaardige thermoplastisch polymeren hebben een groot potentieel in termen van structurele eigenschappen, productiviteit, kostenefficiëntie en recycling. De afgelopen tien jaar is het gebruik van deze relatief nieuwe materialen gestaag toegenomen binnen de luchtvaart- en automobielindustrie. Met deze groei is het thema van hergebruik van de hoogwaardige, maar ook zeer kostbare thermoplastische composieten, steeds belangrijker geworden. Er wordt een aanzienlijke hoeveelheid productieafval gegenereerd tijdens de verwerking van halffabricaat tot eindproduct, bijvoorbeeld bij het snijden van platines of bij het lamineren met thermoplastische prepreg. De efficiëntie van de gehele productieketen kan worden verbeterd door het toevoegen van een productieproces, waarin gebruik wordt gemaakt van het afval dat in het primaire proces ontstaan is. Dit afval kan worden versneden en gebruikt worden in een vormpersproces. Het relatief goede vloeigedrag van de discontinue vezelversterking in het teruggewonnen materiaal biedt de mogelijkheid om complexe geometrieën te persen. Echter, de discontinuïteit in de versterking resulteert in een vermindering van de mechanische eigenschappen ten opzichte van de continue vezelversterking. De toepassing kan daarom liggen bij bijvoorbeeld laag belaste onderdelen.

Dit proefschrift richt zich op het verwerken van vlakke discontinue versterkingen en de resulterende mechanische eigenschappen. Gesneden thermoplastische semipreg met een weefsel versterking, aangeduid als vlokken, wordt beschouwd als een opzichzelfstaande vormmassa binnen dit onderzoek. Een vormpersproces is gebruikt om onderdelen te fabriceren, omdat dit proces complexe geometrieën in combinatie met een lange vezellengte toelaat. Ondanks dat het verwerken van verschillende soorten discontinue versterkingen in het verleden is onderzocht, is het produceren met vlakke versterkingen met een weefselstructuur nog niet bestudeerd.

Het voornaamste doel is het ontwikkelen van een strategie voor het fabriceren van weefselvlokkenversterkte onderdelen met een goede kwaliteit en consistente mechanische eigenschappen. Om dit doel te bereiken is het vloeigedrag van het gesneden weefselmateriaal, inclusief door het proces veroorzaakte vloeibelemmeringen, tezamen met de mechanische eigenschappen van geperste platen experimenteel onderzocht en verklaard aan de hand van theoretische modellen.

Experimenten laten zien dat het reologische gedrag van de gesneden weefselvlokken verandert gedurende het vormpersproces. Daarnaast gaan de willekeurig gepositioneerde vlokken, met een lokale structurele integriteit, conglomereren, waardoor

verdere vloei belemmerd raakt. De mate waarin dit effect voorkomt, wordt bepaald door de vlokgrootte en sluitsnelheid van de mal. De resulterende blokkeringen zijn ongunstig voor zowel de mal als de eigenschappen van het geperste onderdeel en dienen daarom voorkomen te worden. Het is aangetoond dat de overgang van vloei naar blokkering van de smelt wordt veroorzaakt door een toename van de wrijving tussen de samengeperste weefselvlokken. Deze toegenomen wrijving veroorzaakt een overgang van advectieve vloei van de vlokken naar diffunderende vloei van de polymere matrix door het geblokkeerde weefselbed. Het blokkeren van de vlokken kan niet volledig worden voorkomen vanwege de vlokachtige structuur, maar kan worden uitgesteld door de geschikte procesinstelling, vlokgrootte en wanddikte te selecteren. Bovendien is het consolidatieproces rondom de blokkeringen afwijkend van dat van continu-vezelversterkte composieten door de stochastische aard van het materiaal, met name als de polymere smelt vrij is om aan de randen van de matrijs uit te vloeien.

Het fabriceren van onderdelen met geëntegreerde functionaliteit, zoals verstijvingsribben, is één van de aantrekkelijke eigenschappen van het onderzochte materiaal en proces. Om die reden zijn het vulgedrag en de uiteindelijke consolidatiekwaliteit van het gesneden materiaal in geïntegreerde ribben met verschillende hoogte-dikte verhouding bestudeerd. Het onderzoek biedt een aantal procesgerichte basisrichtlijnen voor dergelijke ribachtige structuren.

De mechanische eigenschappen van vlakke laminaten onder trekbelasting is experimenteel onderzocht en blijkt een aanzienlijke spreiding te vertonen. Een eenvoudig fenomenologisch model is gebruikt om het faalgedrag van vlokversterkte composieten te beschrijven. Dit analytische model is in een statistisch kader geplaatst om de onzekerheid in de rekenwaarde (allowable) van de treksterkte te kunnen evalueren. De experimenteel geobserveerde trend in de spreiding is hiermee voldoende gereproduceerd, echter is aanvullend onderzoek nodig om het statistische kader te valideren.

Het onderzoek gepresenteerd in dit proefschrift illustreert de multidisciplinaire aard van het probleem en laat zien dat er een sterke samenhang is tussen het materiaal, het proces en het ontwerp van het onderdeel, waaruit de uiteindelijke producteigenschappen resulteren. Daarom is een verwerkingsaanpak voorgesteld waarin de drie hierboven genoemde hoekstenen voor het produceren van consistente onderdelen is meegenomen. Tot slot is de voorgestelde aanpak gevalideerd door het produceren van een onderdeel op ware grootte. Dit onderdeel bevat typische ontwerpdetails, waarmee de verwerkingsmogelijkheden van het materiaal en het ontwikkelde proces succesvol zijn aangetoond.

# Nomenclature

*The symbols used in this thesis are classified into a Roman or a Greek symbol group. Although some symbols can represent multiple quantities, its intended meaning follows from the textual context.*

## Roman symbols

| | | |
|---|---|---|
| $A$ | scaling factor for fabric compaction stress | [Pa] |
| $A_s, A_f$ | cross sectional area of RVE and flake | [$m^2$] |
| $B$ | power law exponent for fabric compaction stress | [-] |
| $d_r$ | depth of rib | [m] |
| $E$ | flexural stiffness of flake | [Pa] |
| $E_j, E_{uj}$ | compressive stiffness of jammed and unjammed region | [Pa] |
| $F$ | squeeze force | [N] |
| $F_1, F_2$ | tensile force | [N] |
| $F(x), F_e(x)$ | CDF of a random variable $x$ and its empirical estimate | [-] |
| $h, h_0, h_f$ | specimen thickness, initial and final height | [m] |
| $\dot{h}, \dot{h}_c$ | mold closing rate, critical mold closing rate | [m/s] |
| $\dot{h}_{c,l}$ | critical mold closing rate for a certain flake size | [m/s] |
| $I$ | second moment of area | [$m^4$] |
| $K$ | permeability of flake bed | [$m^2$] |
| $k, k_s$ | power law fluid consistency parameter, for shear mode | [$Pa \cdot s^n$] |
| $k_{s,AS}$ | power law fluid consistency parameter for AS load case | [$Pa \cdot s^n$] |
| $k, \hat{k}$ | shape parameter and MLE of shape parameter | [-] |
| $L, L_{sp}$ | length of squeeze specimen and tensile specimen | [m] |
| $L_c$ | critical overlap length | [m] |
| $l, l_{min}, l_{max}$ | length of flake, minimum and maximum | [m] |
| $l_{0,k}$ | overlap length for $k^{\text{th}}$ layer | [m] |
| $m$ | material thickness above rib entry region | [m] |
| $m_p$ | mass of prepreg per unit area | [$kg/m^2$] |
| $n$ | number of adherends | [-] |
| $n, n_s$ | shear thinning index and for shear mode | [-] |
| $n_{s,AS}$ | shear thinning index for AS load case | [-] |
| $P, p$ | pressure | [Pa] |

| | | |
|---|---|---|
| $P_a$ | atmospheric pressure | [Pa] |
| $P_a$ | applied pressure | [Pa] |
| $P_{fl}$ | interstitial fluid pressure | [Pa] |
| $P_e$ | Péclet number | [-] |
| $p$ | quantile | [-] |
| $\text{pdf}(l)$ | probability density function of flake length | [1/m] |
| $R, r$ | radius of squeeze specimen | [m] |
| $r_0$ | initial radius of squeeze specimen | [m] |
| $r_{base}$ | base radius of a spherical cap | [m] |
| $r_e$ | corner radius at rib entrance | [m] |
| $T$ | temperature | [K] |
| $T$ | tortuosity parameter | [-] |
| $T_{0.1}$ | $0.1^{\text{th}}$ quantile of tortuosity distribution | [-] |
| $T^j_{(1)}$ | minimum tortuosity in the $j^{\text{th}}$ array | [-] |
| $T_i$ | tortuosity of $i^{\text{th}}$ link | [-] |
| $T_{req}$ | minimum required tortuosity | [-] |
| $T_\text{g}, T_\text{m}$ | glass transition and melting temperature | [K] |
| $t, t_i, t_j$ | time, $i^{\text{th}}$, $j^{\text{th}}$ instant | [s] |
| $t_b$ | base or flange thickness | [m] |
| $t_f$ | flake thickness | [m] |
| $t_m$ | thickness of interface polymer | [m] |
| $t_s$ | specimen thickness | [m] |
| $\mathbf{u}$ | velocity vector | [m/s] |
| $u_f$ | velocity of fluid | [m/s] |
| $u_{fl}$ | velocity of flake | [m/s] |
| $u_{Darcy}$ | Darcy velocity | [m/s] |
| $v_f, v_f^{init}$ | fiber volume fraction, initial value | [-] |
| $v_i, v_j$ | velocity of flake | [m/s] |
| $v_x$ | component of fluid velocity in $x$ direction | [m/s] |
| $w, w_0$ | width of specimen and initial width of the specimen | [m] |
| $wt$ | weight fraction | [-] |
| $w_r$ | rib width | [m] |
| $X_p$ | $p^{\text{th}}$ quantile of a probability distribution | $[\text{unit}(X)]$ |
| $x$ | random variable | $[\text{unit}(x)]$ |
| $x, y$ | in-plane co-ordinate | [m] |
| $z$ | out-of-plane co-ordinate | [m] |

## Greek symbols

| | | |
|---|---|---|
| $\alpha$ | significance level | [-] |
| $\dot{\gamma}, \dot{\gamma}_a$ | shear rate and applied shear rate | [1/s] |

| | | |
|---|---|---|
| $\delta_{film}$ | thickness of polymer film | [m] |
| $\epsilon$ | strain | [-] |
| $\dot{\epsilon}_{ii}$ | extensional strain rate, where $i \in [x, y, z]$ | [1/s] |
| $\eta, \eta_{fl}$ | fluid viscosity | [Pa · s] |
| $\mu, \hat{\mu}$ | location parameter and MLE of location parameter | [-] |
| $\sigma, \hat{\sigma}$ | scale parameter and MLE of scale parameter | [-] |
| $\sigma, \sigma_e, \sigma_{\mathrm{T}}$ | externally applied stress | [Pa] |
| $\sigma_i$ | applied uniaxial stress in the $i^{\mathrm{th}}$ principal direction | [Pa] |
| $\sigma_{zz}$ | axial compressive stress | [Pa] |
| $\bar{\sigma}_f$ | average fluid pressure | [Pa] |
| $\sigma^{eff}_{flakes}$ | effective stress carried by flakes | [Pa] |
| $\sigma_{eff}$ | effective stress in the lap joint | [Pa] |
| $\sigma_{fabric}$ | fabric compaction stress | [Pa] |
| $\sigma^{ult}_f, \sigma^{ult}_m$ | ultimate tensile strength of the flakes and the matrix | [Pa] |
| $\sigma_{link}$ | maximum stress carried by a link | [Pa] |
| $\tau$ | shear stress | [Pa] |
| $\tau, \tau_{dwell}$ | consolidation dwell time | [s] |
| $\tau_{avg}$ | average shear stress | [Pa] |
| $\tau_d$ | characteristic time scale for diffusion | [s] |
| $\tau_{ij}$ | component of extra stress tensor, where $i, j \in [x, y, z]$ | [Pa] |
| $\tau^y_m$ | yield strength of matrix | [Pa] |
| $\tau_s$ | characteristic time scale for advection | [s] |
| $\chi^2$ | chi-square distribution | [-] |

## Math symbols

| | | |
|---|---|---|
| $\mathcal{O}$ | Landau symbol for order of magnitude | [-] |
| $\mathcal{N}(\mu, \sigma)$ | normal distribution with mean $\mu$ and standard deviation $\sigma$ | [-] |

## Math operators

| | |
|---|---|
| $\nabla$ | gradient operator |
| $\nabla \cdot$ | divergence operator |

## Abbreviations

| | |
|---|---|
| 3D | three dimensional |
| 5HS | 5 harness satin |
| AD | Anderson-Darling |
| AS | axisymmetric |

| | |
|---|---|
| BMC | bulk molding compound |
| C/PPS | PPS with carbon fiber reinforcements |
| CDF | cumulative distribution function |
| CI | confidence interval |
| CRL | continuously reinforced laminate |
| EVS | extreme value statistics |
| FJL | forcibly jammed laminate |
| GEV | generalized extreme value distribution |
| GMT | glass mat thermoplastics |
| HexMC | Hexcel molding compound |
| HQ, LQ | high, low quality |
| LFRT | long fiber reinforced thermoplastic |
| LFS | long fiber suspension |
| LSE | laser speckle extensometer |
| MLE | maximum likelihood estimator |
| MMC | Metropolis Monte-Carlo |
| MR | matrix rich region |
| NI | non-impregnated region |
| OSB | oriented strand board |
| PEEK | poly(ether ether ketone) |
| PEKK | poly(ether ketone ketone) |
| PID | proportional, integral, derivative control |
| PPS | poly(phenylene sulphide) |
| PRC | planar reinforced composite |
| PS | plane strain |
| QI | quasi-isotropic |
| RFL | randomly filled laminate |
| RSA | random sequential adsorption |
| RVE | representative volume element |
| SD | standard deviation |
| SFE | squeeze flow experiment |
| SFRT | short fiber reinforced thermoplastic |
| SMC | sheet molding compound |
| TPC | thermoplastic polymer composite |
| UD | unidirectional |
| V | void regions |

# Contents

**Summary** i

**Samenvatting** iii

**Nomenclature** v

**1 Introduction** 1
1.1 Background . . . 1
1.2 Motivation . . . 3
1.3 Typical process . . . 4
1.4 Objectives and scope . . . 5
1.5 Outline . . . 7
References . . . 8

**2 Rheological behavior of woven flakes** 11
2.1 Introduction . . . 12
2.1.1 Chopped woven reinforcements . . . 12
2.1.2 Problem description . . . 14
2.1.3 Objectives and approach . . . 14
2.2 Literature . . . 15
2.2.1 Classification of flow types . . . 15
2.2.2 Effect of length of reinforcements . . . 17
2.2.3 Effect of fiber content . . . 17
2.2.4 Summary of literature . . . 18
2.3 Squeeze flow modeling . . . 18
2.3.1 Axisymmetric (AS) squeeze flow . . . 18
2.3.2 Plane strain (PS) squeeze flow . . . 18
2.4 Materials and experimental methods . . . 19
2.4.1 Materials and specimen preparation . . . 19
2.4.2 Experimental setup and procedure . . . 21
2.5 Results and discussion . . . 22

2.5.1 Squeeze flow observations . . . 22
2.5.2 Material response . . . 22
2.5.3 Estimation of closing force . . . 28
2.5.4 Practical applicability of the observations . . . 29
2.6 Conclusions . . . 30
References . . . 30
2.A Appendix: Derivation of force response for PS squeeze flow . . . 33

**3 Jamming phenomenon in processing woven flakes 39**
3.1 Introduction . . . 40
3.2 Materials and experimental methods . . . 44
3.2.1 Materials . . . 44
3.2.2 Specimen preparation . . . 44
3.2.3 Experimental setup and procedure . . . 45
3.3 Results and discussion: Jamming . . . 47
3.3.1 Flow regimes and jamming phenomenon . . . 47
3.3.2 Characterization of jamming transition (percolation transition) . . . 50
3.3.3 Jamming transition diagram . . . 53
3.4 Results and discussion: Consolidation dwell time . . . 58
3.4.1 Effect of consolidation dwell in the presence of jamming . . . 58
3.4.2 Consolidation mechanism of jammed regions . . . 58
3.4.3 Validation of results: Effect of consolidation dwell . . . 61
3.5 Applicability in designing a process window . . . 64
3.5.1 Process parameters . . . 64
3.5.2 Orientation of planes of uniform thickness . . . 64
3.5.3 Consolidation dwell . . . 65
3.6 Conclusions . . . 65
References . . . 66

**4 Compression molding of integrated ribs 69**
4.1 Introduction . . . 70
4.1.1 Flow in rib sections . . . 71
4.2 Materials and experimental methods . . . 73
4.2.1 Materials . . . 73
4.2.2 Experimental setup . . . 74
4.2.3 Experimental methods . . . 74
4.3 Results and discussion: Deep rib . . . 76

4.3.1 Measure for part quality . . . 77
4.3.2 Filling of rib . . . 78
4.3.3 Effect of consolidation pressure . . . 79
4.3.4 Effect of flake size . . . 80
4.3.5 Effect of consolidation dwell time . . . 81
4.3.6 Entry radius . . . 83
4.4 Results and discussion: Small rib . . . 83
4.4.1 Rib filling . . . 86
4.4.2 Effect of flake size and consolidation pressure . . . 86
4.5 General discussion: Practical applicability . . . 89
4.5.1 Aspect ratio of rib . . . 90
4.5.2 Entry radius and corner radius . . . 91
4.6 Conclusions . . . 91
References . . . 92

**5 Mechanical performance of woven-flake reinforced composites 95**
5.1 Introduction . . . 96
5.2 Methodology . . . 97
5.2.1 Material definitions . . . 98
5.2.2 Chopped prepregs: process and properties . . . 99
5.2.3 Mechanics of load transfer and failure . . . 100
5.2.4 Extreme (minimum) value of strength . . . 105
5.2.5 Generation of random overlaps and tortuosity estimation . . . 107
5.3 Experimental work . . . 110
5.3.1 Materials and methods . . . 110
5.3.2 Manufacturing of flake reinforced laminates . . . 110
5.4 Results and discussion . . . 111
5.4.1 Experimental results . . . 111
5.4.2 Extreme values of tortuosity . . . 112
5.4.3 Statistically based design value . . . 116
5.5 Conclusions . . . 117
References . . . 117

**6 Discussion** **121**
6.1 Overview of the problem . . . 121
6.2 Multidisciplinary framework . . . 122
6.2.1 Part design . . . 123
6.2.2 Material . . . 124
6.2.3 Process . . . 127
6.2.4 Other factors . . . 129
6.3 Processing approach . . . 130
6.3.1 Proposed strategy for parameter selection . . . 130
6.3.2 Process window . . . 133
6.4 Application: Manufacturing of an access panel door . . . 134
6.4.1 Material, design and process parameters . . . 136
6.4.2 Results: Part quality . . . 136
6.5 Concluding remarks . . . 139
References . . . 140

**7 Conclusions and recommendations** **141**
7.1 Conclusions . . . 141
7.2 Recommendations . . . 142

**Acknowledgments** **145**

**Publications** **149**

# Chapter 1

# Introduction

## 1.1 Background

Composites are a synergistic combination of two or more different materials which bring out the advantages of the constituents in the resulting combination. The major advantage of composites is the ability to be tailored for the required purpose. Hence a higher strength and stiffness can be achieved with a relatively low density material compared to, for example, metals.

Composite materials in general are omnipresent in the nature on different hierarchical scales such as in wood, teeth and seashells, to name a few [1]. In structural engineering applications, especially in the field of aerospace, man-made composites have been used for around five decades [2]. The most commonly used constituents in engineering applications are highly stiff and strong continuous fiber reinforcements made of carbon or glass and a polymer matrix based on thermosets or thermoplastics. Furthermore, the proportion of composites being used in the aerospace sector is ever increasing, from less than 12 %wt in a Boeing B737 aircraft (1967) to more than 50 %wt in Boeing B787 (2011) and Airbus A350 (2015) aircraft [3, 4]. The prevailing situation in the automotive sector is similar, as can be seen from the release of BMW i3 (2016) with most of its structural components made from carbon fiber reinforced polymer [5].

In recent years, interest in continuously reinforced thermoplastic composites (TPC) has grown considerably owing to their superior toughness, increased processability, cost efficient manufacturability and inherent recyclability compared to their thermoset counterparts. The enhanced processability stems from the ability of the polymer to re-melt, which enables thermoforming and the use of various joining techniques such as resistance, ultrasonic and induction welding [6]. Reinforcements such as unidirectional fibers and woven fabrics with high fiber volume content are being utilized to achieve high mechanical properties. In terms of the polymer matrix, high performance polymers such as polyphenylene sulphide (PPS), polyether ether

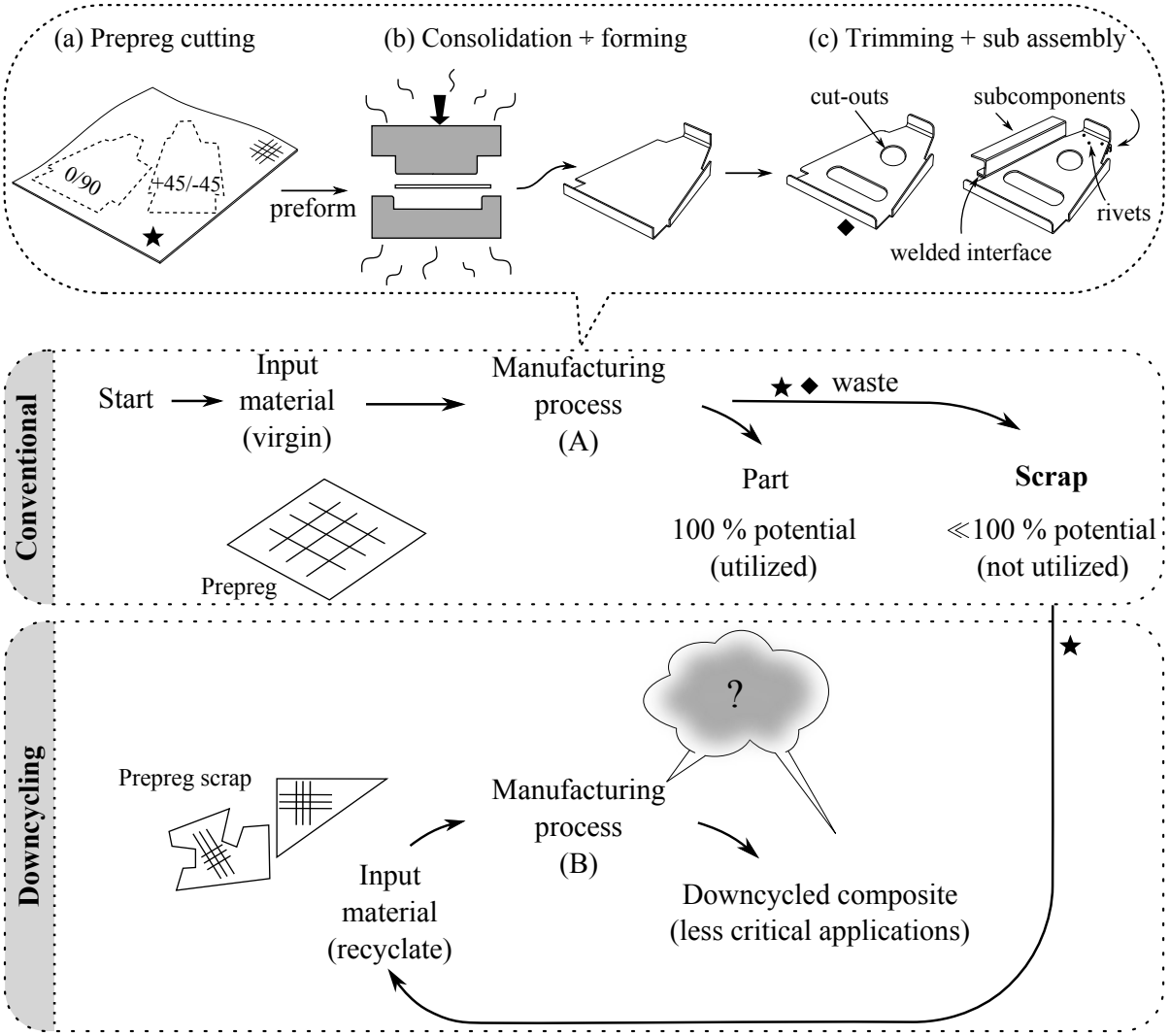


**Figure 1.1** *Value chain of thermoplastic composite manufacturing. Source of unconsolidated (★) and consolidated (◆) wastes. Preforms for thermoforming generate consolidated waste in stage (b).*

ketone (PEEK) and polyether ketone ketone (PEKK) are being used for their excellent mechanical properties, chemical and moisture resistance.

Figure 1.1 shows a simplified illustration of the conventional value chain in the TPC manufacturing process. The cycle starts with the virgin pre-impregnated reinforcements (prepreg) being input to a suitable manufacturing process. Based on the chosen manufacturing process such as autoclave or press consolidation, the prepregs are laid up with the required orientation of the plies. The preform for the next stage, (b), can be either laid-up prepregs cut in the shape of the part for autoclave consolidation or a pre-consolidated laminate trimmed to an approximate shape of the part for the thermoforming process. The illustration shows a thermoforming process as an example for stage (b). The pre-consolidated laminate is usually heated to the

forming temperature and is press-formed with a mold under high pressure. The press-formed laminates are then trimmed to the net-shape of the part and which is then finished with drilling and other subsequent operations in stage (c). Finally, the subcomponents are assembled with rivets or with the other joining techniques mentioned earlier. It can be observed that in the prepreg cutting stage, a significant amount of virgin material is wasted. Further in stage (c) a considerable amount of consolidated material is trimmed to obtain the net shape of the part. In essence, the manufacturing process (denoted by A) transforms a portion of the virgin material into a usable part and rest of the irregular shaped scrap material with reduced potential is discarded. The present thesis focuses on utilizing these discarded materials in the production of usable parts.

## 1.2 Motivation

Although continuously reinforced composite materials have many advantages, one of the major disadvantages of using continuous reinforcements is the limitation to manufacture complex shapes without processing defects such as wrinkles [7, 8]. Therefore, complex parts are manufactured by assembling relatively simple press-formed shapes as shown in Figure 1.1. Another major disadvantage is the wastage of material incurred during the production process. These disadvantages form the basis of the motivation for the work presented in this thesis.

With respect to the first disadvantage, studies have been performed in the past to improve the formability of continuous reinforcements by introducing discontinuities in the fibers. Various methods such as slitting [9], pre-stretching consolidated lamina [10] have been used to improve the formability to some extent, but accompanied with a reduction in mechanical properties. However, to manufacture complex three dimensional structures with integrated functional features and inserts, the composite material has to experience a considerable amount of flow. Further increasing the number of discontinuities in the material to improve the flow of the material leads to a limit case of discontinuously reinforced molding compound. The limit case arises as a balance between the properties and processability. Materials such as chopped unidirectional tapes (TCAC BMC [11] and HexMC [12]) or chopped fiber mats (GMT and SMC) cater to this limit case, in which the first example in each type is based on thermoplastic matrix and the second material is based on thermoset matrix.

The second disadvantage of material wastage is tackled by reclaiming the fibers from the unconsolidated (★) and consolidated (◆) waste using various methods, as illustrated schematically in the downcycling loop in Figure 1.1. These methods include for example, incineration and chemical processes. In other cases the scrap is ground into short fibers or to a fine powder to be used as particulate fillers in polymeric materials [13].

However, for woven fabrics, maintaining the architecture of the reinforcements can be beneficial, apart from the length of the reinforcements, while subjecting it to a size reduction process. The woven architecture provides a local structural integrity to the chopped flakes and hence a two dimensional reinforcing effect can be achieved. Moreover, the woven structure of the flake also prevents disintegration of the flakes, unlike chopped unidirectional tapes that can get split in the transverse direction during the molding process. Since a flake can be mobile and is also unlikely to get disintegrated by the flow, the processing behavior can be expected to be different compared to GMT or chopped tapes. This leads to the question: what kind of process can be used to recover the potential in the scrapped woven prepreg materials? A solution to this question is addressed in this thesis.

## 1.3 Typical process

Undoubtedly, the recyclate from the prepreg cutting process is a good source of virgin material although it may have irregular shapes. The potential in the virgin material can be partly preserved by maintaining the architecture in the form of a two dimensional reinforcement. Moreover, the chopped prepreg material can be used as a standalone molding compound. Additionally, a compression molding process is chosen to manufacture parts, as it allows for complex geometries while retaining a long fiber length [14]. Thereby, a part of the manufacturing value addition loop can be closed by better utilization of the raw material yet with reduced mechanical properties of the part.

Figure 1.2 shows a proposed solution with different routes for chopping the prepreg materials. The process starts with a size reduction process to chop the prepreg scrap followed by a classification process to sieve the different sizes of chopped flakes. The classified flakes are then metered to be used in a compression molding process. The mold is loaded with the uniformly thick chopped material and is subjected to a compression molding cycle. The randomness in loading the material and the amount of material flow inside the mold during the process creates a pseudo-random arrangement of the flakes in the flake reinforced composite.

The size reduction process shown in Route 1 is a more natural route for an established process by shredding the wastes. However, the shredded flakes can have random shapes and irregular orientations of fibers in the flakes. Moreover, during the molding process as the material flows, the fiber bundles at the shorter edges of the flakes can get disentangled. Such additional inconsistencies in the material can potentially cause a large scatter in the experimental measurements, apart from the inherent randomness in the meso-structure. This might inhibit the fundamental understanding of the material behavior. Therefore, the problem can be made tractable with a constant shape of flake, as shown in Route 2, which provides a constant length

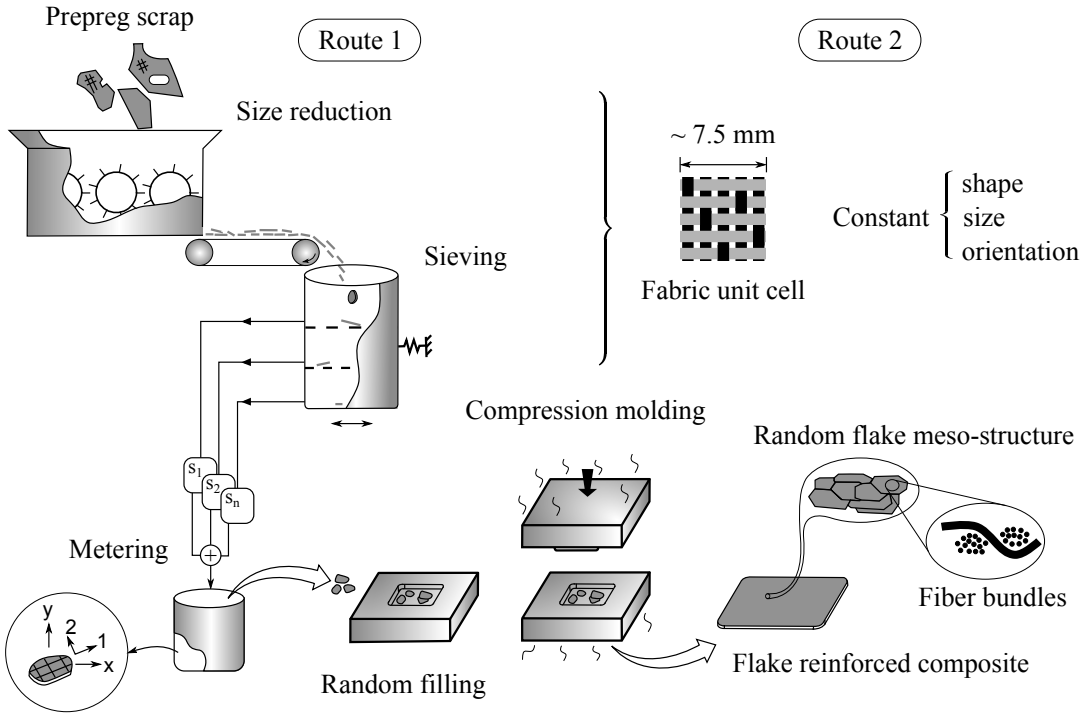


**Figure 1.2** *Conceptualized process cycle. Fabric unit cell corresponds to a 5 harness satin weave with 3K fibers in each bundle.*

of fibers. Additionally, the choice of a constant size based on the fabric unit cell and a constant orientation of fibers in the flake will prevent any other flow-related effects on performance during the processing of the material.

## 1.4 Objectives and scope

The main objective of this thesis is to develop a strategy for the manufacturing of parts from chopped woven thermoplastic composite flakes with good quality and consistent mechanical properties. A fundamental understanding of the chopped woven material is required to achieve the goal. Figure 1.3 shows a typical molding process with chopped flakes and a typical process cycle consisting of different stages.

For producing repeatable and reliable parts with a reduced scatter in their properties, an understanding of the material behavior during filling and consolidation stages is indispensable, since the material flow occurs in those stages. Furthermore, the properties of the molded part depend on the relationship between the process and the process parameters. For instance, the rheology of the reinforced polymer melt is a function of a non-exhaustive list of parameters like the geometry of reinforcements, reinforcement volume fraction, polymer properties, evolving meso-structure and the

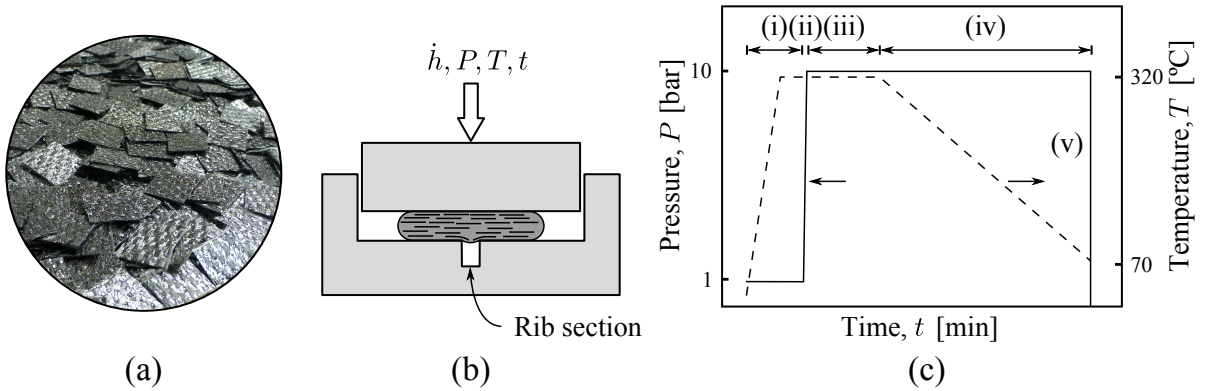


**Figure 1.3** *(a) Chopped prepreg flakes, (b) Typical compression molding process with a defined closing rate of mold $\dot{h}$ (c) Typical process cycle comprising of stages (i) heating (ii) filling, (iii) consolidation dwell (iv) cooling and (v) demolding.*

process parameters. The final meso-structure is a function of the rheology of the reinforced melt, geometry of the part and the processing method and conditions. Additionally, the woven nature of the material affects the mobility of the flakes in combination with the closing rate of the mold ($\dot{h}$). Consequently, the mechanical properties of the consolidated part are a function of the final meso-structure in the part. Therefore, a feasible process window should be identified in the domain of the design, material and process parameters in order to properly fill the mold cavity and to achieve a good consolidation.

A lot of research has been performed in the past to understand the flow behavior of chopped materials such as GMT and SMC with relatively low fiber volume content [15–20] and chopped UD materials with relatively higher fiber volume content [21, 22]. However, literature on chopped woven materials is scarce and this thesis intends to expand knowledge about such materials. In summary, the approach to achieving the objective is as follows,

(a) obtain a fundamental understanding of the processing of the chopped woven material,

(b) develop a preliminary strategy to identify a feasible process window while addressing the critical issues such as efficient material flow with minimal jamming and its connection to the change in the key process parameters, and

(c) assess the variability in the final part properties (simple flat structure) with respect to the flake size and specimen size.

A typical aerospace grade prepreg material from TenCate Advanced Composites is used throughout the study. The prepreg consists of a 5 harness satin (5HS) woven carbon fabric reinforcement and 50 vol% of PPS polymer matrix. The material is obtained from the actual cutting wastes incurred in the manufacturing process of aircraft parts from Fokker Aerostructures.

## 1.5 Outline

Figure 1.4 shows a schematic outline of the main chapters of the thesis. The chapters are reproduced from research papers, hence, some of the essential details are repeated in every chapter. The author apologizes for any inconvenience caused due to the repetition. However, the chapters are self-contained which enables them to be read separately without losing sight of the bigger picture.

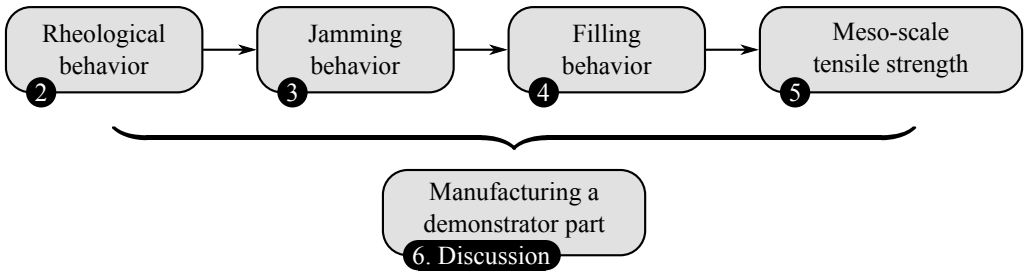


**Figure 1.4** *Outline of the thesis.*

To start with, the rheological behavior of the chopped woven prepreg is studied in Chapter *two*. The flow stress in the chopped material under squeeze flow condition was investigated with different material and process parameters such as flake size and closing rate of the mold. Furthermore, the material behavior was characterized under two different flow boundary conditions namely, axisymmetric and plane strain conditions. The physical observations and the trend in the parameters of the material model are explained phenomenologically.

The randomly positioned woven flakes, with local structural integrity, were found to agglomerate and mechanically jam during the squeezing process. The jamming phenomenon is studied in Chapter *three*. The jamming of the material was considered to be based on the dominance of the type of flow existing in the material such as advective or diffusive type of flow. The relative importance of the type of flow was characterized with scaling arguments based on the Péclet number, for different flake sizes and closing rate of the mold.

As mentioned earlier, one of the major advantages of chopped materials is the ability to take up complex shapes and fill intricate features such as ribs. To explore such capabilities, Chapter *four* focuses on the filling behavior of the chopped material in integrated ribs with different aspect ratio. The consolidation quality in terms of voids and matrix rich regions was investigated experimentally for different flake sizes, consolidation pressures and consolidation dwell times.

Chapter *five* focuses on the mechanical performance of the material in terms of the tensile strength of flat sections. The scatter observed in the measured tensile strength values was approximated with a simple analytical model. Statistical principles were used to analyze the uncertainty in the modeled tensile strength.

As a closure to the thesis, a comprehensive overview of the process and the obtained results are discussed in Chapter *six*. A preliminary strategy to obtain the range of feasible parameters in terms of the design, material and process is proposed based on the results from the study. Furthermore, the results are utilized to manufacture a full scale demonstrator part. The selection of parameters and the qualitative results are presented briefly. Finally, the important conclusions and the recommendations for future work are presented in Chapter *seven*.

# References

[1] P. Fratzl, J. W.C. Dunlop, and R. Weinkamer. *Materials Design Inspired by Nature*. RSC Smart Materials. The Royal Society of Chemistry, 2013.

[2] P. K. Mallick. *Fiber-Reinforced Composites: Materials, Manufacturing, and Design, Third Edition*. CRC Press, November 2007.

[3] B. Griffiths. Boeing sets pace for composite usage in large civil aircraft. Composites World, 2005. URL *http://www.compositesworld.com/articles/boeing-sets-pace-for-composite-usage-in-large-civil-aircraft*, Retrieved on 05 Apr. 2016.

[4] Airbus website, A350XWB family. URL *http://www.airbus.com/aircraftfamilies/passenger-aircraft/a350xwbfamily/technology-and-innovation/*, Retrieved on 05 Apr. 2016.

[5] BMW Leipzig: The epicenter of i3 production : CompositesWorld, April 2016.

[6] F.C. Campbell. *Manufacturing Processes for Advanced Composites*. Elsevier, December 2003.

[7] S.P. Haanappel. *Forming of UD fiber reinforced thermoplastics*. PhD thesis, University of Twente, Enschede, The Netherlands, 2013.

[8] Ulrich Sachs. *Friction and bending in thermoplastic composites forming processes*. PhD thesis, University of Twente, Enschede, The Netherlands, 2014.

[9] I. Taketa, T. Okabe, H. Matsutani, and A. Kitano. Flowability of unidirectionally arrayed chopped strands in compression molding. *Composites Part B: Engineering*, 42(6):1764–1769, September 2011.

[10] C. Stephen, Dustin L. Levin, Dequine, and John P. Crocco. Formability of thermoplastic stretch-broken carbon fiber vs. thermoplastic continuous carbon fiber. In *SAMPE Technical conference proceedings*, 2013.

[11] D. DeWayne Howell and Scott Fukumoto. Compression molding of long chopped fiber thermoplastic composites. In *CAMX conference proceedings*, 2014.

[12] J. Fudge. "HexMC - Composites in 3D" a new high performance molding compound. In *SAMPE Technical conference proceedings*, 2001.

[13] Soraia Pimenta and Silvestre T. Pinho. Recycling carbon fibre reinforced polymers for structural applications: Technology review and market outlook. *Waste Management*, 31(2):378–392, February 2011.

[14] Isayev. *Injection and Compression Molding Fundamentals*. CRC Press, June 1987.

[15] G. Kotsikos, J. H. Bland, and A. G. Gibson. Rheological characterization of commercial glass mat thermoplastics (GMTs) by squeeze flow testing. *Polymer Composites*, 20(1):114–123, February 1999.

[16] Ronnie Törnqvist, Paul Sunderland, and Jan-Anders E. Månson. Determination of the rheological properties of thermoplastic composites for compression flow molding. *Polymer Composites*, 21(5):779–788, October 2000.

[17] M. A. Dweib and C. M. ÓBrádaigh. Extensional and shearing flow of a glass-mat-reinforced thermoplastics (GMT) material as a non-Newtonian viscous fluid. *Composites Science and Technology*, 59(9):1399–1410, July 1999.

[18] Roberto J. Silva-Nieto. *Prediction and characterization of compression mould flow for unsaturated polyester resin sheet moulding compound*. PhD thesis, Loughborough University, 1980.

[19] G. Kotsikos and A. G. Gibson. Investigation of the squeeze flow behaviour of Sheet Moulding Compounds (SMC). *Composites Part A: Applied Science and Manufacturing*, 29(12):1569–1577, December 1998.

[20] P. Dumont, L. Orgéas, S. Le Corre, and D. Favier. Anisotropic viscous behavior of sheet molding compounds (SMC) during compression molding. *International Journal of Plasticity*, 19(5):625–646, May 2003.

[21] Paolo Feraboli, Elof Peitso, Francesco Deleo, Tyler Cleveland, and Patrick B. Stickler. Characterization of Prepreg-Based Discontinuous Carbon Fiber/Epoxy Systems. *Journal of Reinforced Plastics and Composites*, 28(10):1191–1214, May 2009.

[22] Gilles-Philippe Picher-Martel. *Compression moulding of randomly-oriented strands thermoplastic composites: A study of the flow and deformation mechanisms*. PhD thesis, McGill University, Quebec, Canada, 2015.

# Chapter 2

# Rheological behavior of chopped fabric reinforced thermoplastic prepreg: Squeeze flow*


### *Abstract*

Fundamental understanding of the rheological behavior of molding compounds is indispensable for developing a process window for compression molding. For this purpose, constant volume squeeze flow experiments are performed on this material under both axisymmetric and plane strain conditions. The response of the material consisting of different flake sizes is studied at different mold closing rates. An analytical solution with a power law constitutive model, as a first approximation, was used to characterize the melt flow behavior in both loading conditions. An in-plane isotropic flow behavior was observed. The experimentally obtained rheological parameters were found to be a function of flake size and instantaneous height of the cavity. Jamming induced processing limit was observed with larger flakes at lower closing rates.


*Reproduced from: M.I. Abdul Rasheed, B. Rietman, H.A. Visser, R. Akkerman. Rheological behavior of chopped fabric reinforced thermoplastic prepreg: Squeeze flow. To be submitted to *Composites Part A: Applied Science and Manufacturing*, **2016**.

## 2.1 Introduction

High performance thermoplastic polymer composites (TPC) with continuous fiber reinforcements are increasingly being introduced in aerospace and automotive applications. Both unidirectional and woven reinforcements with high fiber volume content are being used. The major driving factors being, superior mechanical performance, cost efficient manufacturability, increased processability and being recyclable compared to thermosets. However, manufacturing complex shapes with continuously reinforced materials is limited by the formation of processing defects such as wrinkles. Therefore, complex parts are made as sub-assemblies of parts with simple shapes. A number of previous studies in the literature have tried different ways to overcome this limitation by adding discontinuities in the fibers such as by slitting the prepreg [1] or by pre-stretching the laminae after manufacturing [2]. The introduction of such discontinuities improves the formability of the material to a certain extent. However, for manufacturing non-shell-like structures or voluminous 3D geometries, a discontinuously reinforced molding compound is a more suitable alternative [3].

### 2.1.1 Chopped woven reinforcements

A discontinuous molding compound consisting of chopped woven prepreg (flakes) with a large planar aspect ratio is considered in this study. Figure 2.1 shows a typical chopped prepreg flake investigated in this study compared to a long fiber pellet with aligned fibers. The motivation to choose planar reinforcement stems from its ability to reinforce in two dimensions locally and the ability to achieve quasi-isotropic properties [4, 5] on a macroscopic scale. The latter can be achieved by randomizing the initial mold filling process, which is relatively straightforward compared to the tedious lay-up design in the case of continuous reinforcements. Upon choosing a suitable manufacturing process, such as compression molding, parts with functional features and high fiber volume content can be molded in one shot. Additionally, near-net shaped parts as well as high production rates can be obtained. Suitable application areas include semi-structural and less critical parts in the aerospace and automotive industry since the inhomogeneity of the material leads to a lower structural performance.

Previous studies on similar discontinuous materials focused on reinforcements such as chopped rovings, dispersed filaments and entangled glass mats with thermoset and thermoplastic matrices. However, materials with relatively low fiber content in the range of 20-30 % by weight were investigated, since the maximum reinforcement content and the form of the reinforcement that could be used is usually limited by the manufacturing process. Moreover, the particular case of chopped woven prepregs with relatively high fiber volume content of nearly 50 % has not been explored so far.

Besides, such planar reinforcements can be derived by shredding the large amount of process scrap generated in the conventional production processes of woven TPCs. Hence, the study of such a material system is also interesting in the perspective of recycling.

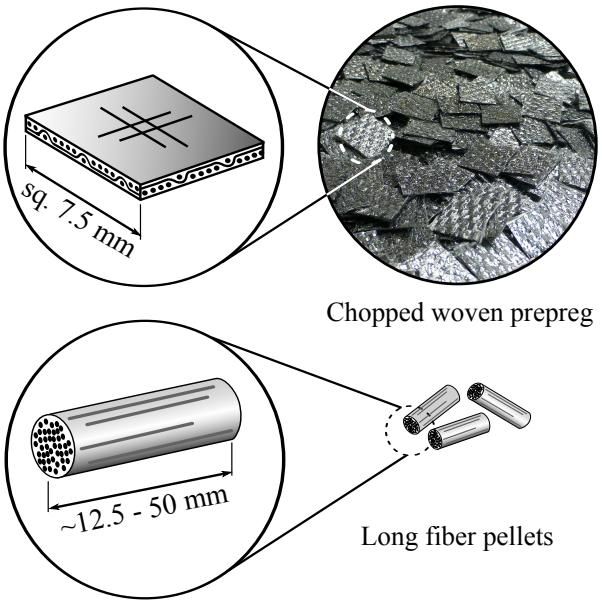


**Figure 2.1** *Top: Conventional chopped long fiber compound. Fiber filaments (dark) surrounded by matrix polymer (light). Bottom: Typical chopped woven prepreg flakes used in this study. Reinforcing fabric consisting of fiber bundles (dark) and partially impregnated regions (light).*

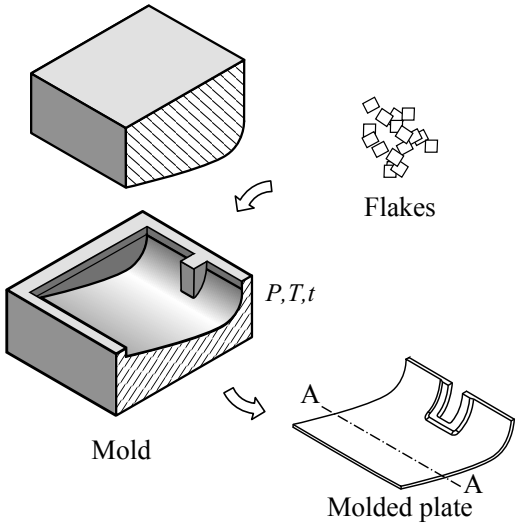


**Figure 2.2** *Illustration of an actual compression molding process with a certain a pressure, temperature and time, and the resulting part.*

### 2.1.2 Problem description

A typical manufacturing cycle starts with filling the prepreg flakes in the compression mold cavity and subsequently heating, compressing, consolidating and cooling the material. The left pane in Figure 2.2 shows the physical process with a positively closed mold. Depending on the charge placement and part design, during the compression stage, the material first flows in all directions on the meso-scale (flake level) as the pressure increases. The material might experience a uniaxial flow, when part of the melt front reaches the mold boundaries. Finally, the material undergoes a triaxial compression after filling the entire mold [6, 7] and subsequently gets consolidated on the micro-scale (filament level).

Consequently, the attainable complexity of the molded part depends on the ability of the reinforcements to move [8]. Furthermore, the bulk flow of the material has an influence on the final meso-structure and thereby on the mechanical properties of the consolidated part.

Clearly, this shows that understanding the rheological behavior of the molding material and its processing limits is the key to manufacturing parts with consistent quality. This paper investigates the rheological behavior of the planar-reinforced polymer melt under axisymmetric and uniaxial flow conditions.

### 2.1.3 Objectives and approach

The objective of this study is to investigate the effect of parameters such as flake size and mold closure rate on the flow behavior of the chopped woven prepreg under a constant volume compression molding scenario. Squeeze flow experiments were selected for the characteristics of the flow and because it can handle materials with relatively high fiber volume content and large sized reinforcements, compared to other standard rheometric experimental techniques. Two conditions are evaluated, firstly, an axisymmetric (AS) flow in all planar directions and secondly, a plane strain (PS) flow idealized as a strip of material bounded by two mold walls limiting the flow to one axis [6]. The mold interfaces in both types of tests are not lubricated. The boundary condition at the mold-material interface and the flow stress under isothermal conditions are investigated with different constant rates of closures. Apart from the matrix polymer present in the prepreg, no additional matrix polymer is added to the compound. The planar aspect ratio of the prepreg flakes is set to one to avoid any unwarranted higher order effects in the flow due to the shape of the flakes. A theoretical analysis of the flow is performed and an analytical solution is devised to describe the flow and obtain the necessary flow parameters.

The subsequent sections of the article contain a brief review of the literature, the analytical solution to the problem and a discussion of the results obtained in the experimental investigation followed by conclusions and future work.

## 2.2 Literature

This section provides a brief review of the literature on concentrated fiber suspensions to highlight the important results observed in similar materials as well as to aid in the design and analysis of the experiments performed for this study.

Literature on the flow of polymer melt suspended with woven flakes is scarce. However, studies on similar discontinuous materials such as short or long fiber reinforced thermoplastics (SFRT, LFRT), glass mat thermoplastic (GMT) materials, chopped unidirectional materials and sheet molding compounds (SMC) with thermoset polymer matrix are considered as a suitable choice for a theoretical reference. An additional aspect to consider in the case of the woven flakes is the local structural integrity of the flakes provided by the architecture of the weave (see Figure 2.1). Compared to the other discontinuous material, the local structure enables the flakes to move as a single unit or to get agglomerated as a stack of flakes through the thickness.

### 2.2.1 Classification of flow types

Figure 2.3 shows the theoretical approximation of the flow in a flat section. Considering a flow in a thin section two extreme cases of flow can be assumed to exist [9]. They are: a shear flow where the mold-material interface is non-slipping (Figure 2.3 (a)) and a plug flow where the material interface slips generating an extensional deformation [10, 11]. Table 2.1 shows a summary of the studies performed in the past with different materials along with the assumed boundary conditions and the material model. Among others, for GMTs with a non-woven mat structure, the studies assumed the presence of a thin lubricating layer at the mold-material interface leading to an extensional type of flow.

However, in practical situations a pure plug flow or a pure shear flow condition may not exist. Instead a mixture of both might be present [12–18] as illustrated in Figure 2.3 (c). Furthermore, in [16] it was found that for materials, such as GMT, with relatively low power law index values of around 0.5, the energy that dissipated in the extensional deformation is very small and has little effect in the average response of the material. Additionally, in the case of highly concentrated suspensions, the bulk fluid properties obtained through the experiments were found to be a function of the local interaction between the reinforcements and were less influenced by the boundary condition at the mold-material interface [7]. Therefore, taking into account the aforementioned observations, the assumption of shear flow is relatively adequate for the characterization of the average material response for the case of chopped woven prepreg with high fiber content.

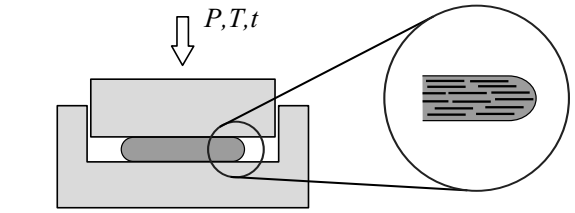


Simplified mold section at A-A

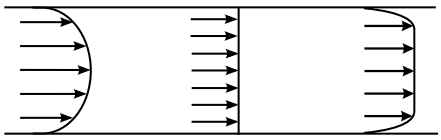

(a) Shear flow (b) Plug flow (c) Mixed flow

Velocity profiles

**Figure 2.3** *Illustration of a simplified process showing a typical flow of flake reinforced polymer melt in a flat cross section (A-A in Figure 2.2). Inset shows the flow front of the flake reinforced polymer melt at steady state. Different possible velocity profiles (a, b, c) are shown in the bottom characterized by their interaction with the mold wall.*

| Material | Description | Ref. |
|---|---|---|
| | Boundary condition and material model | |
| BMC<br>SMC | Shear flow, power law | [19]<br>[20] |
| GMT | Extensional flow, power law<br>Shear and extensional flow | [7, 12, 21–23]<br>[12–18] |
| | Physical effects | |
| LFS | Yield stress increases with length of reinforcement.<br>Frictional effects at low deformation rates and hydrodynamic lubrication between reinforcements at higher rates. | [8, 24] |
| GMT | Yield stress effects were insignificant.<br>Similar frictional effects as LFS.<br>High density of contact points increase the overall stress. | [17, 23]<br><br>[22, 24, 25] |
| | Fiber content | |
| BMC<br>LFS | Increases non-Newtonian behavior. | [19, 26] |
| LFS | Fiber-matrix separation due to non-affine flow. | [27] |

LFS: Long fiber suspensions

**Table 2.1** *Summary of the important observations from the literature.*

### 2.2.2 Effect of length of reinforcements

The length of the suspended fibers has a major role in the rheological behavior at higher concentrations. The effects are observed in the form of deformation-rate dependent lubrication between reinforcements and yield stress of the material. Firstly, at lower rates of deformation the inter-fiber frictional effects were found to be prominent due to the formation of dry contacts between reinforcements. However, at higher rates hydrodynamic interactions were induced by faster relative motion of the fibers, which thereby reduced the normal force at the interaction points. Secondly, the study in [17] showed that the effect of yield stress is less significant in the squeeze flow behavior of GMT compared to frictional effects.

The present case of a bed of chopped woven flakes lies in between the long fibers and GMT. In GMT, the structure of the entangled mat does not allow the individual fibers to move freely, whereas the flakes can slide past each other and also have different periods (order of flake length) of inter-flake interactions at meso-scale. Thus both hydrodynamic as well as frictional effects between the flakes at different deformation rates gives rise to distinct behavior for flake suspensions. That is, it has the ability to flow or to get mechanically jammed as a function of the imposed deformation rate and flake size.

### 2.2.3 Effect of fiber content

The increase in reinforcement content reduces the average inter-fiber distance and hence, both hydrodynamic interactions and frictional contacts between fibers become more important. This effect causes an increase in the non-Newtonian behavior due to the existence of a competitive balance between the fiber-fluid viscous drag force and fiber-fiber interactions [19, 26]. A similar effect was observed when the fiber bundles filamentize in to individual filaments increasing the effective area for the hydrodynamic interaction, for a fixed reinforcement content [19]. In [27], a rigorous mathematical analysis has been carried out considering particle motions with frictional contacts giving rise to bulk stresses. The rise in stress during the initial flow of a statistically homogeneous material with affine flow conditions is due to the energy dissipations required to accommodate the change in orientation states of the particles. Once the particles get aligned the stress drops rapidly due to loss of contacts. Upon relaxing the conditions such as homogeneity and uniform fiber fraction, the flow is no longer affine leading to flow induced segregation or fiber-matrix separation.

### 2.2.4 Summary of literature

Table 2.1 summarizes the important observations from the literature on similar discontinuous materials. From the literature survey, the following assumptions are made as follows. (a) A shear type of flow is considered for the development of the analytical solution for the plane strain load case. (b) As the behavior of the chopped prepreg material is expected to be a function of the flake size, different flake sizes are studied. One of the sizes was chosen to be smaller than the unit cell size of $\sim 7.5$ mm, for a 5 harness satin weave, to determine the effect of disentanglement.

## 2.3 Squeeze flow modeling

This section devises the analytical solutions for the squeeze flow problem under study. The assumptions considered for the solution of the force response are as follows: the material is incompressible, statistically homogeneous, the material sticks at the mold interface, the thin film approximation holds and as a first approximation a power law constitutive model is assumed for the chopped prepreg material. Furthermore, a constant volume squeeze flow experiment is considered in this study. Therefore, by volume conservation the measured instantaneous height $h$ gives the average instantaneous radius $R$ or width $w$ of the specimen in contact with the mold, for the case of axisymmetric flow and plane strain flow, respectively.

### 2.3.1 Axisymmetric (AS) squeeze flow

The problem of an isothermal axisymmetric squeeze flow of a power law fluid between impermeable parallel plates with no-slip boundary conditions was solved by Scott and is given in [28]. The squeeze force $F$ required to maintain a constant rate of mold closure $\dot{h}$ is given as,

$$F_{squeeze,AS} = \left(\frac{\dot{h}^n}{h^{2n+1}}\right)\left(\frac{2n+1}{n}\right)^n\left(\frac{2\pi k_s R^{n+3}}{n+3}\right), \tag{2.1}$$

where $\dot{h}$ is the closing rate of the mold in mm/s, $h$ is the instantaneous height of the specimen in mm, $k_s$ in MPa $\cdot$ s$^n$ is the power law fluid consistency in shear mode, $n$ is the shear thinning index, $R$ is the radius of the specimen in mm.

### 2.3.2 Plane strain (PS) squeeze flow

For the case of plane strain squeeze flow, the material is constrained in the $y$-axis and is allowed to flow only in the $x$-axis as shown in Figure 2.4, corresponding to

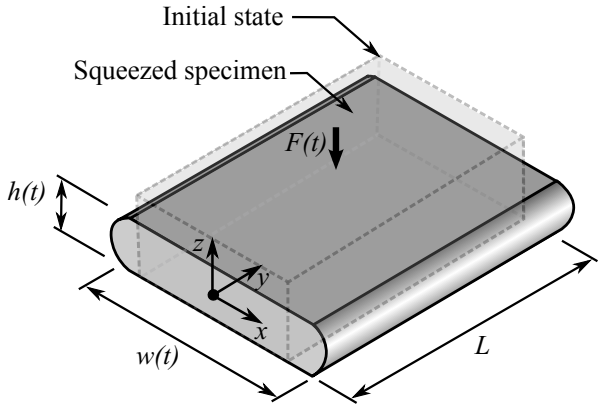


**Figure 2.4** *Plane strain squeeze flow configuration (the flow constraining blocks in the y-direction are not shown).*

a uniaxial flow. Appendix 2.A shows a detailed derivation of the force response and gap-wise shear rates for a shear flow under plane strain boundary condition, following the general solution principles of [9, 28].

The squeeze force $F$ is found to be,

$$F_{squeeze,PS} = \left(\frac{\dot{h}^n}{h^{2n+1}}\right)\left(\frac{2n+1}{n}\right)^n\left(\frac{k_s L w^{(n+2)}}{n+2}\right), \tag{2.2}$$

where $L$ and $w$ are the length and width of the specimen as defined in Figure 2.4.

The material parameters ($k_s$ and $n$) fitted to the equation Eq. (2.1) were found to be constant for a constant mold closing distance $h$, in the case of random GMT [18]. This is primarily due to the evolving structural arrangement of the reinforcements. Furthermore, it can be observed from Eq. (2.24) that the shear strains are not constant throughout the test and within the specimen. Additionally, the randomness of the material leads to an untrackable local stress-strain situation and hence, only an average material behavior is envisioned.

## 2.4 Materials and experimental methods

### 2.4.1 Materials and specimen preparation

The experimental work was performed on the cutting waste of CETEX ® Carbon/-poly(phenylene sulphide) (C/PPS) semi-pregs from TenCate Advanced Composites. The partially pre-impregnated material consists of woven reinforcing fabric with a 5 harness satin architecture spray coated with PPS polymer matrix. The thickness of a consolidated lamina is 0.31 mm with a fiber volume fraction $v_f$ of 50 %. The

polymer has a glass transition temperature ($T_g$) of 90 °C and a nominal processing temperature of 320 °C. The semi-pregs are chopped into squares with side lengths 5, 7.5 and 12.5 mm for manufacturing three different plates. The warp and weft directions of the fabric is made to coincide with the edges of the flakes. The planar aspect ratio of one is chosen for maintaining a constant fiber length in both primary directions of the chopped flakes. Each charge, a total of 496 grams, of chopped flakes is filled in a picture frame mold of 250 x 250 mm$^2$ to obtain a plate of 4 mm final thickness. The plates are compression molded at 4 bar pressure and 320 °C with a consolidation dwell time of 15 minutes and a set-point cooling rate of 15 °C/min. The consolidated plate is then cut into circular disks of diameter 25 mm for the

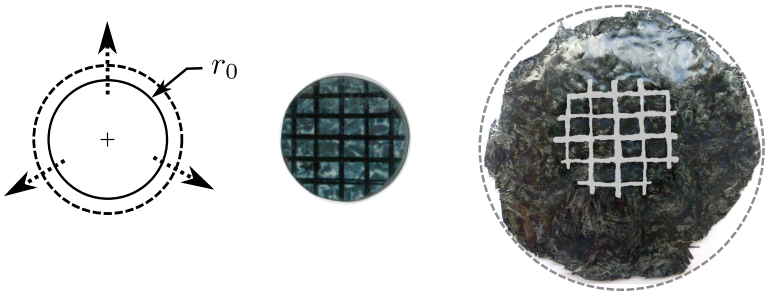


(a) Axisymmetric squeeze specimen

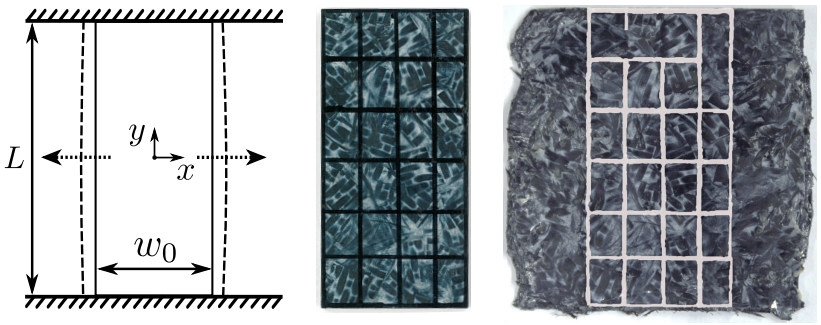


(b) Plane strain squeeze specimen

**Figure 2.5** *(a) Axisymmetric and (b) Plane strain schemes used in this study. Solid lines represent specimens with initial dimensions $r_0$ and $w_0$. Dashed lines show the flow front at time $t > 0$ in the direction of flow shown with dotted arrows. Specimens with grids are shown in a state before and after the test (visible grid in the squeezed specimen is shown in white color).*

AS case and in a rectangular shape with a dimension of 60 x 30 x 4 mm$^3$ for the PS experiments. Figure 2.5 (a,b) shows the AS and PS specimens before and after squeezing respectively. An equidistant grid is drawn on the top surface of the specimens to identify the mold-material interface boundary condition.

### 2.4.2 Experimental setup and procedure

**Experimental setup**

An instrumented squeeze flow setup, as shown in Figure 2.6, is used in this study to perform the squeeze flow experiments. The dimension of the flat surface of the mold platens is 60 x 60 $mm^2$. The setup consists of a moving top half, which is fixed to the crosshead of a Zwick Z100 universal testing machine. The lower mold half is fixed to the stationary frame of the machine with a revolute joint to align the two mold surfaces so they are parallel. Removable side walls are attached to the lower half to constrain the flow in y-axis for the PS condition and also to compensate for the heat loss in the mold gap. Heating cartridges are used to heat the mold and side walls with PID controllers fed with temperature measurements from thermocouples in the mold. The instantaneous mold separation is measured with a Messphysik laser speckle extensometer close to the mold gap. The force exerted on the mold, the displacement and the temperature of the mold halves are recorded using a data acquisition system. Moreover, due to the finite stiffness of the machine and the mold setup, the observed rate of closure $\dot{h}$ is not exact to the set point value. The $\dot{h}$ values used in the analysis are the actual rate calculated with the measured mold displacement data obtained from the laser speckle extensometer.

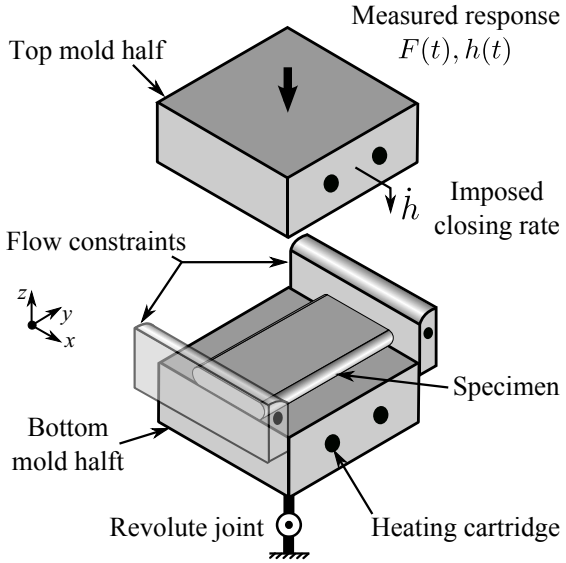


**Figure 2.6** *Squeeze setup showing the top and bottom mold half, and the side elements used to constrain the flow in the case of plane strain flow. The other two side walls are not shown in the figure for brevity.*

**Experimental procedure**

The mold is heated until it saturates to the processing temperature of the C/PPS material of 320 °C and thereafter is held constant. The specimen is placed in the mold gap with polyimide foils on both faces to provide a consistent surface quality at the mold-melt interface. The material is heated for a constant time period of 120 seconds. The heating time was fixed based on the measurements made, at the mid plane of trial specimens, prior to actual tests. After the set heating time is reached, the mold closes at the constant rate of closure to a final height of 25 % and 60 % of the initial specimen thickness ($h_0$) for AS and PS experimental conditions, respectively. The rate of closures investigated for the AS experiments were 0.05, 0.5 and 3 mm/s and 0.005, 0.05, 0.5 and 2 mm/s for the PS experiments.

## 2.5 Results and discussion

The material response in the two different squeeze flow configurations (AS and PS) is explained in the following subsection and a theoretical estimate of the PS squeeze pressure is calculated to validate the obtained material parameters of AS condition.

### 2.5.1 Squeeze flow observations

Two types of compression tests were investigated in this study to characterize the flow properties of woven flake reinforced materials for a compression molding process. This section describes the general observations on the mold-material interface and overall flow behavior. The grid drawn on the specimen is observed to be in an undeformed state after the squeeze test. Hence, the mold-melt interface is considered non-slipping, showing a dominant shear flow behavior. Moreover, the average response of the material can be considered as in-plane isotropic since the material flows almost equally in all directions as shown in Figure 2.5, especially in the AS case (b). In general, partial closure experiments also suggest an isotropic behavior with uniform flow fronts.

### 2.5.2 Material response

The material response in terms of the axial stress $\sigma_{zz}$ versus normalized instantaneous gap $h/h_0$ is shown in Figures 2.7 and 2.8 for a typical AS test on 5 mm flakes and a PS test of 12.5 mm flakes, respectively. The axial stress in the specimen is calculated from the measured force and area based on the constant volume approach as mentioned earlier. Due to the limitation in the size of the compression platen for performing a constant volume test, the maximum strain reachable in the PS

experiment is smaller than the AS case. The results shown are an average of three specimens per experimental condition. The error bars show one standard deviation at some measurement points for clarity. It can be observed that in both cases the maximum axial stress is a function of the rate of closure. The trend in the stress response is similar in both the PS and AS loading conditions.

In the initial periods of closing the mold, before the onset of the flow, an increasing stress response is observed in the PS condition (visible in 0.5 mm/s specimen in the PS response) as the mold starts to close. This can be attributed to several effects such as the elastic response of the material and the inter-flake friction effects at the initial stage [27], as mentioned earlier in Section 2.2.3. It is observed to have an increasing trend with flake size and is found to be smaller in the case of AS condition due to the free flowability in all directions.

As the flow progresses a monotonic response in stress is expected according to Scott's relation shown in Eq. (2.1) and (2.2). However, physical phenomena occur, such as flattening of the bundles due to bundle compaction, fiber-fiber interactions and fiber-matrix separation [9, 12, 21, 23, 24], as the mold gap becomes smaller and the response starts to deviate as the test progresses. Hence, the power law behavior via Scott's relation seems to be valid only for a certain regime beyond which meso-structural changes affect the rheology [26].

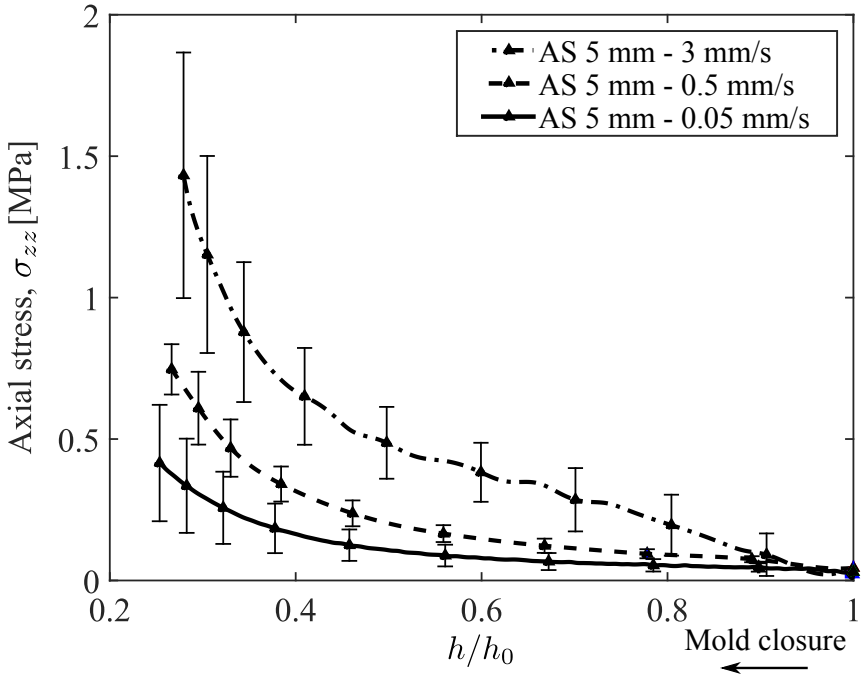


**Figure 2.7** *Experimentally observed axial stress vs. instantaneous mold gap for specimens with 5 mm flake size for different closing rates, under AS condition. Limited numbers of error bars are shown for clarity.*

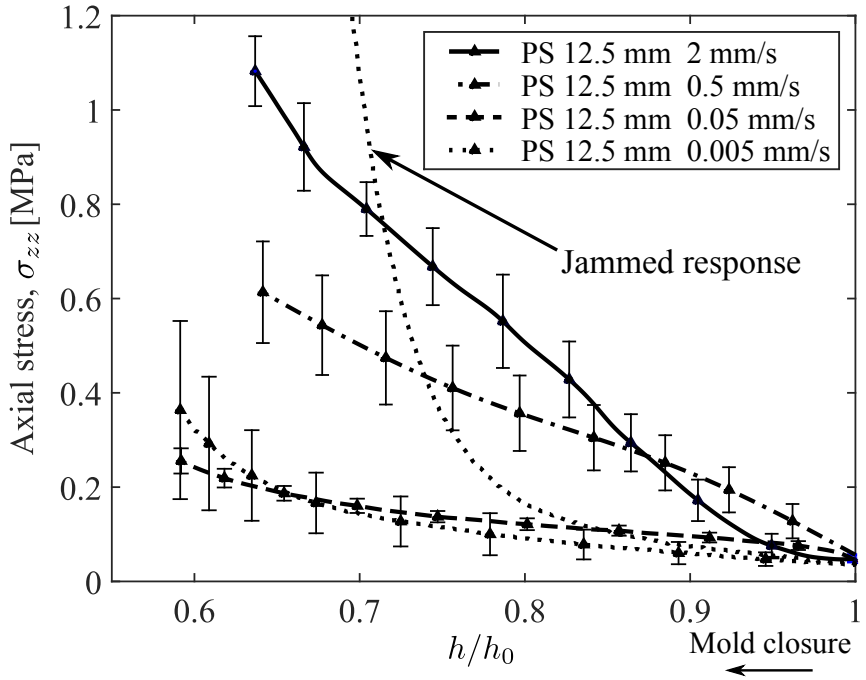


**Figure 2.8** *Experimentally observed axial stress vs. instantaneous mold gap for specimens with 12.5 mm flake size for different closing rates, under PS condition. Dotted line without error bar: The jammed response of a trial at 0.005 mm/s rate of closure. Limited numbers of error bars are shown for clarity.*

At lower closing rates, for instance the PS response corresponding to 12.5 mm flake size and 0.005 mm/s (jammed response in Figure 2.8), a rapid rise in stress is observed after a certain strain. This behavior is significantly different compared to the responses with higher closure rates and is due to the jamming of the material. At low rates of deformation, frictional contacts develop between the flakes resulting in agglomeration of flakes which form a network. They tend to carry most of the squeeze load and thus cause a dry fiber-bed-like region deprived of matrix polymer. A similar observation was made in dough molding compounds, GMT and SMC [12, 15, 19, 27]. The immobility of the reinforcements at lower closing rates and percolation of polymer matrix was considered as the major reason for the occurrence of jamming. In such a case, the jammed region hinders the macroscopic flow of the material and the flow front becomes non-uniform both in the case of PS and AS configuration. However, the observed severity in formation of dry and jammed regions was found to be higher in the case of PS specimens than in AS specimens. It can be attributed to the presence of a constrained flow direction ($y$-axis) in the PS flow, which might induce a size-effect with respect to the ratio of flake size to mold dimension. The occurrence, characterization and the adverse effects of jamming phenomenon are discussed elaborately in the next chapter (Chapter 3).

The relationship between the squeeze stress and global shear rate can be better

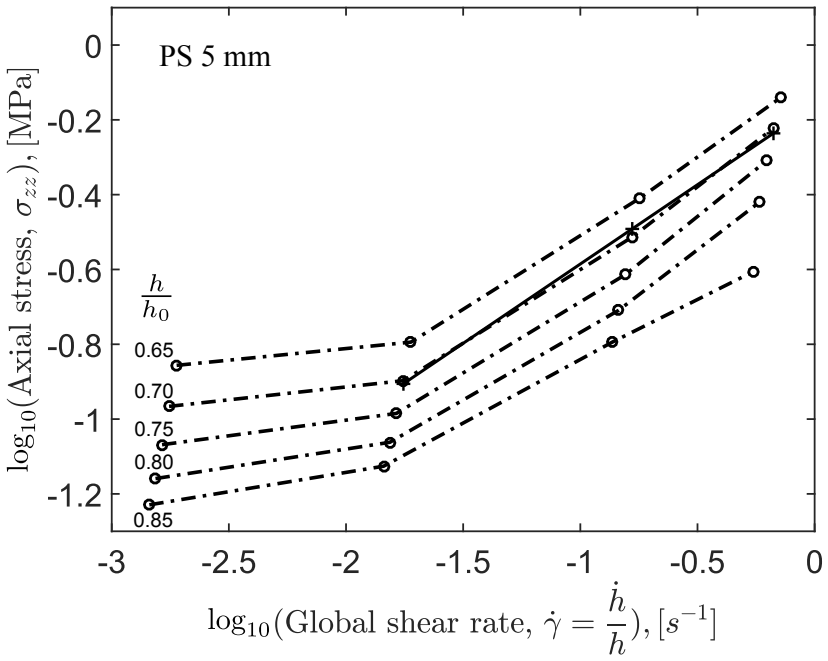


**Figure 2.9** *Synthesis of shear power law parameters for 5 mm flake PS experimental data. A double logarithmic plot shows axial stress vs. global shear rate at a constant instantaneous mold gap $h/h_0$. Dash-dotted lines depict the trend. Solid line: One example of a linear fit at $h/h_0 = 0.70$. The fitting omits the lowest shear rate value due to a jamming induced nonlinear response.*

observed on a double logarithmic plot as shown in Figure 2.9. The trend of the data points for each constant $h/h_0$ is shown in dashed lines. Based on the assumptions of the constitutive model, the slope of the lines should correspond to the power law index $n$ of the material and the intercepts are related to the consistency parameter $k_s$ of the material at that mold opening gap. The observed deviation, from the linear behavior in the log-log plot, at lower closing rates is due to the jamming phenomenon discussed above. Since the developed equation is not valid in those situations and the closing rate is far from actual processing rates, data points corresponding to the lowest closing rate of 0.005 mm/s are neglected for further analysis. A fitted line example considering the other data points for $h/h_0 = 0.7$ is shown as a solid black line.

Figures 2.10 and 2.11 show the variation of the power law indices and consistency parameters for different flake sizes in AS experimental conditions. The values of $n$ and $k_s$ are observed to vary with mold opening gap $h$. In a typical squeeze flow the shear rate is not constant, it varies with $h$ and also along the specimen length as a linear function of $r$ and as $z^{(1/n)}$ through the thickness. Therefore, interpretation of the obtained $n$ and $k_s$ is not straightforward but aids in interpreting the type of deformation observed in the compression molding of flakes. Nevertheless, by

assuming a constant average shear rate at every instant, $n$ and $k_s$ of the suspension can be considered as the bulk material parameters with a certain meso-structure.

**Suspension power law index, $n$**

Figure 2.10 shows the change in the apparent shear thinning behavior of the suspension as a whole at different specimen thickness. It shows a trend with increasing values in the beginning followed by a plateau and then decreases as the mold closes further. As the mold gap reduces, the flow becomes more non-affine causing the particles to lag behind the flow. Moreover, the large planar aspect ratio of the flake creates a large period for the flakes to remain overlapping with each other and therefore promotes development of lubricated contacts. Furthermore, the space between the reinforcements becomes smaller leading to higher local shear rates [17]. This effectively reduces the viscosity of the suspending polymer locally. Hence, the apparent behavior of the suspension becomes more shear thinning as $h/h_0$ reduces further. It can be observed that this trend is the same for all the flake sizes investigated.

Owing to the randomness of the material, agglomerated blocks of flakes can be present in the specimen. These agglomerates initially might cause increased viscous behavior in the process of getting oriented to the flow, but get broken during the flow [27]. The initial rise in the $n$ and the plateau formation can be attributed to this

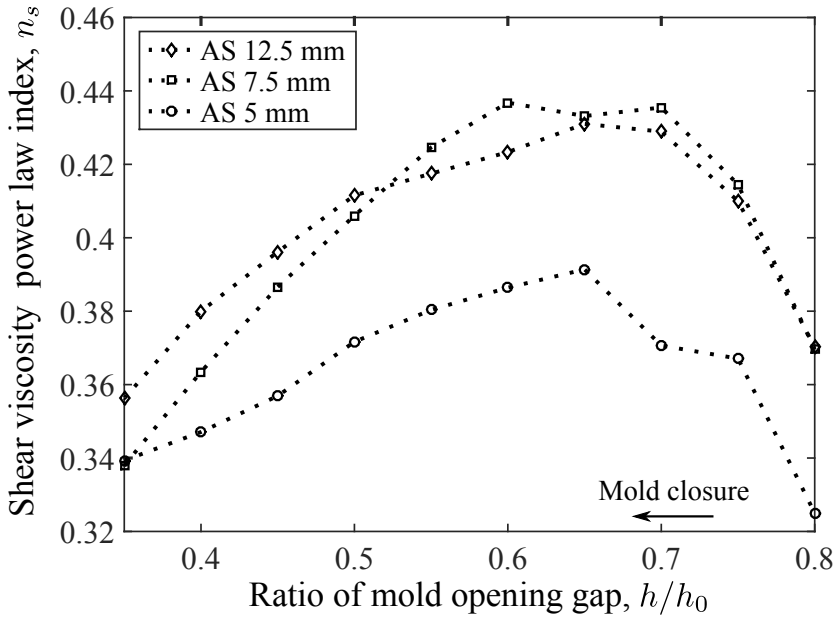


**Figure 2.10** *Variation of power law index (for shear viscosity under AS load case) with instantaneous mold gap for different flake sizes. The dotted lines depict the trend.*

effect. Once the flakes are aligned in-plane, temporary reduction of contact points occur leading to a reduced resistance to flow.

In the case of 5 mm flakes, the values are observed to be lower, but follow the same trend as the other two. This can be explained by the disentangling of the fiber bundles from the woven structure. Since the unit cell size of a 5 harness satin weave is around 7.5 mm, the 5 mm flakes have a greater chance of becoming disentangled. Thereby, the effective aspect ratio of the suspended reinforcements increases while the reinforcement fraction is constant. This effect of filamentization also increases the density of fiber-fiber interaction and thereby reduces the apparent $n$ of the suspension, analogous to the observation in [19].

### Suspension power law consistency, $k_s$

Figure 2.11 shows the change in the apparent consistency $k_s$ of the suspension as a whole at different thicknesses. Complementary to the arguments made above for the observed apparent $n$, the apparent $k_s$ has a decreasing trend with decreasing mold gap $h/h_0$. This effect is not observed in the case of GMT or SMC in the literature. One major difference between the flake reinforced polymer suspension used in this study and the GMT, SMC is the entangled mat-like structure found in the latter materials. The flakes, on the contrary, are uniformly thick and clear flake-flake interfaces exist locally, which can be assumed to be meso-level slipping planes. Hence, the effective

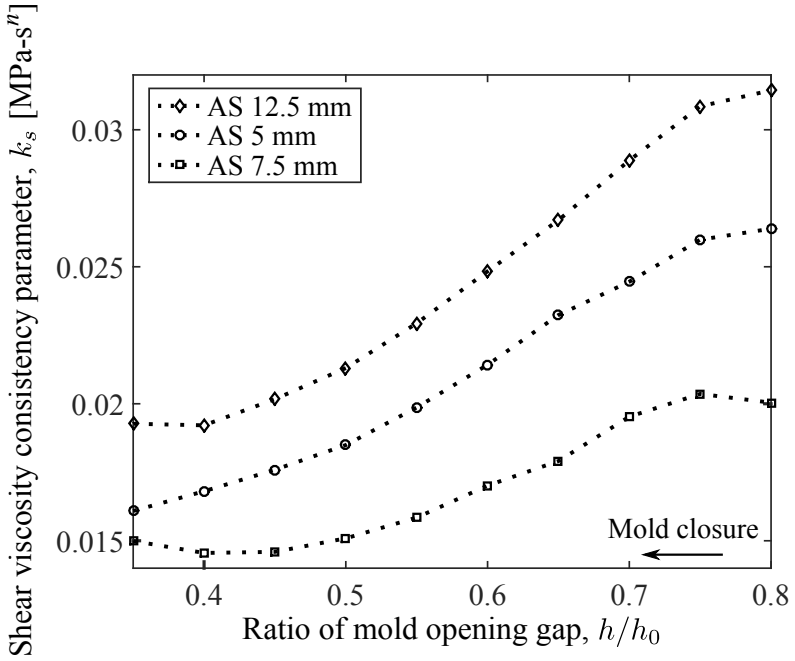


**Figure 2.11** *Variation of consistency parameter (for shear viscosity under AS load case) with instantaneous mold gap for different flake sizes. The dotted lines depict the trend.*

hydrodynamic volume is smaller than the mat structure and remains the same unless the bundles get disentangled from the weave. The hydrodynamic volume is proportional to the amount of reinforcement surface interacting with the fluid flow. Since the permeability of the bundles (micro-scale) is very small compared to the inter-flake permeability (meso-scale), fluid flow at meso-scale can be assumed to be easier than the micro-scale. Therefore, the fibers inside the bundles do not directly account for the hydrodynamic volume in the case of a flake.

The apparent consistency $k_s$ of the suspension with large flakes (12.5 mm) is found to be larger compared to smaller flakes. This can be attributed to a larger contact area and prolonged contact due to the larger aspect ratio. The prolonged contact increases the density of fiber-fiber interactions and frictional behavior [29] leading to an increased apparent $k_s$ of the suspension. The duration of contact based on the aspect ratio is also the basis for the jamming phenomenon at lower rates.

The 5 mm flakes have a larger apparent consistency compared to 7.5 mm flakes due to disentangling and filamentization effects discussed in Section 2.5.2. The loose fibers create a larger effective hydrodynamic volume occupied by the reinforcements [19]. Hence, it results in a larger viscous drag and in the shift of the apparent $k_s$ value to the higher side, compared to the case of 7.5 mm flakes.

### 2.5.3 Estimation of closing force

The constitutive parameters of the suspension $n_{s,AS}$, $k_{s,AS}$ obtained from the AS experiments are utilized to estimate the closing force given the flake size, mold closing rate and final thickness ratio $h/h_0$ for a plane strain flow. The estimated values are compared with the PS experimental data to validate the parameters across different flow boundary conditions. The squeeze force relation derived for PS conditions shown in Eq. (2.2) was used to estimate the squeeze force.

Figure 2.12 shows the estimated squeeze stress and the experimental values for the PS experimental condition for specimens consisting of 7.5 mm flakes at mold gaps ($h/h_0$) of 0.7 and 0.8. An average value of $n_{s,AS}$, $k_{s,AS}$ obtained from Figure 2.10 and Figure 2.11 corresponding to the AS experiments was used for this estimate. The range of $h/h_0$ between 0.6 and 0.7, where a consistent plateau exists in $n_{s,AS}$, was chosen to calculate the average. In this range of mold opening gap, the obtained constitutive parameters for the AS load case are assumed to be primarily influenced by hydrodynamic interactions rather than flake-flake interactions and are free from the effects of fiber-matrix separation. The respective average values are $n_{s,AS} = 0.435$, $k_{s,AS} = 0.018$ MPa $\cdot$ s$^n$. It can be observed that the estimated force values for the PS load case are in close agreement with the corresponding experimental values at larger rates of closure (see Figure 2.12). However, at slower rates of closure the estimated values underestimate the behavior due to the fiber-matrix separation and jamming effects observed in the PS experiments. As discussed before, at these rates the single

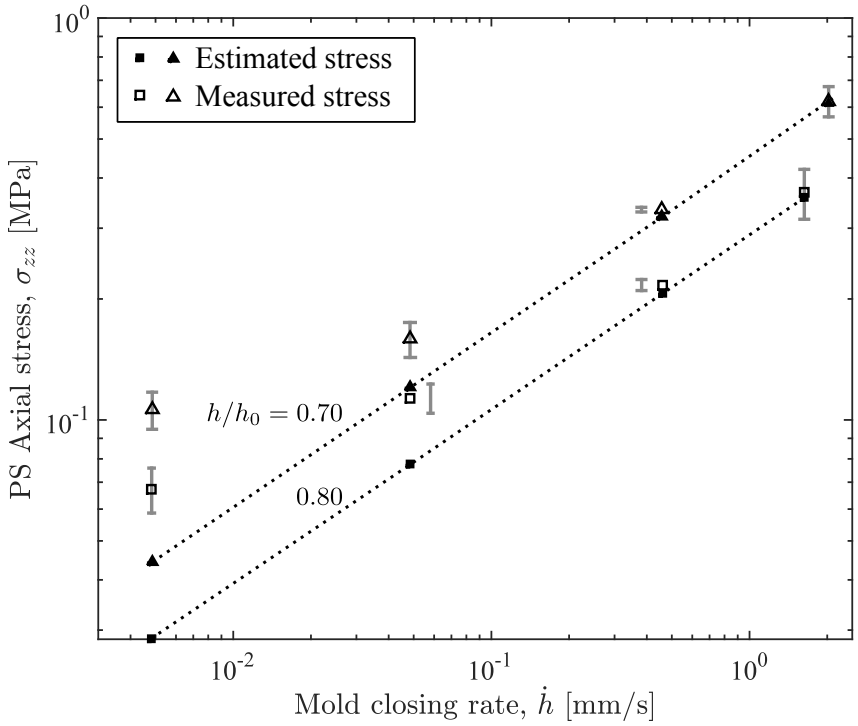


**Figure 2.12** *Estimated axial stress for the PS load case (with material constitutive parameters synthesized from AS experimental data) for different closing rates at a fixed mold gap $h/h_0$. Open symbols show the experimentally observed axial stress for PS load case, with error bars. Dotted lines depict the trend in the estimated stress. Error bars show one standard deviation from mean and in some cases are shown offset for clarity.*

phase behavior is no longer valid and the developed relations start to break down leading to a larger deviation. A critical mold closing rate of approximately 0.05 mm/s can be defined, for this case, beyond which the deviations vanish.

### 2.5.4 Practical applicability of the observations

The observations and the analyzed results from this study can be used as a pointer to construct a process window for the materials investigated and for the selection of a basic flake size based on the design of the part. The findings are,

(a) In general, the consistency of the material increases as the flake size increases. However, just below a critical flake size (a size less than the unit cell size of the weave) the material disentangles and becomes more shear thinning despite consistency being relatively larger. Such behavior can be utilized for filling intricate features in cases where filling with large flakes would be difficult. The proposed idea is that the mold is filled initially with small flakes with a filling pattern such that a flow is induced near the intricate features. The regions with less flow may remain as flakes, whereas the smaller features can be filled with

the induced flow. However, a trade-off should be sought, between the filling ability and the attainable mechanical properties, which is beyond the scope of this article.

(b) A first level approximation of the closing stress required to spread the material in the mold can be estimated from the constitutive parameters characterized from the tests. The estimation can be improved by eliminating the size effects in the experiments, if any, by experimenting with different ratios of flake size to specimen size.

(c) The identification of the jamming phenomena which is crucial for defining the bounds of the process window in terms of rate of closure, size of the flakes and thickness of the part. Following this study, the obtained bulk rheological data can be used to further characterize the jamming behavior of the flakes.

## 2.6 Conclusions

An experimental investigation of the squeeze flow behavior of woven flake reinforced polymer melt has been presented. Two different loading conditions, namely axisymmetric (AS) bi-axial shear flow and plane strain (PS) flow conditions, were investigated. The experimental observations show that the material behavior is in-plane isotropic and the force response has a strong dependency on the rate of closure of the mold and flake size. The plane strain squeeze flow was modeled as shear flow with no-slip boundaries at the mold wall. The estimated mold closing force required for a certain mold gap was calculated with the constitutive parameters synthesized from AS experiments. It shows good agreement with the experimental data from PS experiments at larger closing rates. The discrepancy between measured and estimated forces at smaller closing rates was attributed to the jamming of the flakes, where the analytical solutions become invalid. Jamming of the material was found to be squeeze rate dependent and, combined with the flake size, causes fiber-matrix separation during the process, thereby limiting the process window. In the future, a process window developed with the help of the material and process parameters with appropriate go and no-go regions can help engineers to choose a suitable form of the chopped material for the part design. Further analysis is required to characterize the jamming behavior with respect to the material and process parameters which will be the subject of future study.

## References

[1] I. Taketa, T. Okabe, and A. Kitano. A new compression-molding approach using unidirectionally arrayed chopped strands. *Composites Part A: Applied Science and Manufacturing*, 39(12):1884–1890, December 2008.

[2] C. Stephen, Dustin L. Levin, Dequine, and John P. Crocco. Formability of thermoplastic stretch-broken carbon fiber vs. thermoplastic continuous carbon fiber. In *SAMPE Technical conference proceedings*, 2013.

[3] The Boeing Company. Compression Molding Method and Reinforced Thermoplastic Parts Molded Thereby, 2011, US20110111172 A1.

[4] G. E. Padawer and N. Beecher. On the strength and stiffness of planar reinforced plastic resins. *Polymer Engineering & Science*, 10(3):185–192, 1970.

[5] J. Rexer and E. Anderson. Composites with planar reinforcements (flakes, ribbons)-A review. *Polymer Engineering & Science*, 19(1):1–11, January 1979.

[6] A.I.A. Malkin, A.Y. Malkin, and A.I. Isayev. *Rheology: Concepts, Methods & Applications*. ChemTec Pub., 2006.

[7] Chao-Ming Lin, Cheng-I Weng, and Cheng-Ter Ho. Anisotropy in sheet molding compounds during compression molding. *Polymer Composites*, 18(5):613–622, 1997.

[8] S. G. Advani, T. S. Creasy, and S. F. Shuler. Rheology of long fiber-reinforced composites in sheetforming. In D. Bhattacharyya, editor, *Composite Materials Series*, volume 11 of *Composite Sheet Forming*, pages 323–369. Elsevier, 1997.

[9] Isayev. *Injection and Compression Molding Fundamentals*. CRC Press, June 1987.

[10] S.G. Advani and E.M. Sozer. *Process Modeling in Composites Manufacturing, Second Edition*. CRC Press, 2012.

[11] M. R. Barone and D. A. Caulk. A model for the flow of a chopped fiber reinforced polymer compound in compression molding. *Journal of Applied Mechanics*, 53(2):361–371, June 1986.

[12] G. Kotsikos, J. H. Bland, A. G. Gibson, and H. W. Chandler. Squeeze flow testing of glass mat thermoplastic material. *Composites Part A: Applied Science and Manufacturing*, 27(12):1195–1200, 1996.

[13] A. G. Gibson and S. Toll. Mechanics of the squeeze flow of planar fibre suspensions. *Journal of Non-Newtonian Fluid Mechanics*, 82(1):1–24, April 1999.

[14] M. A. Dweib and C. M. ÓBrádaigh. Extensional and shearing flow of a glass-mat-reinforced thermoplastics (GMT) material as a non-Newtonian viscous fluid. *Composites Science and Technology*, 59(9):1399–1410, July 1999.

[15] M. A. Dweib and C. M. ÓBrádaigh. Anisotropic modeling of isothermal squeezing flow of glassmat reinforced thermoplastics (GMT). *Polymer Composites*, 19(5):588–599, October 1998.

[16] G. Kotsikos, J. H. Bland, and A. G. Gibson. Rheological characterization of commercial glass-mat thermoplastics (GMTs) by squeeze flow testing. *Polymer Composites*, 20(1):114–123, February 1999.

[17] Ronnie Törnqvist, Paul Sunderland, and Jan-Anders E. Månson. Determination of the rheological properties of thermoplastic composites for compression flow molding. *Polymer Composites*, 21(5):779–788, October 2000.

[18] M. A. Dweib and C. M. ÓBrádaigh. Compression molding of glass reinforced thermoplastics: Modeling and experiments. *Polymer Composites*, 21(5):832–845, October 2000.

[19] K. S. Gandhi and R. Burns. Rheological properties of glass fiber reinforced dough molding compounds. *Transactions of The Society of Rheology (1957-1977)*, 20(4):489–502, December 1976.

[20] Roberto J. Silva-Nieto. *Prediction and characterization of compression mould flow for unsaturated polyester resin sheet moulding compound*. PhD thesis, Loughborough University, 1980.

[21] G. Kotsikos and A. G. Gibson. Investigation of the squeeze flow behaviour of Sheet Moulding Compounds (SMC). *Composites Part A: Applied Science and Manufacturing*, 29(12):1569–1577, December 1998.

[22] P. Dumont, L. Orgéas, S. Le Corre, and D. Favier. Anisotropic viscous behavior of sheet molding compounds (SMC) during compression molding. *International Journal of Plasticity*, 19(5):625–646, May 2003.

[23] S. M. Davis and K. P. McAlea. Stamping rheology of glass mat reinforced thermoplastic composites. *Polymer Composites*, 11(6):368–378, December 1990.

[24] Colin Servais, Andre Luciani, and Jan-Anders E. Månson. Squeeze flow of concentrated long fibre suspensions: experiments and model. *Journal of Non-Newtonian Fluid Mechanics*, 104(23):165–184, June 2002.

[25] Pierre Dumont, Jean-Pierre Vassal, Laurent Orgéas, Veronique Michaud, Denis Favier, and Jan-Anders E. Månson. Processing, characterisation and rheology of transparent concentrated fibre-bundle suspensions. *Rheologica Acta*, 46(5):639–651, February 2007.

[26] Steven Le Corre, Pierre Dumont, Laurent Orgéas, and Denis Favier. Rheology of highly concentrated planar fiber suspensions. *Journal of Rheology*, 49(5):1029–1058, September 2005.

[27] Staffan Toll and Jan-Anders E. Månson. Dynamics of a planar concentrated fiber suspension with non-hydrodynamic interaction. *Journal of Rheology*, 38(4):985–997, July 1994.

[28] R. B. Bird, R. C. Armstrong, and O. Hassager. *Dynamics of polymeric liquids. Vol. 1: Fluid mechanics*. NewYork: Wiley., 1987.

[29] Philippe Coussot. *Rheometry of Pastes, Suspensions, and Granular Materials: Applications in Industry and Environment*. John Wiley & Sons, June 2005.

[30] K. Balaji Thattaiparthasarthy, Selvum Pillay, and Uday K. Vaidya. Rheological characterization of long fiber thermoplastics - Effect of temperature, fiber length and weight fraction. *Composites Part A: Applied Science and Manufacturing*, 40(10):1515–1523, October 2009.

# 2.A Appendix: Derivation of force response for PS squeeze flow

For the plane strain squeeze flow configuration shown in Figure 2.4, the approximated force experienced by the top moving platen is calculated in this appendix. The flow is assumed to be dominated by shear caused by the no-slip boundary condition.

The basic assumptions stated in the main text are summarized below with additional assumptions to solve the problem:

(a) The investigated material is above the melting point of the polymer at a constant temperature, hence the problem can be considered as being isothermal.

(b) The flakes behave as suspended particles in the melt, forming a single phase material.

(c) The reinforced melt is considered to be incompressible.

(d) The flow is constrained in the $y$ direction creating a plane strain loading condition in the $x$-$z$ plane.

(e) The flow of concentrated suspensions can be considered to have a very low Reynolds number [26] and since the specimen mass is relatively small, the inertia terms can be neglected and assume quasi-steady state at every instant [28].

(f) There is no slip at the melt-platen interface (conforming to the experimental observation).

(g) The thickness to width ratio ($h/w$) is smaller than 1 and in combination with the previous assumptions the hydrodynamic lubrication theory can be assumed to be valid.

It is worth noting that the assumptions (e)-(g) lead to a Hele-Shaw type of flow widely used for the analysis of compression molding [9, 10].

## *Equations of motion*

The governing equations of motion neglecting inertia and other body forces in a compact form can be written as,

$$0 = -\nabla p + \nabla \cdot \tau_{ij}, \tag{2.3}$$

where $p$ is the hydrostatic pressure and $\tau_{ij}$ is the extra stress tensor.

Considering a shear flow in Cartesian co-ordinates, the equations of motion reduce to [28],

$$\frac{\partial p}{\partial x} = \frac{\partial \tau_{xx}}{\partial x} + \frac{\partial \tau_{zx}}{\partial z} \tag{2.4a}$$

$$\frac{\partial p}{\partial y} = \frac{\partial \tau_{yy}}{\partial y} + \frac{\partial \tau_{zy}}{\partial z} \tag{2.4b}$$

$$\frac{\partial p}{\partial z} = \frac{\partial \tau_{zz}}{\partial z}. \tag{2.4c}$$

## Conservation of mass

The conservation of mass in the system is given by,

$$\nabla \cdot u = 0, \tag{2.5}$$

where $u$ is the velocity vector the fluid element is subjected to during the flow.

## Constitutive model for the reinforced fluid

The AS specimens have shown that the circular specimens remain circular during the bi-axial squeezing experiment. Thus an in-plane isotropic behavior of the material can be assumed. Experiments with similar discontinuous materials such as GMT, LFT in the literature have shown nonlinear behavior with respect to the strain rate [14, 30]. In this study, in addition to the assumption of the material being one-phase, the response is assumed to be non-Newtonian with a power law dependency.

$$\tau = k(\dot{\gamma})^n, \tag{2.6}$$

where $k$ is the power law consistency index with units $\mathrm{Pa} \cdot \mathrm{s}^n$ and $n$ is the non-dimensional power law index.

## Boundary conditions

From Figure 2.4 the boundary conditions for the flow can be derived as given below:

No-slip at melt-platen interface states:

$$v_x = 0 \quad \text{at} \quad z = \pm(h/2). \tag{2.7a}$$

Symmetry of gap velocity profile states:

$$\frac{\partial v_x}{\partial z} = 0 \quad \text{at} \quad z = 0 \tag{2.7b}$$

$$v_z = \begin{cases} 0 & \text{at} \quad z = 0 \\ -\dot{h}/2 & \text{at} \quad z = h/2. \end{cases} \tag{2.7c}$$

Pressure boundary conditions:

$$p = \begin{cases} P & \text{at} \quad x = 0 \\ P_a & \text{at} \quad x = \pm(w/2). \end{cases} \tag{2.7d}$$

## *Expression for gap velocity profile and pressure profile*

While considering the assumptions stated above, an order of magnitude analysis shows [9] that the velocity gradients in the $x, y$ directions are smaller than the $z$ direction.

$$\left\{ \frac{\partial v_x}{\partial x} = \mathcal{O}(1/l^2) \right\} << \left\{ \frac{\partial v_x}{\partial z} = \mathcal{O}(1/h^2) \right\}. \tag{2.8}$$

Hence, the stresses $\tau_{xx}$ and $\tau_{yy}$ associated with an $\mathcal{O}(1/l^2)$ can be considered negligible compared to the shear stress in the $x$-$z$ plane. Moreover, the thickness of the specimen is much smaller than the in-plane dimensions hence the pressure in the $z$ direction can be considered to be uniform. Consequently, the equations of motion Eq. (2.4) reduce to:

$$\frac{\partial p}{\partial x} = \frac{\partial \tau_{zx}}{\partial z} \tag{2.9a}$$

$$0 = \frac{\partial \tau_{zy}}{\partial z} \tag{2.9b}$$

$$0 = \frac{\partial \tau_{zz}}{\partial z}. \tag{2.9c}$$

Using the constitutive model of the material defined in Eq. (2.6),

$$\frac{\partial p}{\partial x} = k \frac{\partial}{\partial z} \left( \frac{\partial v_x}{\partial z} \right)^n \tag{2.10}$$

and integrating twice with respect to $z$ and substituting the boundary conditions Eqs. (2.7a-2.7b), the gap velocity profile is obtained as below:

$$v_x(z) = \frac{1}{\left(\frac{1}{n}+1\right)} \left(\frac{1}{k}\frac{\partial p}{\partial x}\right)^{\frac{1}{n}} \left[z^{\frac{1}{n}+1} - \left(\frac{h}{2}\right)^{\frac{1}{n}+1}\right]. \tag{2.11}$$

The volume flow rate across a section at $x$ assuming incompressibility is given by,

$$Q = 2L\int_0^{\frac{h}{2}} v_x(z)dz = \frac{Lh^2}{2\left(\frac{1}{n}+2\right)} \left(\frac{h}{2k}\frac{\partial p}{\partial x}\right)^{\frac{1}{n}}. \tag{2.12}$$

It is worth noting that the volume flow rate obtained is similar to an axial flow in a rectangular slit shown by Bird et al. [28]. Since the top platen is moving with a constant closure rate of $(-\dot{h})$, the average rate of change of volume $Lx(-\dot{h})$ should be equal to $Q$ in Eq. (2.12), thus we obtain the relation for the presssure gradient as,

$$Lx(-\dot{h}) = \frac{Lh^2}{2\left(\frac{1}{n}+2\right)} \left(\frac{h}{2k}\frac{\partial p}{\partial x}\right)^{\frac{1}{n}} \tag{2.13}$$

$$\frac{\partial p}{\partial x} = \left(\frac{-\dot{h}}{h}\right)^n \left(\frac{1+2n}{n}\right)^n \left(\frac{2}{h}\right)^{n+1} kx^n. \tag{2.14}$$

Substituting the pressure gradient in Eq. (2.11), the velocity profile is given by,

$$v_x(x,z) = (-\dot{h}) \left(\frac{1+2n}{1+n}\right) \left(\frac{1}{h}\right)^{\frac{1+2n}{n}} (2)^{\frac{1}{n}+1} \cdot x \cdot \left[z^{\frac{1}{n}+1} - \left(\frac{h}{2}\right)^{\frac{1}{n}+1}\right]. \tag{2.15}$$

Integrating Eq. (2.14) with boundary condition in Eq. (2.7d) with respect to $x$ and assuming $P_a = 0$ to be a relative datum,

$$P(x) = \left(\frac{-\dot{h}}{h}\right)^n \left(\frac{1+2n}{n}\right)^n \left(\frac{1}{h}\right)^{n+1} \frac{2k}{n+1} \left[x^{n+1} - \left(\frac{w}{2}\right)^{n+1}\right]. \tag{2.16}$$

## Expression for the force response

The integral of the pressure distribution over the mold-melt interface area gives the force required to push the platens at the constant rate of $\dot{h}$. Assuming the material remains homogeneous, it follows:

$$F = 2L\int_0^{w/2} P(x)dx, \tag{2.17}$$

$$F = \frac{kL\dot{h}^n}{(n+2)} \left(\frac{1+2n}{n}\right)^n \left(\frac{1}{h}\right)^{2n+1} w^{n+2}. \tag{2.18}$$

## Expression for the strain rates

Following a similar analysis carried out for the AS flow in [18], the strain rates can be calculated for the PS case from the above relations. The longitudinal velocity $v_x$ of the fluid given by Eq. (2.15) is a function of both $x$ and $z$. Hence, there exists a non zero extensional strain rate $\dot{\epsilon}_{xx}$ with respect to each $z$ location and is given by,

$$\dot{\epsilon}_{xx} = \frac{\partial v_x}{\partial x} = (-\dot{h}) \left(\frac{1+2n}{1+n}\right) \left(\frac{1}{h}\right)^{\frac{1+2n}{n}} (2)^{\frac{1}{n}+1} \left[z^{\frac{1}{n}+1} - \left(\frac{h}{2}\right)^{\frac{1}{n}+1}\right]. \tag{2.19}$$

From the continuity equation one can obtain the axial strain rate $\dot{\epsilon}_{zz}$ since the constraint in the transverse flow forces $\dot{\epsilon}_{yy} = 0$;

$$\dot{\epsilon}_{xx} + \dot{\epsilon}_{yy} + \dot{\epsilon}_{zz} = 0 \tag{2.20}$$

$$\dot{\epsilon}_{zz} = -\dot{\epsilon}_{xx}. \tag{2.21}$$

The axial velocity $v_z$ is obtained upon substituting Eq. (2.19) and integrating with respect to $z$.

$$v_z = (-\dot{h}) \left(\frac{1+2n}{1+n}\right) \left(\frac{1}{h}\right)^{\frac{1+2n}{n}} (2)^{\frac{1}{n}+1} \left[z\left(\frac{h}{2}\right)^{\frac{1}{n}+1} - \frac{z^{\frac{1}{n}+2}}{\frac{1}{n}+2}\right]. \tag{2.22}$$

Subsequently, the shear strain rate at every $x$ and $z$ location can be computed with,

$$\dot{\gamma}_{xz} = \left(\frac{\partial v_x}{\partial z} + \frac{\partial v_z}{\partial x}\right). \tag{2.23}$$

Since $v_z$ is a function of only $z$, $\dot{\gamma}_{xz}$ reduces to,

$$\dot{\gamma}_{xz} = (-\dot{h}) \left(\frac{1+2n}{n}\right) \left(\frac{1}{h}\right)^{\frac{1+2n}{n}} (2)^{\frac{1}{n}+1} \cdot x \cdot (z)^{\frac{1}{n}}. \tag{2.24}$$

For the axisymmetric case, a similar exercise as shown above can be done in a cylindrical coordinate system. It has been derived in existing literature [28] and is not repeated here.

# Chapter 3

# Experimental investigation of flow phenomena in processing woven composite flakes: Jamming*


### *Abstract*

Compression molding of discontinuous thermoplastic composite materials provides a higher degree of freedom for designing complex shapes with integrated functional features compared to continuously reinforced materials. Chopped planar reinforcements (flakes) with a large in-plane aspect ratio and a high fiber content can be used to attain improved in-plane isotropic mechanical properties compared to short fibers. However, processing limits can be observed with large flakes at lower compressive strain rates and at longer consolidation dwell times due to mechanical jamming. In this study, the jamming phenomenon, observed under squeeze flow conditions, is characterized with scaling arguments based on the Péclet number. A semi-quantitative jamming transition diagram was constructed. The effect of consolidation dwell time on the intensification of jamming was analyzed with scaled model experiments. An increase in dwell time increases the severity of jamming and induces more voids due to uneven pressure distribution and the presence of material flash.


*Reproduced from: M.I. Abdul Rasheed, W.J.B. Grouve, S. Wijskamp, H.A. Visser, R. Akkerman. Experimental investigation of flow phenomena in processing woven composite flakes: Jamming. To be submitted to *Composites Part A: Applied Science and Manufacturing*, **2016**.

## 3.1 Introduction

Composites with continuous fiber reinforcements and a high performance thermoplastic polymer, thermoplastic composites (TPCs), have become an attractive choice of material in aerospace and automotive industries in recent years. The motivation is due to their superior mechanical performance, processability and recyclability compared to thermoset materials. However, the highly stiff fibers restrict the formability of the material into complex shapes and may lead to processing defects such as wrinkles in the part. The formability of TPCs can be improved by adding discontinuities in the fiber phase by slitting [1] or pre-stretching [2] the conventional laminae. However, at present, parts with complex 3D geometries are manufactured as separate components with simple shapes which are subsequently assembled using various joining techniques.

Discontinuous molding compounds can be used to overcome the aforementioned limitations and enable manufacturing of complex 3D geometries with integrated functional features [3–5]. A class of discontinuous reinforcements, namely chopped woven prepregs (see Figure 3.1), was studied in Chapter 2 to assess the rheological behavior of the material to be used in a compression molding process. Investigation of such material is interesting since parts made from cutting wastes (production scrap) of woven prepregs can be put to use in semi-structural and less critical applications in aerospace and automotive industries.

Manufacturing parts with consistent quality requires knowledge of the material behavior during the manufacturing process. A typical compression molding process

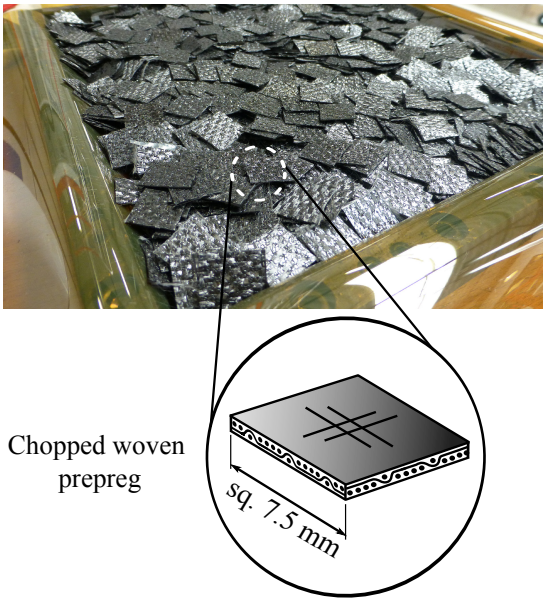


**Figure 3.1** *Chopped woven flakes in the shape of a square from 5 harness satin C/PPS semi-preg cutting waste.*

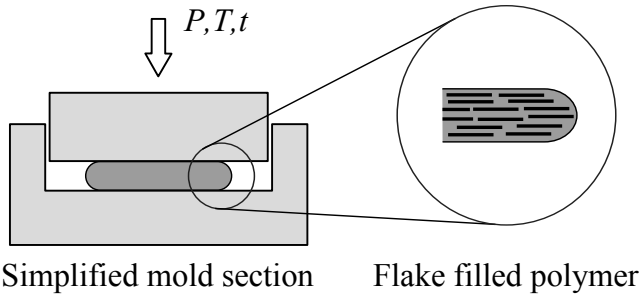


**Figure 3.2** *Schematic representation of a typical compression molding process. The flake reinforced polymer melt is shown to be compressed inside a mold cavity with an applied pressure (P), temperature (T), for a certain time (t).*

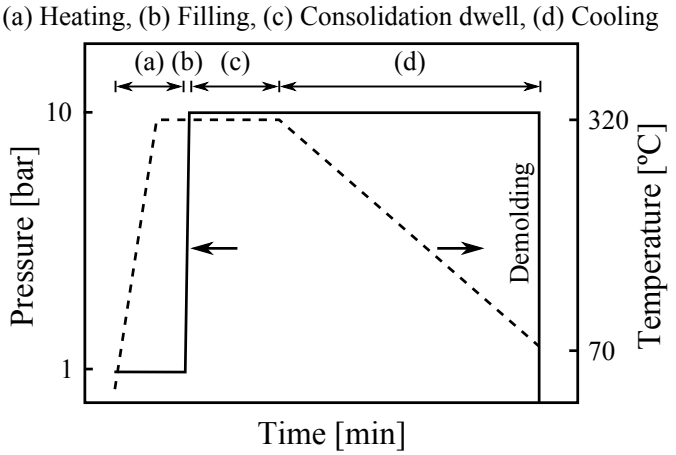


**Figure 3.3** *Schematic representation of the typical compression molding cycle for flake reinforced thermoplastic composites. Typical heating time is around 8 minutes and a cooling time of around 30 minutes in a 60 x 60 mm$^2$ mold.*

is illustrated in Figure 3.2 where the material in melt state is compressed to fill the mold. A representative process cycle is shown in Figure 3.3, which involves heating of the charge material inside the mold, filling the mold cavity under pressure by closing the mold and finally consolidating the composite material before cooling and demolding. In the filling phase the material flows due to the squeezing action of the mold halves closing at a constant displacement rate. In the previous study it was concluded that apart from the flow being a function of the flake size and mold closing speed, processing limits were observed which lead to jamming of material in the mold. This was attributed to the woven architecture of the reinforcements providing local integrity to the flakes, which leads to process induced fiber-matrix separation.

The phenomenon of jamming in this context is the aggregation of a stack of flakes analogous to an immobilized fiber mat in the case of glass mat thermoplastics (GMT) or epoxy based sheet molding compounds. The material flow behavior in such a

condition is overridden by the jammed stack potentially leading to incomplete mold filling. Further, the minimum thickness of compression molded parts is limited by this phenomenon.

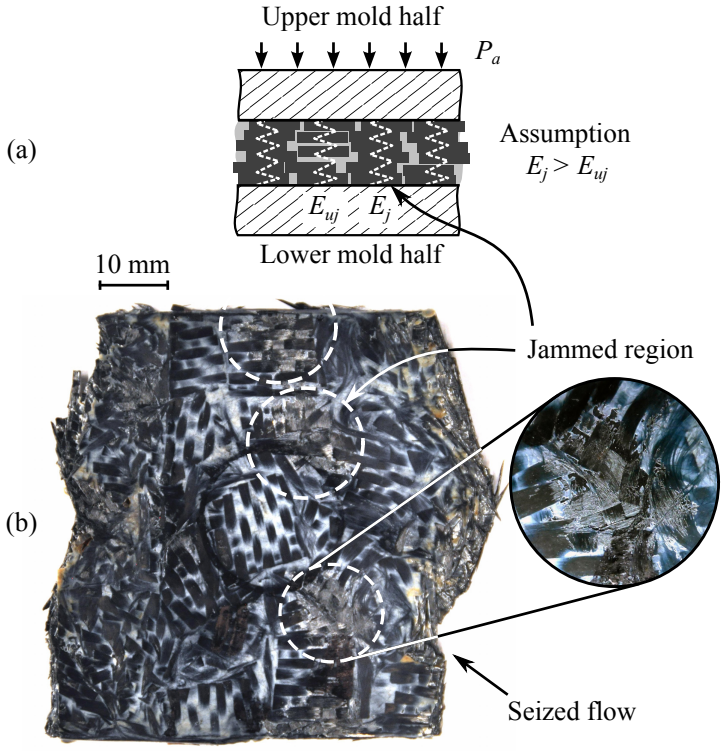


**Figure 3.4** *(a) Schematic of a small section of the mold filled with flakes. Stiffness of a potentially jammed region is illustrated as $E_j$ and for an unjammed region as $E_{uj}$. (b) Jamming observed in squeeze flow experiments. Due to jamming, the flow in the bottom right side has seized. (Inset) Dry fabric visible in the jammed spot.*

Figure 3.4 (a) shows a typical section of a filled mold in a compression molding scenario. The flakes are rendered as rectangles surrounded by polymer matrix. A probable case of a jammed stack of flakes is illustrated along with an analogy of parallel springs representing the jammed and unjammed regions. The compressive stiffness, $E_j$, of the jammed fabric is assumed to be much larger due to the dense packing of filaments compared to the adjacent unjammed region. The formation of such jammed regions, on the one hand, seizes the consolidation process globally by forming alternate load bearing paths giving rise to a poorly filled and a poorly consolidated part with resin rich regions (see Figure 3.4 (b)). On the other hand, the locally jammed region undergoes further consolidation during the consolidation phase and forms a dense stack of incompressible reinforcements (see Figure 3.3 (b:Inset) giving rise to large local stress in the mold. In extreme cases these stress peaks cause local deformations in the mold. Therefore, jamming of material is detrimental to both the mold life and the mechanical performance of the molded part.

Literature on the jamming behavior of flake reinforced composites is scarce. However, experiments on similar discontinuous materials such as glass fiber reinforced dough molding compounds and GMT show deviations from the nominal stress-strain behavior at lower strain rates [6–10]. This is attributed to the separated flow of matrix and the compaction of an entangled network of fibers at low strain rates. However, no attempt was made to characterize this effect, since most of the material investigated had a relatively low fiber volume content of around 20 %. In [9] a two-phase model was solved with a finite element approach to qualitatively capture the trend of the fiber volume fraction along the squeezed specimen. Nevertheless, the influence of squeezing velocity on the point at which the magnitude of a separated flow affects the flow behavior was not studied.

Fluids loaded with a high volume fraction of solid particles are often referred to as concentrated suspensions. In this case the particles are chopped prepregs in the form of platelets and the suspending fluid phase is the polymer matrix. The concept of phase separation in concentrated suspensions and granular pastes is well studied including the effects of particle interactions, lubrication effects and fluid-solid coupling using non-dimensional parameters to find their relative importance [11–13]. The effect of flow induced heterogeneity in the case of particle reinforced slurries under squeeze flow configurations was studied on concentrated suspensions of spheres [14], pastes [15, 16], on soft solids [17] and on sewage sludge [18]. In this case, the scenario of compression molding of flake laden polymer melt can be assumed to be analogous to a squeeze flow condition. Therefore, the aforementioned theories can be applied to characterize the flow induced heterogeneity in the system under study.

In [14], Delhaye et al. reported that at high closing rates the behavior of the concentrated suspension of spheres was observed to be non-Newtonian, with particles moving with the flow. Whereas, at lower rates it almost behaved like a sponge-foam under compression, where the fluid percolates or gets filtered through the bed of particles. They proposed a critical velocity at which the mechanism of filtration competes with the global flow of the suspension. It was also noted that the separation of the phases is dependent on the size of the reinforcing particles, particle volume fraction and the viscosity of the suspending fluid. In [17], it was shown that for the case of perfect slipping mold-material interface (pure extensional flow), the filtration effect was not present due to the absence of a pressure gradient. In Chapter 2 it was shown that, for the case discussed in the present study, the mold-material interface is non-slipping, and hence the flow was assumed to be shear dominant. However, the squeeze flow of suspended polymers is a mix of both shear and extensional flow. Additionally, the stochastic nature of the flake reinforced material causes heterogeneities in the stress gradients due to sudden changes in the material form.

The first part of this study aims to investigate the flow regimes observed during

squeeze flow in Chapter 2 and to characterize the jamming phenomenon as a function of the squeeze velocity and flake size. The squeeze flow rheology data under axisymmetric (AS) and plane strain (PS) flow conditions is obtained from the previous study in Chapter 2. The second part investigates the effect of the consolidation dwell time on the formation of voids around the jammed region. It is a common practice to increase the dwell time to improve the consolidation quality by allowing more time for the polymer to impregnate the fiber bundles and also to suppress the voids. However, the molding compounds with chopped flakes were found to behave differently, which should be understood. Therefore, consolidation experiments with different dwell times are performed with a randomly filled mold and a model laminate with induced jamming. The void contents are compared to validate the hypothesis that, in small parts with flash, jammed regions induce fluctuations in the resin pressure during the consolidation phase, such that the suppression of voids near the jammed region is hindered.

## 3.2 Materials and experimental methods

This section describes the materials used, method of specimen preparation and the details of the consolidation experiments performed in this study. For completeness, an excerpt of the specimen preparation and experimental method followed for squeeze flow experiments in Chapter 2 is also provided in this section.

### 3.2.1 Materials

The experimental work was performed on cutting waste of CETEX® Carbon/poly-(phenylene sulphide) (C/PPS) semi-preg from TenCate Advanced Composites. The semi-preg consists of a 5 harness satin (5HS) fabric partially pre-impregnated with polymer spray. The thickness of the consolidated lamina is 0.31 mm and the fiber volume fraction $v_f$ of the material is 50 %. The polymer has a glass transition temperature ($T_g$) of 90 °C and the nominal processing temperature is 320 °C.

### 3.2.2 Specimen preparation

**Squeeze flow specimens**

Compression molded plates with chopped semi-pregs were used as preforms for the squeezing experiments. Square shaped flakes were chosen to maintain a constant fiber length. Flakes with lengths 5 mm, 7.5 mm, and 12.5 mm were investigated. Circular disc shaped specimens with a diameter of 25 mm, cut from the compression molded plates, were used for the AS experiments. PS experiments were performed on

rectangular specimens, cut from the compression molded plates, with the dimensions of 60 x 30 x 4 $mm^3$.

**Consolidation specimens**

Two types of specimens are prepared for consolidation experiments. Table 3.1 shows the specimen configurations for the consolidation experiments. For the case of randomly filled laminate (RFL), the mold cavity is filled with 16.5 g of flakes to mold plates of dimension 60 x 60 x 3 $mm^3$. For forcibly jammed laminates (FJL), a laminate with continuous plies of 10 layers is prepared with a cross-ply layup. Additional flakes were placed in between the layers, symmetrically about the mid plane, to enable jamming. Furthermore, a 10 layer continuously reinforced laminate (CRL) in cross-ply layup was prepared as a reference laminate.

### 3.2.3 Experimental setup and procedure

An instrumented mold setup, as shown in Figure 3.5, is used in this study to perform the consolidation experiments. The same setup was used to perform the squeeze

| Manufacturing phase† | (b) Filling (§ 3.3) | (c) Consolidation dwell (§ 3.4) | | |
|---|---|---|---|---|
| Experiment type | Squeeze flow* | Consolidation | | |
| Parameters | Values | | | |
| Name | SFE | RFL | FJL | CRL |
| Preform | Yes | No | No | No |
| Filling | Random | Random | Cross ply layup + flakes | Cross ply layup |
| Flake size [mm] | 7.5, 10, 12.5 | 7.5 | 12.5 | - |
| Specimen dimensions [mm] | $\phi$25x4 (AS), 60x30x4 (PS) | 60x60x3 | 60x60x3 | 60x60x3 |
| Closing rate [mm/s] | 0.005, 0.05, 0.5, 2, 3 | 0.5 | 0.5 | 0.5 |
| Consolidation pressure [bar] | - | 10 | 10 | 10 |
| Consolidation dwell time [min] | - | 5, 10, 20 | 5, 20 | 5, 20 |

†Refer to Figure 3.3, (§) refers to the respective results and discussion section.

*Experimental data obtained from Chapter 2.

SFE: Squeeze flow experiment, RFL: Randomly filled laminate, FJL: Forcibly jammed laminate,

CRL: Continuously reinforced laminate

**Table 3.1** *Summary of experimental settings.*

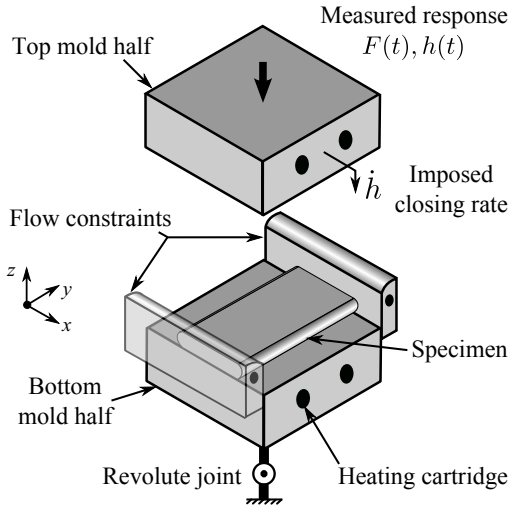


**Figure 3.5** *Illustration of the squeeze setup showing the top and bottom mold half, and side elements to constrain the flow in the case of plane strain flow. The other two sides are also closed to avoid heat loss in the gap, but is not shown in the figure for clarity.*

flow experiments in Chapter 2. The setup consists of a moving top half which is fixed to the cross head of a universal testing machine. The lower half of the mold is fixed to the stationary frame of the machine with a revolute joint to align the two mating surfaces so they are parallel and is locked in position. Removable side walls are attached to the lower half to form a picture frame mold. In the case of PS squeeze flow they constrain the flow in $y$-axis. Furthermore, the side walls compensate for the heat loss in the mold gap. Heating cartridges are used to heat the mold halves and side walls in conjunction with PID controllers and thermocouples in the mold halves and side walls. A laser speckle extensometer (LSE) is used to measure the instantaneous mold separation. The force exerted on the mold, displacement and temperature of the mold halves are recorded using a data acquisition system.

### Squeeze flow experiments

The squeeze flow specimens are heated to the processing temperature of 320 °C and the mold is closed at a specified velocity. This is similar to the transition from (a) to (b) illustrated in Figure 3.3. After reaching a final mold separation of 25 % and 60 % of the initial specimen thickness for AS and PS experimental conditions respectively, the specimen is taken out. The closing rates investigated for the AS experiments were 0.05, 0.5 and 3 mm/s and for the PS experiments were 0.005, 0.05, 0.5, 2 mm/s. For more detailed information on the squeeze flow experiments, readers are referred to Chapter 2.

**Consolidation experiments**

For the consolidation experiments performed in this study, the mold cavity is prepared as stated in Section 3.2.2. The laminates are consolidated with the process cycle illustrated in Figure 3.3 and with the respective process settings from Table 3.1.

## 3.3 Results and discussion: Jamming

The first part of the results and discussion provides the analysis of the flow regimes and jamming phenomenon. The next section discusses the results on the effect of consolidation dwell time on the resulting part quality in the presence of jammed regions.

### *3.3.1 Flow regimes and jamming phenomenon*

In the previous study (Chapter 2), the flake reinforced suspension was considered as a single phase material. The material response observed under the imposed experimental conditions indicates that the flow cannot be considered as a monophasic squeeze flow for the entire duration of the experiment. The assumptions of squeeze flow are only valid within a certain range of compressive strain beyond which the flow conditions are observed to be different due to the evolving meso-structure as well as the formation of mechanically jammed regions. In Chapter 2, the initial regime, the state of squeeze flow with no-slip boundary condition was analyzed and the material parameters were identified with an assumption of a power-law material behavior. The present study characterizes the jamming phenomenon at different closing rates with a phenomenological approach.

**Flow regimes**

A pattern in the flow curves can be observed upon carefully examining the stress responses leading to jamming. Figure 3.6 shows the different regimes for a typical jammed response as in SFE 2. Initially the flow starts in Regime 1 where a squeeze flow behavior is evident with a steady monotonic increase in stress. As the gap reduces further, the flakes come into closer contact with each other depending on the mobility of the flakes. A transition region can be observed where the stress response starts to deviate from Regime 1.

Finally, the material enters the third regime of flow when the mold opening gap is a few multiples of flake thickness, the flakes get jammed and the stress response rises rapidly with respect to the imposed strain. This effect can be correlated with the arguments in [19] that the power law behavior deviates considerably due to structural

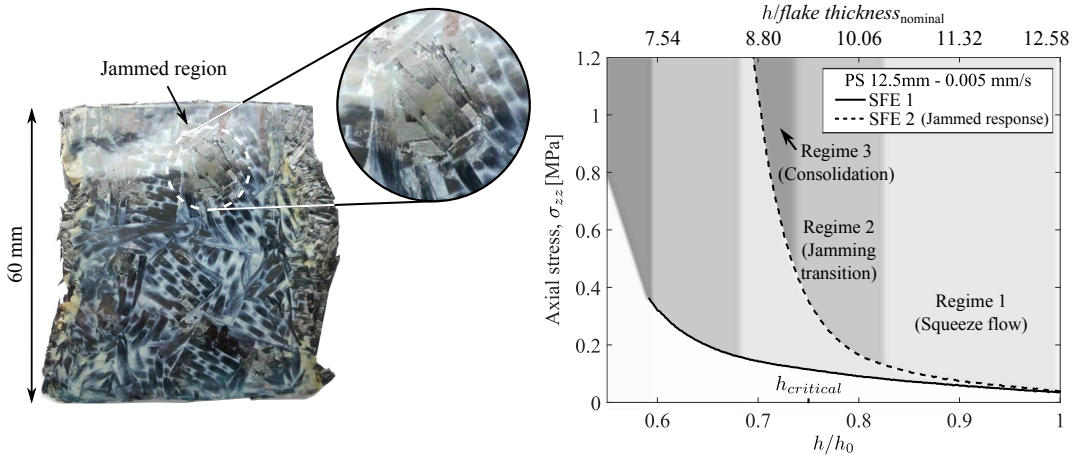


**Figure 3.6** *Right: The stress response showing the different flow regimes valid for the system under study with a nominal flake thickness of 0.31 mm. A hypothetical critical height, $h_{critical}$, is located at the intersection of the slopes of the two extreme regimes of SFE 2. Left: A photograph of a jammed region in the specimen devoid of polymer.*

changes and reinforcement interactions. However, the width of these regimes and their relative position is not well defined. SFE 1, which is of the same experimental configuration as SFE 2, shows that the Regime 1 extends further in this case and that the others are shifted and occur at lower instantaneous height $(h)$ of the specimen. This indicates that the occurrence of jamming and the gap at which it occurs has a stochastic nature.

### Jamming phenomenology

In the present study, the reinforced polymer melt is considered as a highly concentrated suspension made of incompressible constituent materials. Considering a two phase behavior, the external stress required to shear the material is a function of the stress in the interstitial fluid and the stress required for the deformation of the reinforcement network [12, 13]. However, the stress in the interstitial fluid varies with the deformation of the network. Moreover, the stiffness of the network can be highly nonlinear leading to a coupled problem. In general the process depends on the evolving structure of the flake bed and additional boundary conditions like seepage of fluid from the bed in between the mold parting surfaces [12].

In the case of flake reinforced suspensions, the network formed by the flakes can be considered as a deformable porous medium. On a mesoscopic scale, at the flake level, the flakes can have interactions which can be due to a direct contact or a lubricated contact in the presence of a polymer film at the interface. In the initial state a thin polymer film is assumed to be present between the flakes. The illustration in Figure 3.7 (a) shows a small representative part of a squeeze specimen (in the

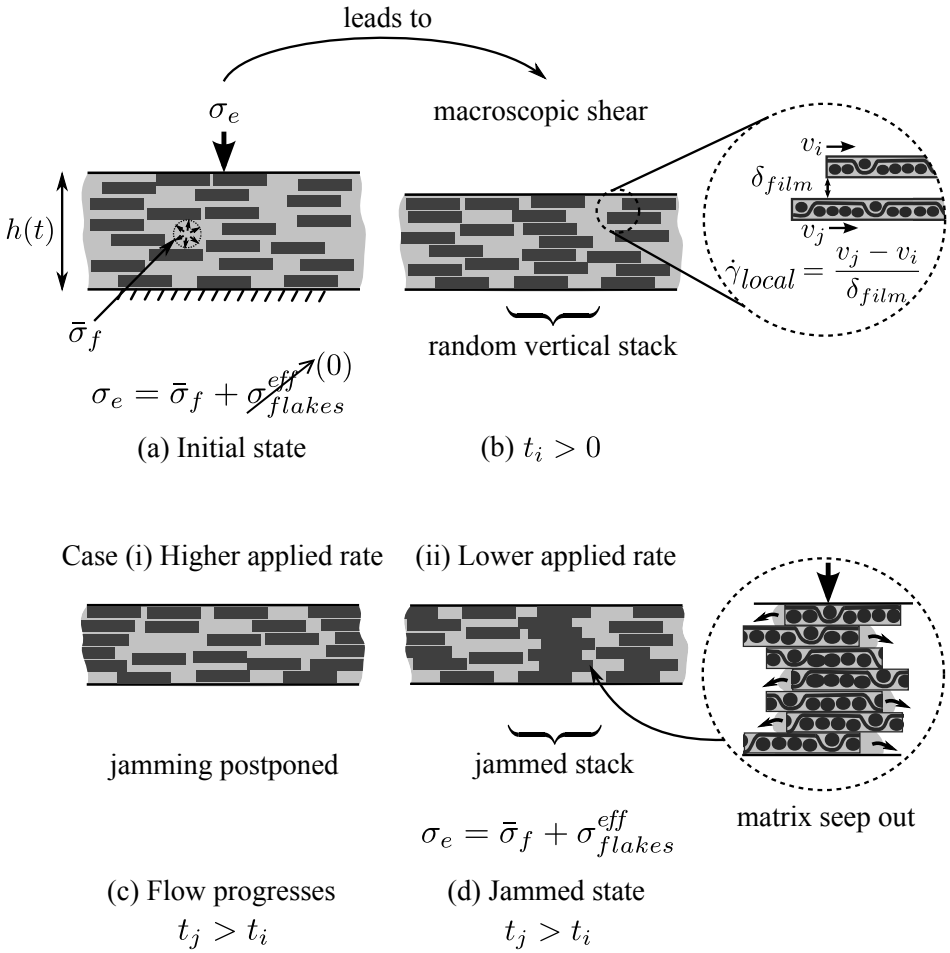


**Figure 3.7** *Illustration of the different states of the squeeze flow process leading to jamming or postponement of jamming depending on the applied closing rate. (a) Initial state. (b) A state after a certain amount of flow. (b:Inset): The local shear rate as a function of film thickness between the flakes. From the state shown in (b), the flow can proceed in any of the two ways depicted in (c) or (d) based on the applied closing rate. (d:Inset): effective stress in the locally jammed stack is large causing the matrix to diffuse out, creating a matrix rich region adjacent to the fiber rich jammed spot.*

$x$-$z$ plane of Figure 3.5) with flakes idealized as rectangular plates surrounded by the interstitial fluid. In the initial state the material is assumed to be statistically homogeneous, with flakes and fluid (resin) pockets spread out uniformly in a randomly packed bed of flakes. Hence, the fluid pressure is assumed to be close to the average fluid pressure $\bar{\sigma}_f$ in the specimen.

As the external stress is applied in the form of a compressive displacement, by the conservation of mass and momentum, and assuming a no-slip mold-material interface, a macroscopic shear flow sets in, as illustrated in (b) at a time $t_i > 0$. The portion of axial stress carried by the flakes, the effective stress $\sigma^{eff}_{flakes}$, is assumed to be very small during the initial states and the flakes are assumed to flow with the fluid.

As flow progresses, the effective stress borne by the reinforcement bed or flake stacks varies since it is related to the amount of contacts present in the mobile network [13] of flakes, as illustrated in Figure 3.7 (d).

The average distance between the flakes reduces as the concentration of the flakes increases. At high concentrations, such as the presently studied material, the inter-flake separation can be much smaller compared to the specimen thickness. Figure 3.7 (b:Inset) shows a typical local structure where two flakes are separated by a small gap. At higher closing velocities, the local shear rate $\dot{\gamma}_{local}$ in the thin fluid film, $\delta_{film}$, separating the flakes can become larger than the average imposed shear rate. Thereby, creating a situation for the contacts to remain hydrodynamically lubricated [13, 20].

During the initial period of imposing a large closing velocity, the pressure in the interstitial fluid rises rapidly considering a finite amount of permeability of the flake bed. The fluid pressure temporarily limits the effective stress carried by the flake bed network [21] and also causes a reduced shear resistance. Thereby, it aids the initiation of the hydrodynamic lubrication with reduced chance of forming dry contacts by breaking of the thin fluid film. As the compression proceeds further, the effective stress carried by the network starts to increase as the compaction of flake bed increases, leading to a relatively large total stress compared to an unjammed response at lower velocities.

At lower closing velocities, the relative motion of the reinforcements is small and therefore, frictional contact starts to develop between the flakes. The rise in the interstitial fluid pressure gets dissipated as the fluid percolates through the flake network. The reduced mobility of the flakes causes stacks of flakes to mechanically jam through the thickness, as illustrated in Figure 3.7 (d). Subsequently, the stress carried by the fiber bed or the jammed stack of flakes rapidly increases as the compression proceeds further.

### 3.3.2 Characterization of jamming transition (percolation transition)

The following assumptions are made based on the jamming phenomenology described in the previous section: (a) The fibers and the polymer matrix are incompressible. (b) The deformable porous bed of flakes is fully saturated with resin, since the preform used for squeeze flow is a consolidated laminate. (c) The flake bed and the associated meso-scale permeability of the bed is statistically homogeneous. (d) The meso-scale permeability is mainly due to the inter-bundle space. (e) The percolation of polymer through the porous bed is assumed to follow Darcy's law. (f) The percolating polymer is assumed to behave as a Newtonian fluid. (g) The global

shear flow of the suspension is assumed to be non-Newtonian, the parameters of which are obtained from previous study. (h) Inertial effects and gravity are neglected.

The flow mechanisms described earlier, namely shear flow and percolation flow, are assumed to compete with each other during the squeeze flow process. The characteristic time scales for these effects can be compared to give a macroscopic view of the coupling between the two phases [12]. The deformation of the suspension is mainly advective in the flow direction before jamming occurs. However, after jamming occurs the polymer flow can be considered to be dominated by percolation. Therefore, the following characteristic times can be defined, namely $\tau_s$ the time scale for the deformation of the whole suspension and $\tau_d$ the time scale for the diffusive behavior [12, 18].

The time scale $\tau_s$ is given by the global shear rate, $\dot{\gamma}_a = \frac{\dot{h}}{h}$ applied to the material causing the advection of the material and is given by,

$$\tau_s = 1/\dot{\gamma}_a. \tag{3.1}$$

The time scale $\tau_d$ is formally defined by a Darcy type of percolation flow through a porous bed of fibers and is given by,

$$\tau_d = h/U_{Darcy}, \tag{3.2}$$

where $U_{Darcy}$ is the average relative velocity of the suspending fluid with respect to the reinforcement phase and $h$ is the instantaneous height of the specimen. For a Newtonian fluid, the relative velocity is given as,

$$U_{Darcy} = (u_{fl} - u_f) = -\frac{K(v_f, l)}{\eta_{fl}} \nabla P_{fl}, \tag{3.3}$$

where $u_{fl}$ and $u_f$ are the velocities of fluid and the flake, respectively, $K$ is the permeability of the flake bed as a function of fiber volume fraction $v_f$ and flake size $l$, $\eta_{fl}$ is the fluid viscosity and $\nabla P_{fl}$ is the pressure gradient in the interstitial fluid in the direction of flow. The permeability of a randomly packed bed of particles varies with the size and aspect ratio of the particles owing to difference in the packing efficiency. Hence, $K$ is a function of both fiber volume fraction (microscopic scale) and flake length (mesoscopic scale).

The Péclet number is defined as the ratio of the two characteristic times $\tau_d$ and $\tau_s$ [12],

$$P_e = \frac{\tau_d}{\tau_s} = \frac{h\dot{\gamma}_a}{U_{Darcy}}. \tag{3.4}$$

It can be observed that the $P_e$ is a function of the gradient of the interstitial fluid pressure and permeability of the flake bed through the variable $U_{Darcy}$.

As mentioned earlier in Section 3.3.1, the interstitial fluid pressure is a variable coupling the deformation of the flake bed and the fluid percolation process. Therefore, the fluid pressure has to be obtained by simultaneously solving both the flake bed deformation and a Darcy type of percolation flow problem. For such a full solution, parameters related to compressibility of the random flake bed and the change in the permeability of the bed are required which are beyond the scope of the current study.

However, as a first approximation the pressure gradient in the interstitial fluid is assumed to be close to the pressure gradient in the suspension. Furthermore, considering an unjammed response of the material with hydrodynamic lubrication between the flakes, the particle interactions can be assumed to be less influential.

The pressure gradient along the flow, under squeeze flow condition, is created by the total deformation of the suspension. The momentum balance states that the divergence of the stress in the suspension is balanced by the pressure gradient in the direction of flow and is given by (Chapter 2),

$$\frac{\partial P}{\partial x} = k_s \frac{\partial}{\partial z} \left( \frac{\partial v_x}{\partial z} \right)^{n_s}, \tag{3.5}$$

where $P$ is the pressure in the suspension, $n_s$, $k_s(v_f, l)$ are the power-law material parameters of the suspension in shear flow conditions, $v_x$ is the velocity of the suspension in the direction of flow. Therefore, Eq. (3.5) can be approximated to:

$$\nabla P_{fl} = \frac{k_s(v_f, l) \cdot (\dot{\gamma})^{n_s}}{h}, \tag{3.6}$$

where $n_s$ and $k_s(v_f, l)$ are obtained from the experimental data of the AS load case (Chapter 2), in the region of $h/h_0$ of 0.8, free from the effect of jamming. Here, $h_0$ is the initial height of the specimen, which is equal to 4 mm.

Upon substituting Eq. (3.6) in Eq. (3.3) and subsequently in Eq. (3.4), the Péclet number is obtained for this specific case as,

$$P_e = \frac{h^2 \eta_{fl}}{K(v_f, l) \cdot k_s(v_f, l) \cdot \dot{\gamma}^{(n_s - 1)}}. \tag{3.7}$$

It is worth noting that the consistency $k_s$ of the suspension increases rapidly as jamming occurs due to the increased physical contacts between the flakes, analogous to the observations in [6]. Furthermore, the local fiber volume fraction also increases, which adds to the increase of the consistency of the suspension resulting in an increased effective stress carried by the jammed stack.

Similarly, the permeability $K$ of the fiber bed reduces as the jamming progresses and as the fiber bed gets further compacted. The most widely used empirical form

to relate the permeability and fiber volume fraction is the Kozeny-Carman equation assuming a flow through packed bed of spheres. In the case of a stack of flakes, it can be considered to be a small representative part of a stacked laminate configuration. Hence, a modified form of Kozeny-Carman [22] can be used to get a first estimate of the permeability. Nevertheless, obtaining an experimentally consistent value for the average permeability of a bed of randomly oriented flakes is non-trivial and the influence of the randomness of packing on the permeability is not taken into account here.

With the definition of Péclet number in Eq. (3.4), we can define three possible regimes [18].

1. Case: $P_e \gg 1$
   In the case of $P_e \gg 1$, the time scale of deformation of the suspension is much smaller than the time scale in which the fluid has to percolate through the interstitial pores. Hence, a macroscopic flow occurs, in which the fluid dominates the flow behavior of the material and the suspended flakes are bounded to the flow [12].

2. Case: $P_e \ll 1$
   In the case of $P_e \ll 1$, the global deformation is slow when compared to the time scale of percolation of the interstitial fluid. Hence, the physical contacts created upon compression of the material sustains themselves. Additionally, with the increasing planar aspect ratio of flakes, the contact duration becomes longer and thus inter-flake friction dominates the flow behavior [13]. This effect causes the material to jam and the force response increases rapidly. Furthermore, the increased pressure causes the interstitial fluid to percolate through the stack of jammed flakes as shown in Figure 3.7. This leads to a dry region at the spots of maximum compression and a resin rich region directly around it due to the seepage as shown in Figure 3.7 (d:Inset).

3. Case: $P_e \approx 1$
   The case in which $P_e \approx 1$ gives a transitional regime in which both diffusive and advective mechanisms mentioned above compete and proceeds further on either sides of the transition zone [11, 18]. At this critical point, a critical shear rate or a critical height exists at which jamming can occur. Hence, setting $P_e = 1$ in Eq. (3.7) gives a critical rate $\dot{h}_c$ for a certain height $h$ and corresponding material parameters of the suspension for the chosen flake size, volume fraction of fibers and interstitial fluid parameters.

### 3.3.3 Jamming transition diagram

From the manufacturing viewpoint, guidelines for a feasible processing window and part design for compression molding using these discontinuous compounds

are required for a consistent part quality. As discussed, the jamming phenomenon is detrimental to the mold as it locally carries most of the applied composite consolidation pressure thereby deforming the mold surface. Furthermore, the composite consolidation pressure is carried by the jammed regions, hence the quality of consolidation of the part is affected in the adjacent regions due to reduced consolidation pressure. Hence, a process map with practical variables identifying the jamming zones will be a valuable design tool.

Liu and Nagel in [23] proposed a conceptual jamming phase diagram which provides a universal framework to explain the jamming phenomenon in a suitable parameter space corresponding to different systems. The generic phase diagram was illustrated in density-temperature-stress space for systems such as glass forming supercooled liquids, suspended particle systems and several other systems which jam in a comparable way. Following their approach, a similar phase diagram adapted from [24] is conceptualized to delineate the boundaries of the jamming transition for the flake reinforced fluid system under study. The following parameters that are applicable for this problem are: flake size, squeeze rate and final achievable thickness.

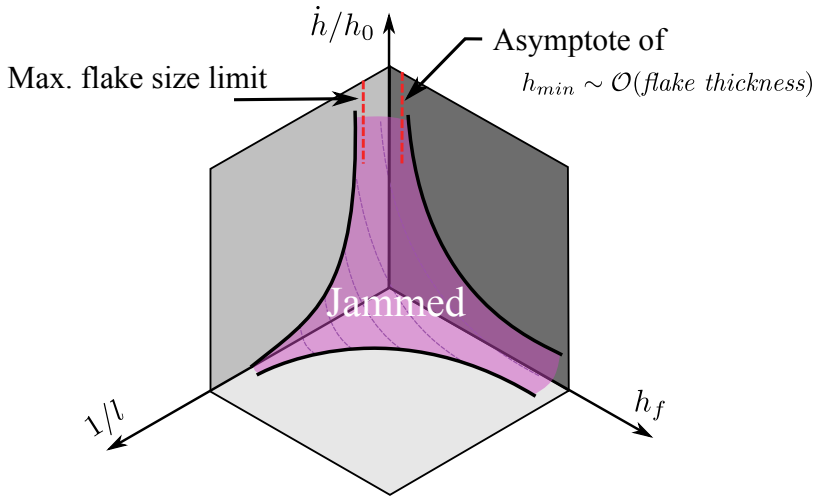


**Figure 3.8** *An adapted phase diagram from [23, 24] incorporating the conceptual transitions and asymptotes showing the limiting behavior of the material.*

Figure 3.8 shows the conceptual phase diagram proposed for the problem studied based on the generic theory [23, 24]. The phase space spans the variables namely, inverse flake size ($1/l$), minimum (final) achievable specimen thickness ($h_f$) and squeeze rate ($\dot{h}$) parametrized with the initial height of the specimen ($h_0$). The plane corresponding to $1/l - \dot{h}/h_0$ is characterized experimentally based on the Péclet number and is discussed below. The curves shown in the other two planes are tentative curves based on phenomenological reasoning. All the three curves form a surface as shown in the figure which characterizes the jamming surface. The points lying between the surface and the origin lead to a jammed state, whereas the points

away from the surface and origin are flowable regions. On these points the jamming is postponed and the process proceeds towards a minimum achievable thickness, which is of a few orders of the flake thickness.

### Phase plane: $\dot{h}/h_0$ vs. Inverse flake size

Figure 3.9 shows the squeeze rate $\dot{h}$ normalized with the initial thickness $h_0$ of the specimen in the ordinate versus inverse flake size. The grid of values plotted in the axes correspond to the PS experiments, in which jamming was primarily observed. The gray level of the points indicate a count of the number of mechanically jammed spots identified visually in the specimens, corresponding to the combination of $\dot{h}/h_0$ and flake size used in the experiment. The counts are normalized with respect to the maximum number spotted, which occurred with the combination of lowest rate and largest flake size (bottom left corner of the plot). Black color signifies the top one third (1-0.67) and gray corresponds to mid one-third (0.33-0.67) and the unfilled circles correspond to the least amount (0-0.33) of mechanically jammed regions identified. The contours labeled 0.05, 0.33 and 0.67 show the respective boundaries.

Figure 3.10 shows the same plot superimposed with a dashed line which qualitatively represents the transition between the practically feasible region (region of unfilled circles) and to-be-avoided jammed region (black circles). The end points of the

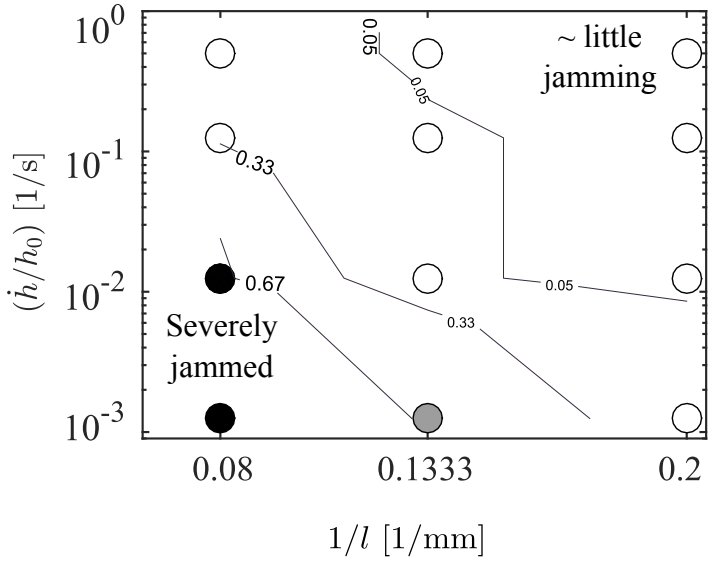


**Figure 3.9** *Jamming observed in the experimental space of shear rate vs. flake size. The solid lines (contour levels of 0.05, 0.33, 0.67) depict the normalized count of dry spots identified in the PS squeeze specimens. The experimental points are indicated with circles. The color indicates the severity of jamming observed in the respective data point. Unfilled circles indicate regions with relatively little jamming (go-region), gray circle indicates a transition region and black circles indicate no-go regions with severe jamming.*

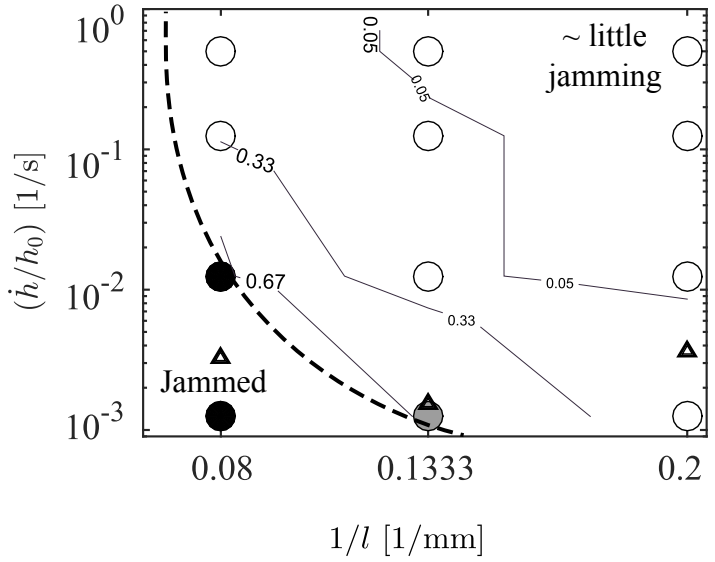


**Figure 3.10** *The jamming transition diagram in squeeze rate vs. inverse flake size space superimposed on the experimental data shown in Figure 3.9. (Dashed lines) tentative transition curve below which the material jams and above the curve the material still flows, (triangles) calculated critical closing rate $\dot{h}$ corresponding to $P_e = 1$ from Eq. (3.7).*

dashed curve (limiting behavior) are discussed here and the approximation of the curve is discussed in the next subsection. On the lower end of the dashed curve, the jamming transition occurs at a certain flake size range at which the jamming becomes important. In this case it occurs in the region near the gray circle corresponding to the 7.5 mm flakes and 0.005 mm/s squeeze rate. On the other end, after a certain limiting flake size the friction behavior will be dominant regardless of the application of a large mold closing rate. A trial experiment with large flakes of size 150 x 150 mm$^2$ placed in a mold of dimension 390 x 390 mm$^2$, showed no movement of flakes, as expected, due to the large area of contact with the adjacent flakes. The flake system jammed severely even though a relatively larger squeeze rate $\dot{h}$ of around 5 mm/s was used. Therefore, the other end of the jamming curve can be thought of as having asymptotic behavior with respect to the ordinate for a certain large flake size as illustrated by the red dashed line in Figure 3.8.

### Calculation of critical closing rates $\dot{h}_c$ for jamming

For the present study, critical mold closing rates $\dot{h}_{c,l}$ were calculated for the three different flake sizes from the equation Eq.(3.7) by setting $P_e = 1$. For a chosen $h/h_0$ of 0.8, values from the $n_{s,AS}$ vs. $(h/h_0)$ and $k_{s,AS}$ vs. $(h/h_0)$ data in Chapter 2 corresponding to different flake sizes were used. The values used are shown in Table 3.2. The constitutive parameters of the suspension from axisymmetric experiments are assumed to be the result of primarily hydrodynamic interactions

| Parameters | Flake size [mm] | | |
|---|---|---|---|
| | 5 | 7.5 | 12.5 |
| $n_{s,AS}$ [-] | 0.325 | 0.369 | 0.370 |
| $k_{s,AS}$ [MPa $\cdot$ s$^n$] | 0.026 | 0.018 | 0.0314 |
| $K(v_f(h/h_0))$ [mm$^2$] | $1.5 \times 10^{-3}$ | | |

**Table 3.2** *Parameters used for calculating the critical closing rate.*

at a large opening gap of $h/h_0 = 0.8$. They are also assumed to have reduced size effects concerning the ratio of flake size and mold dimensions when compared to the plane strain squeeze flow.

The permeability $K$ of the flake bed can be approximated upon considering a limiting case for the structure of a stack of flakes. Figure 3.7 (d:Inset) shows a stack of flakes being compressed. As the height of the stack reduces the matrix seeps out and the fiber volume fraction in the stack increases. The new fiber volume fraction can be approximated at time $t$ by $v_f(t) \sim v_f^{init}(h_0/h(t))$. This effect can be assumed to be a local behavior of the flake bed at lower closing rates due to the development of frictional contacts (as discussed for the case of $P_e \ll 1$) leading to the percolation of polymer matrix.

Grouve et al. in [25] performed a numerical study on a structured arrangement of square packed ellipses analogous to a compressed fabric structure. The transverse permeability of the model structure was characterized along the major and minor axis of the ellipses, taking into account the fiber volume fraction. The non-dimensional permeability in this study was obtained from [25] with the volume fraction of fibers for a certain mold closing gap. The $v_f(t)$ was calculated at $h(t)/h_0 = 0.80$ giving a value of 62.5 % and the corresponding non-dimensional permeability $K(v_f(h/h_0))$ was interpolated from the permeability data in [25] and was found to be in the range of $4 \times 10^{-3}$. Bundle dimensions were measured from cross-sectional micrographs and an equivalent radius was calculated from the measured major and minor axis based on the van West relation [22]. An approximate permeability of $1.5 \times 10^{-3}$ mm$^2$ for the meso-structure was obtained from the equivalent radius and the non-dimensional permeability.

In Figure 3.10 the data points with open triangles show the calculated critical closing rate for each flake size corresponding to $P_e = 1$. Despite all the assumptions and with experimental variability, the values are close to the observed jamming transition based on the number of jammed spots identified in the specimens (3 repetitions per process setting). Hence, the trend of the qualitative jamming transition shown in dashed line can be assumed to be valid within the assumptions made. In the case of 5 mm flakes the calculated critical squeeze rate is larger than the actual

observations. One of the reasons for the discrepancy is that the filamentization of the smaller flakes (since the unit cell size of 5HS weave is larger than 5 mm) causes an increase in the consistency parameter $k_s$ (Chapter 2). The critical squeeze rate as per Eq. (3.7) is directly proportional to the consistency parameter of the suspension raised to $1/(1-n_s)$. Hence, owing to a different type of material behavior, there is an apparent increase in the critical squeeze rate $\dot{h}_c$ for the case of flake sizes smaller than 5 mm. In the processing standpoint, for the flakes smaller than the unit cell size of the fabric architecture ($\sim$ 7.5 mm for 5HS weave), the integrity of the flake might reduce. However, the processability increases due to filamentization which reduces the chance of jamming and also enables filling of intricate design features.

## 3.4 Results and discussion: Consolidation dwell time

This section provides the analysis of results on the second aim of this study, the effect of consolidation dwell time on the resulting part quality in the presence of jammed regions.

### 3.4.1 Effect of consolidation dwell in the presence of jamming

The concept of consolidation dwell in the case of a continuously reinforced laminate is to provide sufficient time for the resin to percolate into the fibrous structure of the fabric or unidirectional fiber reinforcements. This generally reduces the void content and results in a better formation of fiber matrix bonding. However, in the case of discontinuous composites with randomly filled reinforcements, the consolidation dwell time is found to have an upper bound for obtaining a smaller void content. This effect is more pronounced in the presence of jammed regions, as they undergo further consolidation by squeezing out the matrix, resulting in local densification of the jammed stack of flakes. Figures 3.11 and 3.12 show a few representative micrographs of a specimen molded with 5 and 20 minutes consolidation dwell time, respectively, and at a constant consolidation pressure of 10 bar. It is evident that the increased dwell time has led to the formation of voids. The optimal dwell time can only be found when the consolidation mechanism is understood, which is the subject of the next subsection.

### 3.4.2 Consolidation mechanism of jammed regions

The assumptions made for the analysis are as follows: (a) The flakes filled in the mold are initially un-impregnated or partially impregnated. (b) The mold cavity is semi-positively closed, with no mechanical stops and with flash edges. Hence, the matrix material can seep out of the mold cavity through the flash edges. (c) Upon

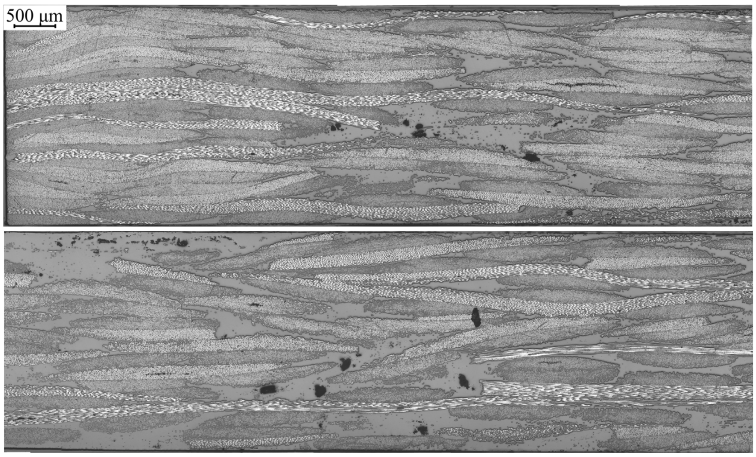


**Figure 3.11** *Cross-sectional micrographs of specimen consolidated for 5 minutes. Black regions are voids.*

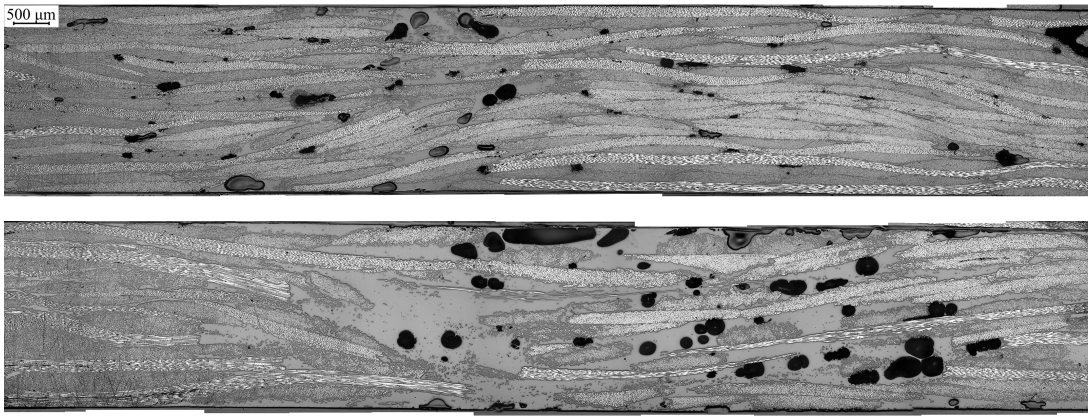


**Figure 3.12** *Cross-sectional micrographs of specimen consolidated for 20 minutes. Black regions are voids.*

application of a certain compressive load, the stress-strain response of the dry flake bed is similar to the compaction of dry fabric. (d) Pockets of air are present due to the random packing of the flakes in the cavity, and is spread uniformly in the cavity. (e) Meso-level impregnation of the flakes is assumed to be complete after holding the material above melting temperature at 1 bar pressure for a very short period, since the polymer from the faces of the flakes has to travel only half the thickness of the flake. (f) Partial micro-level impregnation occurs just after the application of consolidation pressure and, subsequently, filling of the pockets occur.

The concept of interstitial fluid pressure and effective stress in the consolidation of a granular medium, discussed in Section 3.3.1, can be used here to approximate the local interstitial fluid pressure (resin pressure) adjacent to a jammed region bearing

the effective stress. The situation is shown in Figure 3.7 (d). The total external consolidation pressure $\sigma_e$ applied can be divided into the constituent stresses as,

$$\sigma_e = \bar{\sigma}_{f_{fl}} + \sigma^{eff}_{flakes}, \tag{3.8}$$

where $\bar{\sigma}_{f_{fl}}$ is the average interstitial fluid pressure or the average resin pressure and $\sigma^{eff}_{flakes}$ is the effective stress borne by the stack of flakes.

The effective stress of the fiber network formed by the stack of flakes can be experimentally measured by compressing layers of the same type of dry or preferably (wetted for lubrication effects) impregnated woven carbon fabric. Since the applied consolidation pressure is known, the average pore pressure can be calculated from Eq. (3.8) by using the compaction stress-strain curve of the dry fabric as an approximation. However, the resin pressure varies with time and space due to the seepage from the flash edges and as a result of randomness. After a certain time, the resin pressure drops to a level where the seepage seizes.

The fabric compaction stress can be modeled (fitted) with a simple power-law for the type of fabrics used in this study. The compaction stress $\sigma_{fabric}$ is given by,

$$\sigma_{fabric} = A\epsilon^B, \tag{3.9}$$

where $\epsilon$ is the imposed strain (or equivalent change in volume fraction), $A$ and $B$ are fitting parameters.

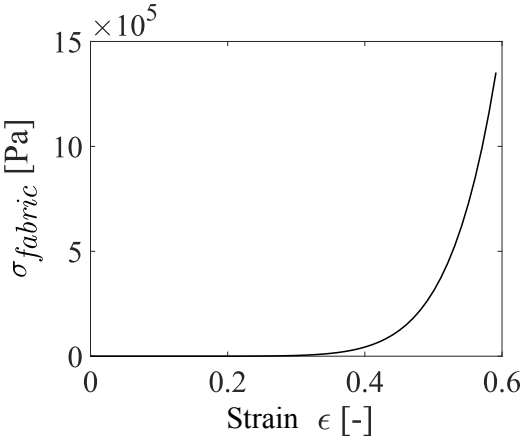


**Figure 3.13** *Compressive stress-strain response of CD286 fabric.*

For the fabric (CD286) used in CETEX laminates the values of $A$ and $B$ were experimentally found to be in the range of $1.38\times10^8$ Pa and 8.80, respectively. The procedure used for measuring the power law constants is similar to the method stated in [26]. It can be observed in Figure 3.13, that the stress increases slowly at small strains. After reaching a certain strain, the stress rises rapidly due to the formation

of close packing of incompressible fibers. Therefore, from Eq. (3.8) and Eq. (3.9) it can be qualitatively concluded that after reaching a certain compaction level the resin pressure surrounding the jammed region is lower than the average consolidation pressure. Thus, further filling of the pockets or the suppression of the existing voids is hindered.

### 3.4.3 Validation of results: Effect of consolidation dwell

Model laminates with forcibly jammed regions (FJL: forcibly jammed laminates) were manufactured as mentioned in Section 3.2.3 with the configuration shown in Figure 3.14, to validate the proposed mechanism. Additionally, conventional continuously reinforced laminates (CRL) with the same material were molded under the same processing conditions for comparison.

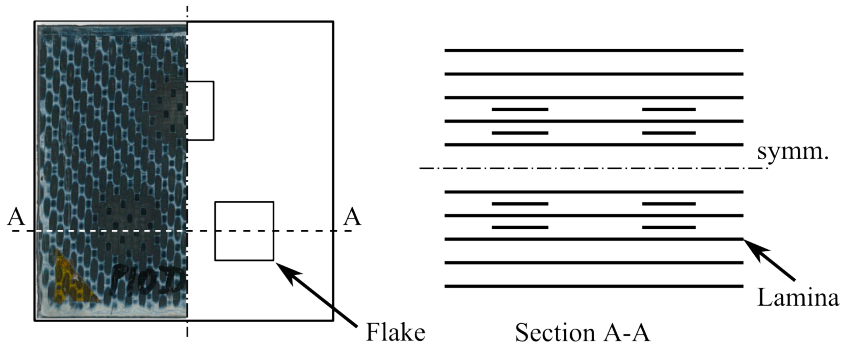


**Figure 3.14** *Configuration of model laminate for consolidation dwell experiment. Flakes are placed symmetrically, in between the continuous layers, about the symmetry plane. Half of the molded specimen is shown on the left with visible jammed region as dark patches.*

Figure 3.15 shows the representative sections of all the laminate configurations, where Figure 3.15 (c,d) shows the cross section at section A-A between the flakes (see Figure 3.14). The region close to the sides of the specimen shows a high fiber content due to the presence of additional flakes causing a locally thick region emulating a jammed region.

It can be observed from the plot in Figure 3.16, that the void content increases in the case of chopped prepreg laminates with longer dwell times. In the case of CRL, the effect of consolidation dwell time is not adverse, unlike the other cases shown. The proposed hypothesis for the consolidation mechanism of chopped prepreg laminates is illustrated in Figure 3.16 (a,b,c) at different locations in the plot corresponding to the chopped prepreg laminate. The situation shown in Figure 3.16 (a) is at the beginning of the application of 10 bar consolidation pressure where the material is already in molten state. Voids are present in the composite level due to the random packing of the flakes and also in the bundle level since the material is a semi-preg.

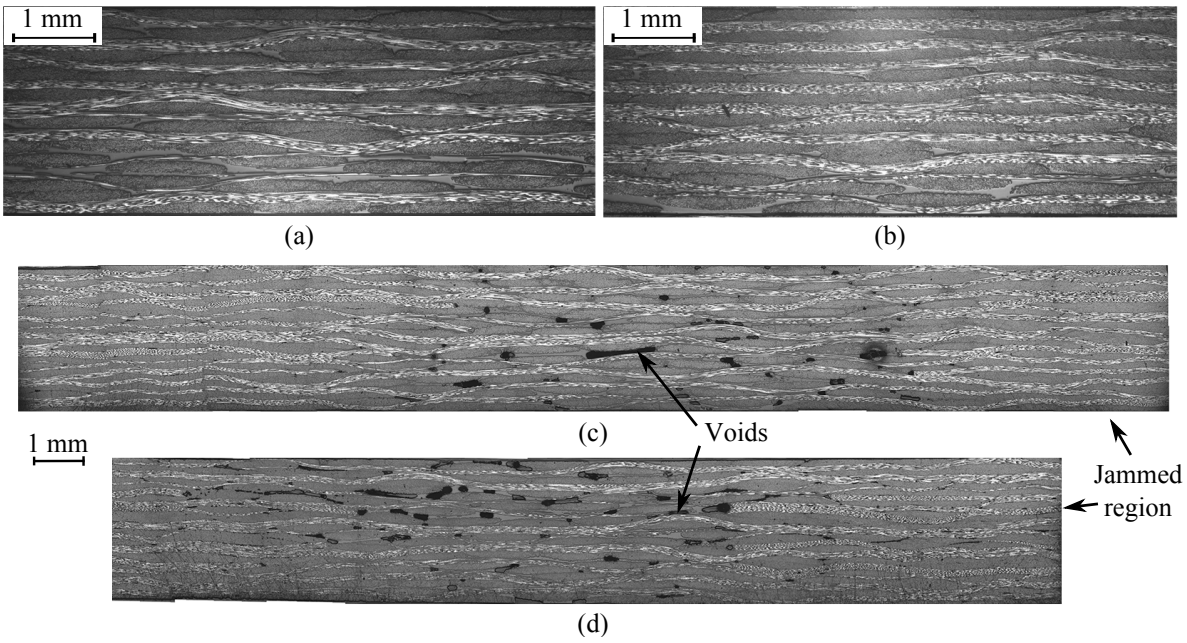


**Figure 3.15** *Cross-sectional micrograph of specimens consolidated at 10 bar pressure. Legend: [laminate type, dwell time in minutes, void fraction in %]. (a) [CRL, 5, -] (b) [CRL, 20, -] (c) [FJL, 5, 1.46] (d) [FJL, 20, 3.1].*

As the consolidation progresses, Figure 3.16 (b), the thickness reduces, the voids are filled with the polymer matrix and the rest of the voids are suppressed due to the existence of resin pressure. In the presence of jammed regions and flash boundary condition, the fiber rich jammed regions start to carry the consolidation load and the resin pressure gradually reduces. Additionally, when the consolidation dwell is prolonged such as shown in Figure 3.16 (c), the suppression of voids is hindered and the final residual void content increases in the part. The forcibly jammed laminates (FJL) are used for validating this hypothesis. The void content measured in the FJL laminates between the two jammed regions in section A-A (see Figure 3.14), shows an increasing trend of residual void content as the dwell time is increased (see plot in Figure 3.16).

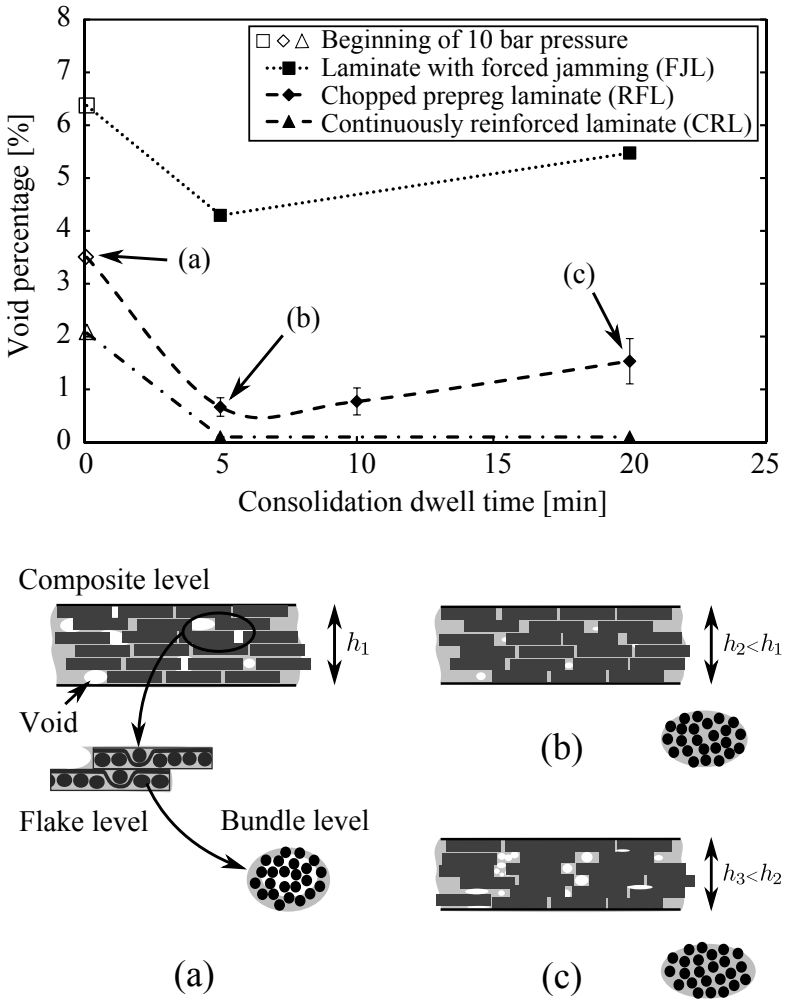


**Figure 3.16** *Top: Void percentage measured from micrographs of different laminate configurations (filled symbols) consolidated with different dwell times. Open symbols indicate void percentage calculated with the cavity volume at the instant of the application of 10 bar pressure. Bottom: The hypothesis for the mechanism of consolidation as time progresses (a,b,c), for chopped prepreg laminates, is illustrated at different scales. The thickness of laminate is denoted by $h_i$ for the $i^{th}$ instant.*

## 3.5 Applicability in designing a process window

The selection of a feasible process window for an unconventional molding material such as chopped woven prepreg is a direct consequence of the choice of material and design parameters. This section summarizes the results with a view to transferring them to real life application.

### 3.5.1 Process parameters

Taking account of the above observations, when molding a relatively large part ($\sim$ 20-30 times larger surface area than the experiments) with a mold initially filled with flakes, the local flow can be assumed to be an axisymmetric flow. However, the flow might be locally constrained depending on the surrounding created by the part geometry and randomly filled mold. Therefore, jamming in flat regions cannot be completely avoided but can be delayed until a certain required final thickness is reached. Furthermore, the smallest part thickness that can be achieved ideally is around 3 to 4 times the flake thickness ($\sim$ 1 mm) considering the observed sticking flow boundary condition at the mold-material interface.

The proposed jamming transition diagram can be used to identify suitable closing rates to avoid jamming for a given flake size. The general guideline for the extreme values (or bounds) for the parameters can be identified from the asymptotic behavior. Further investigation is required to quantify the other planes of the jamming diagram and to estimate the limits of final thickness including the stochastic nature of the mold filling process. Moreover, the possibility of a size effect has to be investigated in the future with various ratios of flake dimension to the mold dimension (or a characteristic mold dimension).

### 3.5.2 Orientation of planes of uniform thickness

The scenario of material planes normal to the compression axis was investigated in this study. However, preliminary compression molding trials with a spherical dome ($r_{base} = 90$ mm, $depth = 40$ mm) mold and shredded laminate scrap[†] material showed a longer flow length for larger flakes compared to smaller flakes. This effect is possibly due to the reduced number of interactions possible between the adjacent flakes, since the number of large flakes for the same mass of input material is less than small flakes. Moreover, a longer contact length or a larger plane might give the flakes greater mobility due to shear when compared to small flakes with many discontinuities. Consequently, a reduced jamming phenomena was also observed.

[†]Flakes with an average minimum Feret diameter [27] of 22 mm and a standard deviation of 4.69 mm.

This observation is noteworthy and a possible explanation could be sought from the theory on unjamming of particle systems subjected to shear stress. The force network developing along the axis of compression of the flake stack (which might potentially jam) can be assumed to be disrupted by the tangential component of stress along the spherical profile and may thereby reduce the possibility of jamming of flakes through the thickness. Furthermore, reduced flake-flake interaction is also probable with fewer numbers of large flakes for the same volume of the material.

Therefore, orientation of the planes of uniform thickness with respect to the compression axis is a parameter to be considered in the design of mold to prevent jamming in the flat regions of the molded part. Eventually, the range of flake sizes that can be used for molding increases and can thereby attain better mechanical properties.

### 3.5.3 Consolidation dwell

The small-scale consolidation experiments have shown that, unlike continuously reinforced composites, the consolidation dwell time for woven flake reinforced composites is bounded on both sides. In the presence of jammed regions or nearly jammed regions, a longer dwell time results in a more dry jammed spot due to squeeze out of resin.

For larger parts with a large ratio of surface area to perimeter, the effect of resin outflow (in flash edges) on the drop in resin pressure near jammed regions can be less influential. Hence, the residual void content near jammed regions can be different for large parts. However, the presence of design features, like rib cavities or regions which could cause a pressure drop, adjacent to the jammed regions can cause resin migration leading to resin starved regions around jammed spots. Further study is needed for evaluating this phenomenon.

Therefore, a time period which ensures a proper consolidation of the part and at the same time does not lead to a dry jammed spot has to be sought. Further study is required to understand the process of resin squeeze out from the jammed stacks along with the overall boundary conditions for the flow of resin in the flake bed.

## 3.6 Conclusions

The jamming phenomenon of woven flake reinforced composites has been investigated under two types of compression molding scenario, namely axisymmetric and plane strain squeeze flow. The effect of consolidation dwell time on the part quality in the presence of jammed regions was studied. Under certain flow conditions, the squeeze flow induces phase separation in the material giving rise to different

regimes of flow. The phase separation was found to be dependent on squeeze rate and flake size which leads to jamming of the material during the squeezing process. Upon jamming and subsequent consolidation, further draining of the jammed region occurs giving rise to dry fiber rich regions surrounded by matrix rich regions. Furthermore, the collapse of voids is hindered due to low average resin pressure. Therefore, local jamming of highly stiff material, such as woven carbon fiber flakes, has detrimental effects on the mold surface and also affects the part quality. It degrades the mechanical performance of the molded part on the one hand and potentially damages the mold on the other hand. Principles from flow of granular materials and soil mechanics were used to identify and explain the phenomenology of the transition from one-phase flow to a phase separated flow, leading to jamming. The different regimes of flow were identified with the use of the Péclet number and a jamming transition diagram was constructed which allows the design engineers to determine a safe operating mold closure rate for a certain flake size and part thickness. Although more data is required to completely define the parameter space, the initial experimental points and the calculated trend are in qualitative agreement and show that the approach presented here is promising and warrants pursuing further. More work is needed to completely characterize the jamming surface with all the practically useful process and material parameters from the manufacturing point of view.

# References

[1] I. Taketa, T. Okabe, and A. Kitano. A new compression-molding approach using unidirectionally arrayed chopped strands. *Composites Part A: Applied Science and Manufacturing*, 39(12):1884–1890, December 2008.

[2] C. Stephen, Dustin L. Levin, Dequine, and John P. Crocco. Formability of thermoplastic stretch-broken carbon fiber vs. thermoplastic continuous carbon fiber. In *SAMPE Technical conference proceedings*, 2013.

[3] Paolo Feraboli, Elof Peitso, Francesco Deleo, Tyler Cleveland, and Patrick B. Stickler. Characterization of Prepreg-Based Discontinuous Carbon Fiber/Epoxy Systems. *Journal of Reinforced Plastics and Composites*, 28(10):1191–1214, May 2009.

[4] M. Selezneva, K. Kouwonou, L. Lessard, and P. Hubert. Mechanical properties of randomly oriented strands thermoplastic composites. In *Proceedings of the International Conference on Composite Materials (ICCM19)*, Montreal, CA,, 2013.

[5] M. I. Abdul Rasheed, B. Rietman, H. A. Visser, and R. Akkerman. A parametric study on compression molding of reference parts with integrated features using carbon composite production waste. In *Proceedings of the 18th International ESAFORM conference on material forming*, pages 458–463, Graz, Austria, 2015.

[6] K. S. Gandhi and R. Burns. Rheological properties of glass fiber reinforced dough molding compounds. *Transactions of The Society of Rheology (1957-1977)*, 20(4):489–502, December 1976.

[7] G. Kotsikos, J. H. Bland, A. G. Gibson, and H. W. Chandler. Squeeze flow testing of glass mat thermoplastic material. *Composites Part A: Applied Science and Manufacturing*, 27(12):1195–1200, 1996.

[8] M. A. Dweib and C. M. ÓBrádaigh. Anisotropic modeling of isothermal squeezing flow of glass-mat reinforced thermoplastics (GMT). *Polymer Composites*, 19(5):588–599, October 1998.

[9] P. Dumont, L. Orgéas, C. Servais, V. Michaud, D. Favier, and J.-A. E. Månson. Influence of material and process parameters on segregation phenomena during compression molding of GMT. In *Proceedings of ESAFORM 2005*, pages 967–970, Cluj-Napoca, Romania, 2005.

[10] Laurent Orgéas, Pierre J. J. Dumont, Veronique Michaud, and Denis Favier. Separation of the polymer matrix and the fibrous reinforcement during compression moulding of glass mat thermoplastics (GMT). *International Journal of Material Forming*, 1(1):929–932, April 2008.

[11] Christophe Ancey, Philippe Coussot, and Pierre Evesque. A theoretical framework for granular suspensions in a steady simple shear flow. *Journal of Rheology*, 43(6):1673–1699, November 1999.

[12] P. Coussot and C. Ancey. Rheophysical classification of concentrated suspensions and granular pastes. *Phys. Rev. E*, 59:4445–4457, Apr 1999.

[13] Philippe Coussot. *Rheometry of Pastes, Suspensions, and Granular Materials: Applications in Industry and Environment*. John Wiley & Sons, June 2005.

[14] N Delhaye, A Poitou, and M Chaouche. Squeeze flow of highly concentrated suspensions of spheres. *Journal of Non-Newtonian Fluid Mechanics*, 94(1):67 – 74, 2000.

[15] J.D. Sherwood. Liquid-solid relative motion during squeeze flow of pastes. *Journal of Non-Newtonian Fluid Mechanics*, 104(1):1 – 32, 2002.

[16] J. D. Sherwood. Liquid-solid relative motion during slow squeeze flow of pastes. *Journal of Non-Newtonian Fluid Mechanics*, 128(23):163–171, July 2005.

[17] Gerald Meeten. Constant-force squeeze flow of soft solids. *Rheologica Acta*, 41(6):557–566, January 2002.

[18] Fami Chaari, Guillaume Racineux, Arnaud Poitou, and Mohend Chaouche. Rheological behavior of sewage sludge and strain-induced dewatering. *Rheologica Acta*, 42(3):273–279, May 2003.

[19] Steven Le Corre, Pierre Dumont, Laurent Orgéas, and Denis Favier. Rheology of highly concentrated planar fiber suspensions. *Journal of Rheology (1978-present)*, 49(5):1029–1058, September 2005.

[20] S. G. Advani, T. S. Creasy, and S. F. Shuler. Rheology of long fiber-reinforced composites in sheetforming. In D. Bhattacharyya, editor, *Composite Materials Series*, volume 11 of *Composite Sheet Forming*, pages 323–369. Elsevier, 1997.

[21] K. Terzaghi. *Theoretical soil mechanics*. J. Wiley and Sons, inc., 1943.
[22] S.G. Advani and E.M. Sozer. *Process Modeling in Composites Manufacturing, Second Edition*. CRC Press, 2012.
[23] Andrea J. Liu and Sidney R. Nagel. Nonlinear dynamics: Jamming is not just cool any more. *Nature*, 396(6706):21–22, November 1998.
[24] Corey S. O. Hern, Leonardo E. Silbert, Andrea J. Liu, and Sidney R. Nagel. Jamming at zero temperature and zero applied stress: The epitome of disorder. *Physical Review E*, 68(1):011306, July 2003.
[25] W.J.B. Grouve, R. Akkerman, R. Loendersloot, and S. van den Berg. Transverse permeability of woven fabrics. In *11th ESAFORM Conference on Material Forming*, 2008.
[26] W. J. B. Grouve and R. Akkerman. Consolidation process model for film stacking glass/PPS laminates. *Plastics, Rubber and Composites*, 39(3-5):208–215, June 2010.
[27] Henk G. Merkus. *Particle Size Measurements: Fundamentals, Practice, Quality*. Springer Science & Business Media, January 2009.

# Chapter 4

# Compression molding of integrated ribs using chopped woven prepreg*


### *Abstract*

The filling behavior of chopped woven reinforcements in rib cavities using a compression molding process has been investigated. An experimental study with different groups of design, material and process parameters, such as rib aspect ratio, flake size, consolidation pressure and dwell time was performed. The observations show that the ribs can be filled completely with the molding material, but with varying volume fractions of reinforcement. Moreover, defects such as voids, non-impregnated regions and fiber-matrix separation may arise depending on the combination of parameters, the presence of flash boundary conditions and a mechanical jamming effect caused by the woven architecture of the flakes. A tendency for a limiting consolidation pressure and dwell time was observed based on the fiber-matrix separation. The requirement of a proper combination of the aforementioned groups of parameters is illustrated via the results obtained. Preliminary recommendations for design rules based on the current results have been discussed.


*Reproduced from: M.I. Abdul Rasheed, W.J.B. Grouve, S. Wijskamp, H.A. Visser, B. Rietman, R. Akkerman. Compression molding of integrated ribs using chopped woven thermoplastic prepreg. To be submitted to *International Journal of Material Forming*, **2016**.

## 4.1 Introduction

Compression molding of discontinuous composite materials has received much attention in the past due to the excellent repeatability of the process and processability of the material. Recently, the extensive use of thermoplastics in structural composites, for their high toughness and recyclability, has widened the scope of the discontinuous molding compounds with high performance thermoplastic matrices. Discontinuous composites have a major advantage over conventional continuous fiber laminates in their ability to take up complex shapes without processing defects such as wrinkles. Furthermore, the possibility of manufacturing near-net shaped parts reduces the excess material used for in-production material handling in multi-step processes and the post production trimming process. Figure 4.1 shows an example of a complex part with functional design features, such as joggles, thickness transitions and stiffeners, which is rather difficult to manufacture with continuous reinforcements.

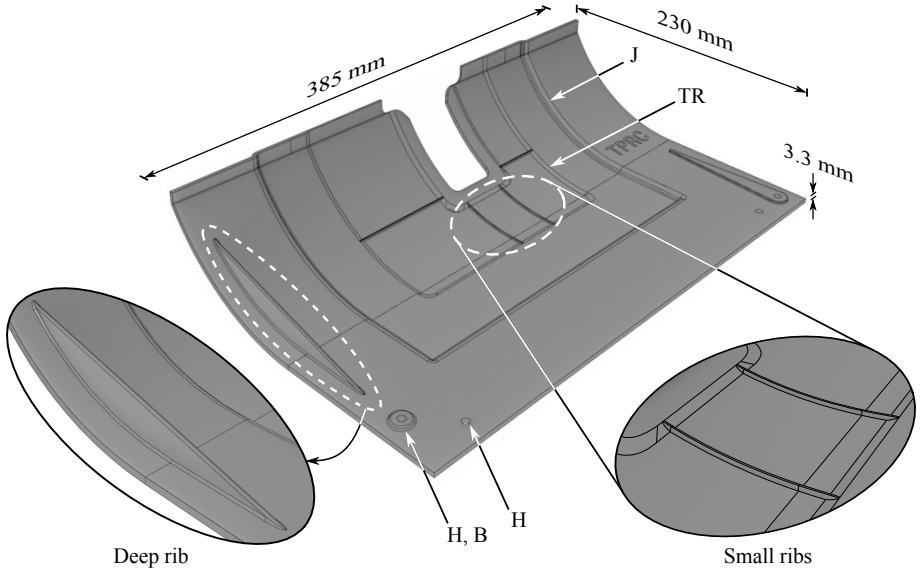


**Figure 4.1** *A demonstrator part with integrated design features like ribs, joggle (J), thickness transitions (TR) and as-molded holes (H) with boss (B). Insets show ribs of different width to depth ratio.*

Several studies have been performed in the past on the flow behavior of discontinuous molding compounds based on both thermoset matrices such as bulk molding compounds (BMC), sheet molding compounds (SMC), chopped unidirectional tapes (HexMC™) [1–7] and thermoplastics such as glass mat thermoplastics (GMT) and chopped unidirectional tapes (TenCate BMC™) [8–11]. The primary reinforcing elements in such compounds are chopped fibers or unidirectional (UD) tapes with a fiber volume content of 20-30 % except for TenCate BMC which is around 55 %. However, literature on chopped materials with a woven architecture is scarce. In this study chopped woven prepreg materials, referred to as flakes, with a fiber volume

content of 50 % are studied. It is interesting to study such a material form since the woven structure provides a local structural integrity to the flakes which provides a two dimensional reinforcing effect. However, it also leads to atypical flow behavior, such as jamming of material, compared to other discontinuous compounds [12, 13] which needs to be taken into account when designing a part. Possible applications include non-load bearing or semi-structural parts with high stiffness requirement in aerospace and automotive sectors.

A typical compression molding process and an accompanying process cycle for such materials is shown in Figure 4.2 and 4.3, respectively. Initially, the mold cavity is loaded with the flakes in a random pattern as shown in Figure 4.2. Subsequently, the material is heated under a small initial pressure (phase (a) of the process cycle) to compact the bulk material and to expel the air in the compound. Upon reaching the processing temperature the mold is closed further at a constant closing rate to fill the entire mold cavity with the molten material. Thereafter, the material is consolidated at a constant pressure prior to cooling and demolding. During the filling process, phase (b), the macroscopic flow of the material is governed by the initial material-loading pattern and the mold geometry. However, local mesoscopic flow of the matrix (at the flake scale) and reinforcements exists, which fills the intricate parts of the mold cavity such as the design features. Furthermore, the reinforcements get reoriented and there is also a possibility of fiber-matrix separation (Chapter 3) due to a change in the resistance to the flow of the material created by the mold geometry.

### 4.1.1 Flow in rib sections

Unlike thin and flat sections, the flow around a design feature is generally more complicated due to the sudden contraction or expansion of sectional area experienced by the reinforced melt. For instance in the case of ribs, there can be loss of pressure in the entrance region of the ribs. Additionally, the mesostructure formed by the flake bed can act as a filter causing the matrix to get separated based on the entrance geometry, such as rib width, base thickness and entry radius. The size of the reinforcements, which can be considered as a material parameter, adds to the above effects making the flow more non-uniform as the size gets larger. Large flakes are far more likely to bridge the rib opening and thus create a matrix rich rib. These effects lead to a reduction in the mechanical performance as well as secondary effects such as sink marks and uneven surfaces.

A lot of studies in the past have analyzed the flow of anisotropic material in flat sections as mentioned earlier and non-flat sections [14–16] with materials such as SMC and GMT which consist of primarily fiber filaments or bundles suspended in a polymer matrix. However, only a few have experimentally characterized the effect of fiber-matrix separation in flat sections using GMT [17] and in non-flat sections such as ribs using SMC [14]. In [14], the authors have developed a model dimensional

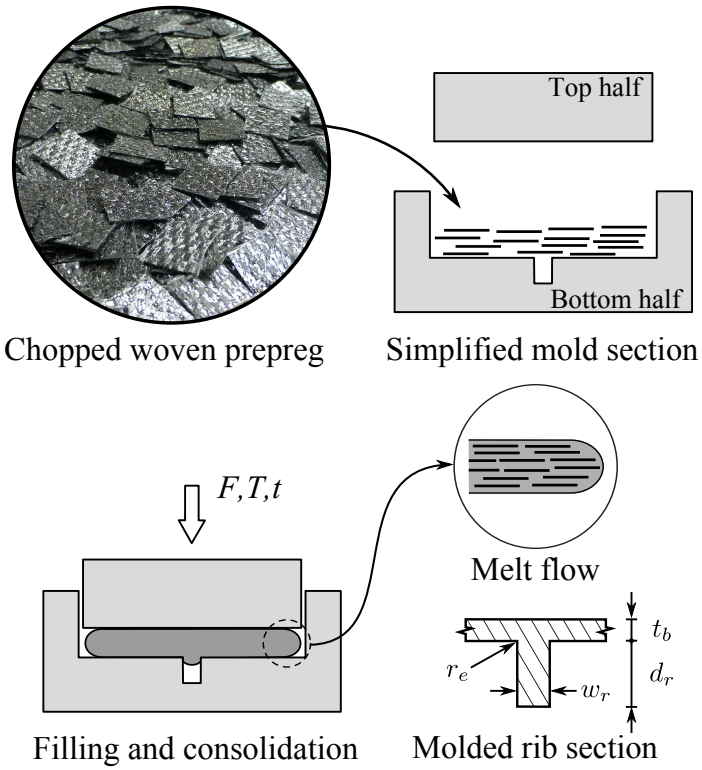


**Figure 4.2** *Illustration of a typical compression molding process with chopped prepreg flakes. Inset shows the melt flow of the polymer material with flakes.*

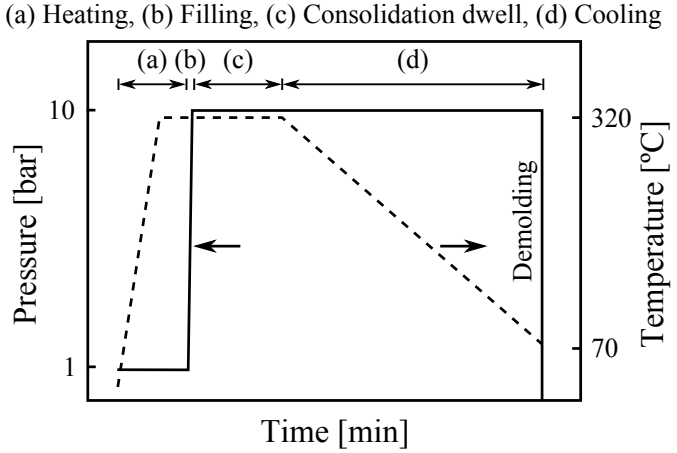


**Figure 4.3** *Schematic of a typical compression molding process cycle.*

analysis based on rib dimensions in which the results show that for a larger rib opening, the resistance to flow into the rib decreases, whereas the pressure loss occurring at the entrance due to a sudden change in section will cause fiber-matrix separation. Moreover, in [17], the experimental results show that the mold closing rate has an influence on the observed non-homogeneity of fiber volume fraction across the flat section. These flow filling studies have been done for fiber bundle reinforced molding compounds such as the materials mentioned earlier. However, the process of filling flaky woven reinforcements into and across non-flat regions has not been explored so far in the literature. This article focuses on the filling behavior of chopped woven materials for a typical non-flat design feature, namely integrated stiffener or rib, which is commonly added to increase the flexural stiffness of the component.

The aim of the first part of this study is to investigate the ability to mold a flat plate with a deep rib using chopped woven materials. The quality of the part is assessed from the matrix distribution in rib and base plate for various combinations of material and process parameters such as flake size, consolidation pressure and consolidation dwell time. The second part of the study is on smaller ribs, focusing on the effect of the rib aspect ratio on the filling quality, in the presence of flash edges.

The following sections of the article describe the materials and experimental methods used in the study. The observed experimental results are presented and discussed followed by the conclusions drawn from the study.

## 4.2 Materials and experimental methods

This section describes the materials used, the details of the molding setup and the procedure for the experiments performed in this study.

### *4.2.1 Materials*

Cutting wastes of CETEX® Carbon/poly(phenylene sulphide) (C/PPS) semi-preg material from TenCate Advanced Composites was used in this study. The semi-preg material is made of 5 harness satin weave fabric, spray coated with polymer matrix. The nominal thickness of a consolidated lamina is 0.31 mm with a fiber volume fraction ($v_f$) of 50 %. The matrix polymer has a glass transition temperature ($T_\mathrm{g}$) of 90 °C, melting point ($T_\mathrm{m}$) of 280 °C and the nominal processing temperature of 320 °C. The semi-preg materials are chopped into square shaped flakes of side length 5 mm, 7.5 mm, 10 mm, and 12.5 mm. The edges of the flakes are maintained parallel to the fiber directions during the chopping process. A square shape was chosen to have the fiber length a constant in the event of disentanglement of the woven structure.

### 4.2.2 Experimental setup

The compression molding experiments are carried out in a small instrumented press setup, having dimensions of 60 x 60 $mm^2$, installed on a universal testing machine. Figure 4.4 shows the molding setup used in this study which consists of a bottom half attached to the stationary frame of the machine and a moving top half attached to the cross head. A spherical joint is used in the stationary part of the setup to accommodate the plates to be installed parallel to each other. Removable side walls are attached on the sides of the bottom half to create the mold cavity. Heating

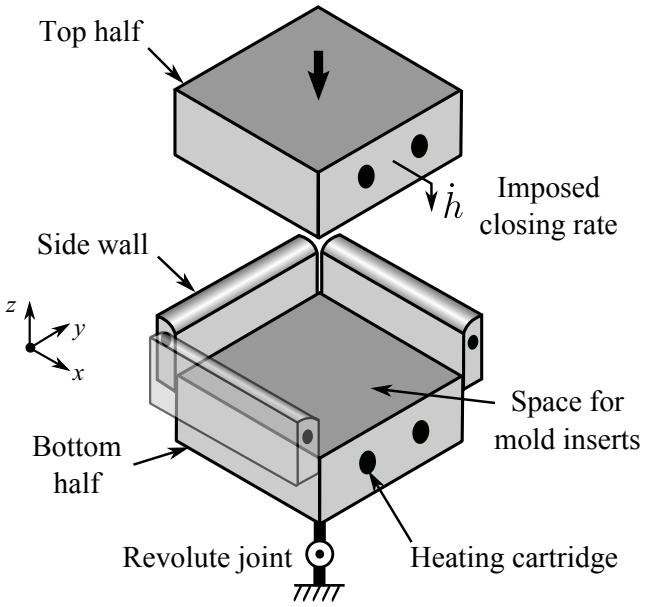


**Figure 4.4** *Illustration of the mini-press setup. The fourth side wall forming the cavity is not shown for clarity.*

cartridges are present in the bottom, top and the side walls to heat the material in the cavity. The temperature of the platens is measured with thermocouples and PID controllers are used to control the temperature of the two halves. The force exerted on the mold, the displacement of the mold and its temperature are logged with a data acquisition system. Modular mold inserts are used for the different rib dimensions investigated in this study as described in the following section.

### 4.2.3 Experimental methods

Two different sets of experiments with different rib geometries, material parameters, process settings and boundary conditions are investigated in this study. The quality of the molded rib sections are analyzed by cross-sectional micrography. The matrix

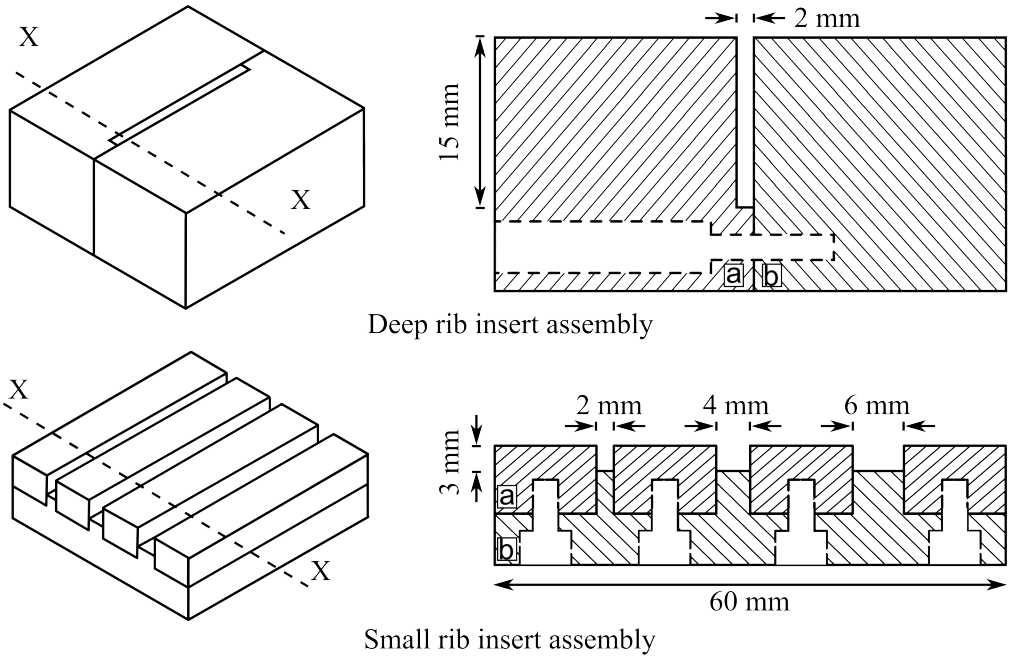


**Figure 4.5** *Left: Isometric view of the mold inserts for the deep rib and small ribs. Right: Sectional view of the inserts at section X-X. Separable parts are marked with labels a and b.*

content and void content is obtained by image analysis using the software package ImageJ [18].

Firstly, a small aspect ratio rib, henceforth referred to as deep rib, is investigated with a nearly no-flash boundary condition. Secondly, ribs with smaller depth compared to the deep rib are investigated with different aspect ratio. The small ribs are investigated with a boundary condition which permits flashing of material. This enables studying the possible effect of seepage in the case of semi-preg materials, which are not fully impregnated prior to processing. By allowing flash, matrix seepage is made possible which potentially causes resin starved regions. In reality, this could be considered as multiple features which might cause additional pressure drops thereby leading to resin starved regions. Moreover, for a semi-positively closed mold, a flash boundary condition exists at the edges of the parts by default.

In both cases of deep ribs and small ribs, the base plate has a dimension of 60 x 60 $mm^2$. The corner radius at the rib entrance is negligible. Table 4.1 summarizes the experimental settings for the two sets of experiments mentioned above.

The manufacturing method for both classes of ribbed plates is the same except for the mold inserts. Figure 4.5 shows the mold inserts used for the two classes of ribs. All mold pieces can be separated for demolding the part. The assembled mold pieces are mounted on the bottom half of the press setup shown in Figure 4.4. A weighed quantity of material based on the volume of the part was added to the cavity and the process cycle (see Figure 4.3) was started with the respective settings from Table 4.1.

| Parameter | | Values | |
|---|---|---|---|
| Class | | Deep rib | Small rib |
| Aspect ratio, $w_r/d_r$ | [mm/mm] | 2/15 | 2/3, 4/3, 6/3 |
| Base thickness, $t_b$ | [mm] | 3 | 2 |
| Flake size | [mm] | 10, 12.5 | 5, 12.5 |
| Consolidation pressure | [bar] | 10, 15, 20 | 5, 10, 15 |
| Consolidation dwell | [min] | 15, 25 | 15 |
| Closing rate | [mm/s] | 0.5 | 2 |

**Table 4.1** *Experimental matrix for the two classes of experiments. See Figure 4.2 for notations.*

During the filling phase, the mold was closed at a constant displacement rate until the required consolidation pressure was achieved.

The analysis of the part quality is performed with light microscopy and image processing. Micrographs of the cross section of the ribs are obtained and thresholded to calculate the different measures of quality. These measures are explained in the results and discussion section.

It is worth noting that the random filling of the mold causes a large scatter in the results. However, this study aims at obtaining a qualitative trend in the material behavior so as to generate a fundamental understanding of the material and the process. For the experiments with deep rib cavity three specimens were molded per process setting and one location was studied. In the small rib case two locations from one specimen per process setting are studied. The reason for the choice of the locations is discussed in the respective sections concerning the results.

## 4.3 Results and discussion: Deep rib

The results from the first part of the molding experiments with a deep rib cavity and negligible flash boundary condition are presented and discussed in this section.

Figures 4.6 and 4.7 show a molded plate with a deep rib and a micrograph of the rib cross-section (A-A) from the center of the plate, respectively. Different regions can be observed in the micrograph, such as impregnated flake regions visible as fiber bundles, pockets of matrix rich regions in many spots and non-uniformity at the rib entry. Moreover, the stochastic nature of the position and orientation of the flakes during the initial filling of the mold cavity leads to scatter in the observed results. However, a qualitative analysis of the filling behavior in the rib sections is performed in this study and the effects of the change in parameters are described.

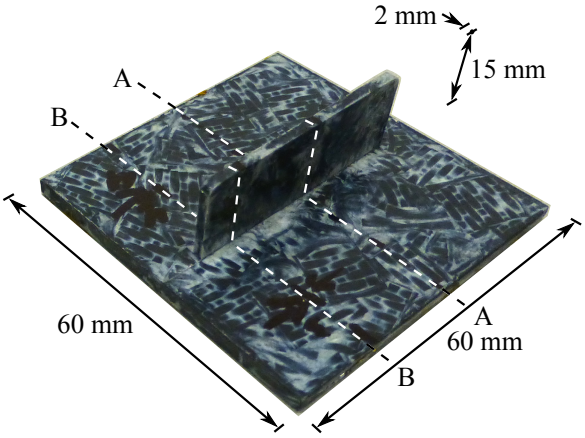


**Figure 4.6** *Plate molded with deep rib. Sections A-A and B-B illustrate the sectioning plane for the micrography.*

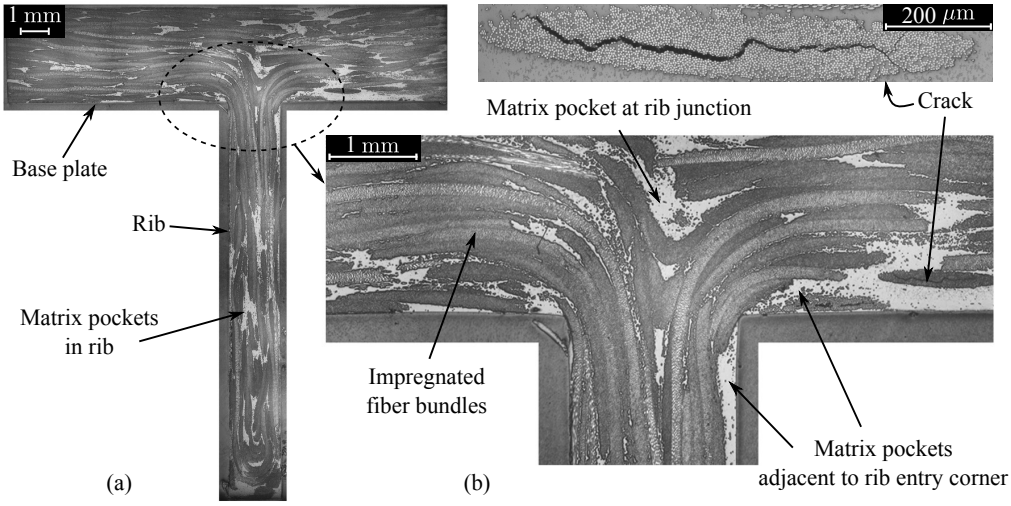


**Figure 4.7** *Micrograph of a typical cross section of a deep rib (A-A in Figure 4.6). Different regions in the micro structure are indicated.*

### 4.3.1 Measure for part quality

The quality of consolidation of a composite part is usually described by the average spatial distribution of fibers, matrix and possibly voids measured from several cross sections, assuming the structure repeats itself. Structures from these chopped materials, however, have a non-homogeneous and random micro-structure which is a function of base materials and process parameters. Therefore, defining a criterion for the quality of filling in the case of non-homogeneous random materials is non-trivial. In this study, the distribution of the resin rich pockets is used to quantify the quality of the filling. Since the mold filling process involves several flow mechanisms such as local bulk flow of matrix and flakes, and percolation flow of the matrix, the matrix rich regions will provide an approximate measure to determine the degree

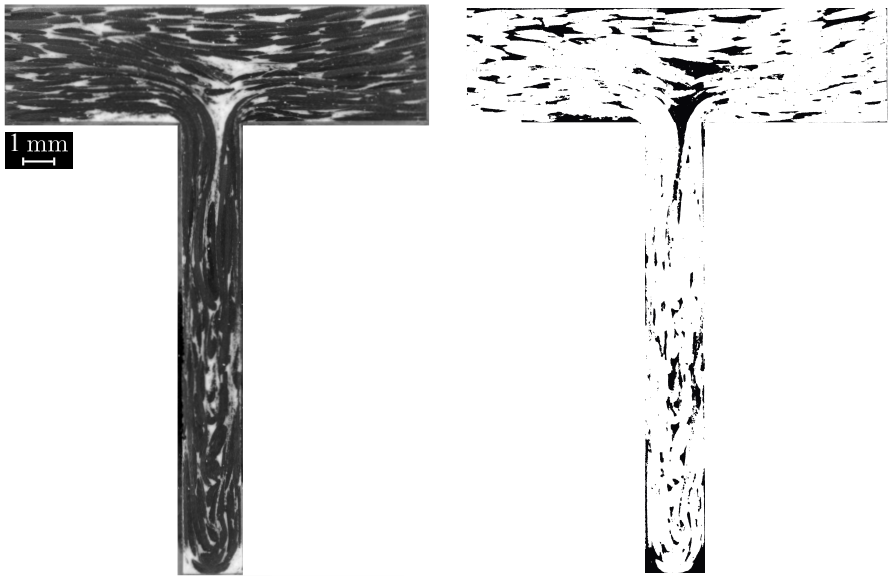


(a) Micrograph (b) Thresholded image

**Figure 4.8** *(a) Micrograph of a typical cross section with dark fibers and white matrix rich regions, (b) the thresholded micrograph showing matrix rich regions as black pixels.*

of homogeneity in the distribution of flakes. The fraction of matrix rich regions is computed from a thresholded image of the micrograph. Figure 4.8 shows a typical micrograph and the thresholded image obtained using ImageJ.

### 4.3.2 Filling of rib

In all the investigated test cases, the deep ribs were observed to be fully filled with the molding material. However, the distribution of fibers and matrix differs with the choice of parameters.

The process of filling the rib with a flake reinforced melt can be described as follows: (a) as the pressure builds up in the material while closing the mold, the material near the rib cavity flows into the rib. The randomly positioned flakes flow with the matrix and are pushed or bent into the rib cavity. (b) The mesoscopic flow of the material seizes once the entry of the rib is bridged or clogged with large flakes. This occurs with insufficient consolidation pressure, or after the rib is filled and the melt front reaches the bottom of the rib cavity. (c) Further compression of the material leads to the meso-structure at the rib entry to act as a filter through which the matrix polymer percolates to fill the regions which were not yet filled with flakes or fibers. Consequently, the fiber volume content in the base increases while the matrix volume content rises in the rib.

Figure 4.9 shows a comparison of the central location and edge of the rib at different pressure settings. A triangular matrix rich region is observed adjacent to the entry

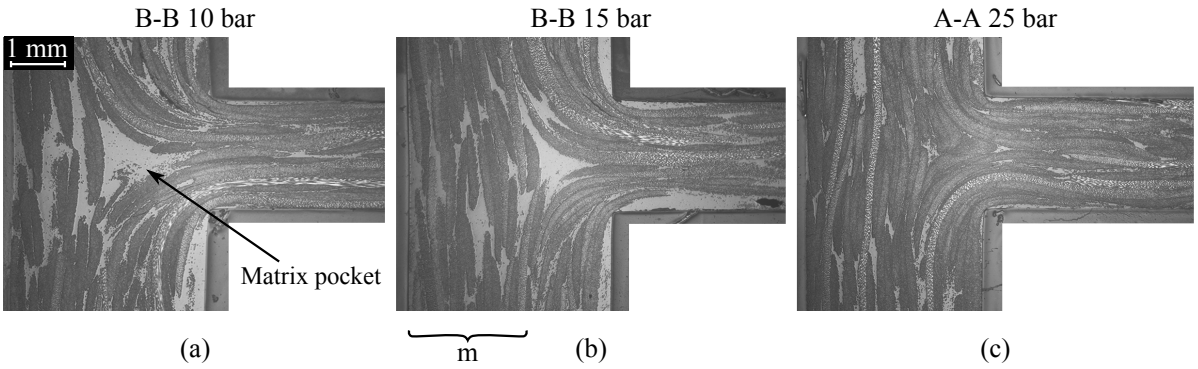


**Figure 4.9** *Cross sections of deep rib showing different size of matrix pocket, visible as a triangular region, at the entrance of the rib. A-A is a section at the center of the plate and B-B is a section at the edge of the rib (see Figure 4.6). The consolidation pressure is indicated in the label. The flake size and dwell time are 10 mm and 15 minutes respectively. The layer of material in the base plate above the triangular matrix pocket is denoted as m.*

of the rib where the flow is non-uniform through the thickness. This effect is also observed in the simplified theoretical analysis performed in [19] for SMC materials and was attributed to the form of the streamlines of the flow. The theoretical flow patterns near the rib entry suggest that, as the flow merges into the rib, a region of non-uniform flow exists at the entrance of the rib. Moreover, the size and location of the matrix pocket depend on: the entrance geometry, the rheological behavior of the material and the boundary conditions [19]. The experimental observations from the present study indicated that the matrix pocket at the rib entry is observed to be more prominent, especially with lower consolidation pressure or at the edges of the rib (close to section B-B, see Figure 4.9) where the rib ends abruptly. The change in the geometry of the rib entry makes the flow more non-uniform. Therefore, the analysis discussed below is focused on the section A-A since the flow mechanism is not the same in section B-B. Moreover, on a long rib, the majority of the rib falls under a scenario of flow similar to section A-A.

Despite the presence of a matrix rich entrance region, sink marks were found to be negligible. This is due to the layer of material present above the entry region in the thick base plate, which masks the matrix rich zone beneath it, denoted by $m$, as seen in Figure 4.9 (b). However, this is a qualitative representation and further study is required to characterize the layer thickness $m$.

### 4.3.3 Effect of consolidation pressure

Figure 4.10 shows the average area fraction of the matrix rich regions measured from the cross-sectional micrograph (section A-A) and the error bars show one standard deviation from the mean. The data is obtained from plates molded with a fixed

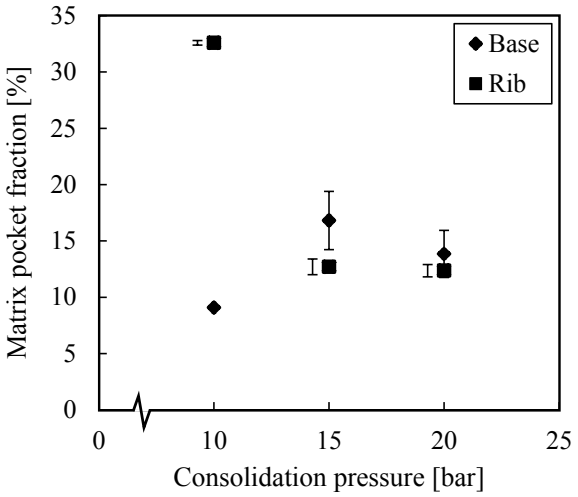


**Figure 4.10** *Area fraction of matrix pockets as a function of consolidation pressure for a flake size of 10 mm and a dwell time of 15 minutes. The error bars show one standard deviation from the mean. Some of the error bars are offset horizontally for clarity.*

flake size of 10 mm and three different consolidation pressures. As the consolidation pressure is increased, the fraction of matrix pockets in the rib tends to reduce. With a large pressure, the flakes can be effectively pushed into the rib overcoming the resistance to flow and the resistance of the flake to deform (bend). The base section shows a complimentary trend due to the conservation of volume of the material. Furthermore, with the largest investigated pressure of 20 bar, the base and the rib section show a similar amount of matrix pockets implying a relatively homogeneous distribution of the matrix pockets compared to a lower processing pressure.

### 4.3.4 Effect of flake size

To study the dependency on flake size, specimens were molded with flake sizes of 10 mm and 12.5 mm with a fixed consolidation pressure of 15 bar. Figure 4.11 shows the average area fraction of matrix rich regions in the rib and base sections for two different flake sizes. As the flake size increases, the ability to fill the ribs reduces for a constant consolidation pressure due to the increased resistance to flow into the rib and due to bridging of the entrance. Consequently, the bridging of flakes at the rib entrance induces a filtering effect or in other words, the percolation flow of matrix tends to dominate due to the pressure difference between the base plate and the rib cavity. This effect can be observed in the increasing matrix pocket fraction in the ribs with an increase in the flake size. As mentioned earlier, the random nature of the material causes larger scatter in the observed values. Nevertheless, the results provide a qualitative understanding of the filling behavior.

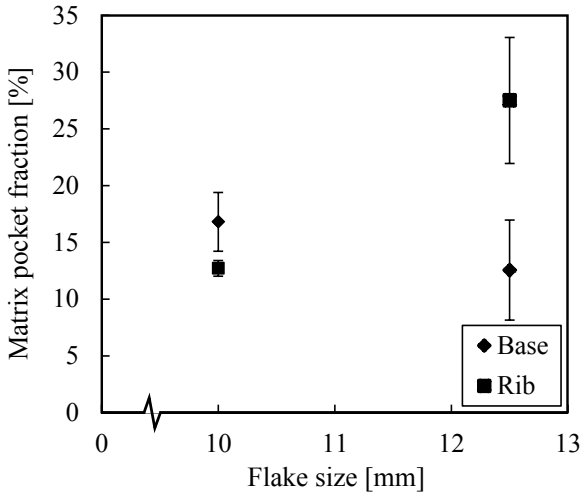


**Figure 4.11** *Area fraction of matrix pockets as a function of flake size with a consolidation pressure of 15 bar and a dwell time of 15 minutes. The error bars show one standard deviation from the mean.*

### 4.3.5 Effect of consolidation dwell time

Figure 4.12 shows the effect of consolidation dwell time on the amount of matrix pockets in the rib and base sections. The specimens were molded with flakes of size 10 mm with a consolidation pressure of 15 bar. As the dwell time is increased, the bed of flakes has more time to get compacted. Therefore, if favorable conditions prevail, the matrix percolates through the bed towards the low pressure regions. In this case the matrix pockets in the rib sections tend to increase as a result of percolation of matrix replacing voids. Moreover, previous studies on woven flake material [12, 13] have shown the possibility of agglomeration of the flakes and formation of a mechanically jammed region at random locations during the mold closing process. Under such conditions, the jammed flakes start carrying a part of the consolidation pressure thereby creating heterogeneously distributed low pressure regions, which further drives the percolation of the matrix. Measurement of the matrix pockets in the jammed regions located randomly in the rib stiffened plate showed a matrix pocket fraction of 17.5 % and 3 % for consolidation dwell time of 15 and 25 minutes respectively. This shows that the resin migration out of the jammed regions makes the jammed region dry and the adjacent regions rich in matrix content. However, with a positively closed mold (no flash boundary condition), this effect should be less prominent since the macroscopic compaction of the fiber bed cannot happen unless the matrix material seeps out of the mold assuming incompressible constituents. Moreover the results presented are from a minimal number of specimens and further effort is needed to establish a quantitative relationship.

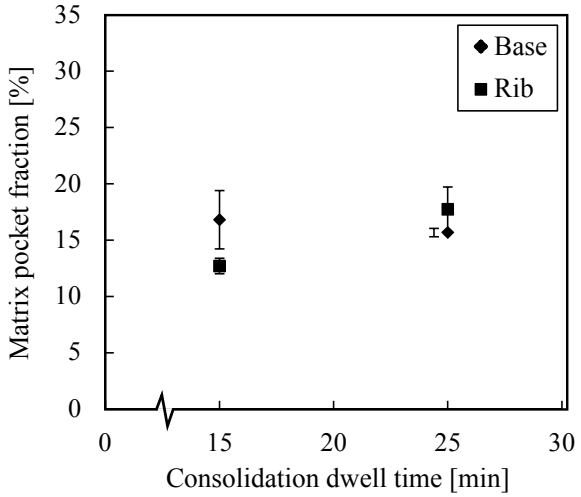


**Figure 4.12** *Area fraction of matrix pockets as a function of consolidation dwell time. The error bars show one standard deviation from the mean. Some of the error bars are offset horizontally for clarity.*

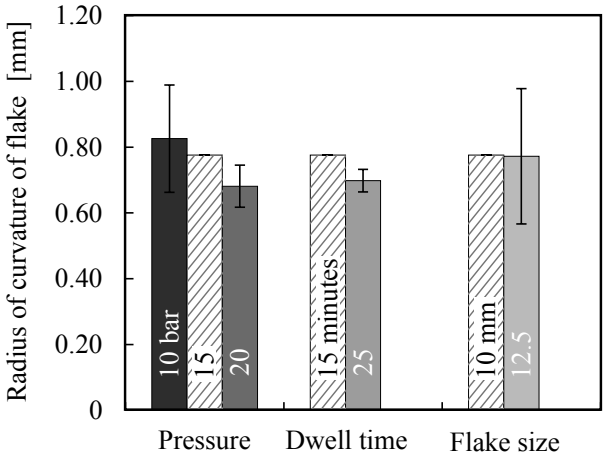


**Figure 4.13** *Radius of curvature of the flakes at the entry corner of the rib ($r_e$) as a function of consolidation pressure, dwell time and flake size. The hatched bars represent the reference configuration. Other bars represent a systematic change of the respective variable from the reference configuration.*

### 4.3.6 Entry radius

Near the corner of the rib entry and the corners at the end of the rib, matrix rich regions are found, as seen in Figure 4.9, since the flakes cannot conform to a sharp corner. However, the flakes bend near the corners and the bending radius reduces as the pressure increases or the dwell time increases. Figure 4.13 shows the observed radius of curvature of the flakes/fiber bundles at the entry corner $r_e$. The effect of pressure, dwell time and flake size is shown. The flexural rigidity ($EI$) of the flake material is the major parameter involved, where $E$ is the flexural stiffness and $I$ is the second moment of area. The parameter $EI$ is a function of the flexural stiffness of the fibers, the architecture of the woven fabric and the frictional behavior of the fibers and bundles making up the fabric. With sufficient applied pressure, the flakes can take the shape of the rib corners.

The consolidation dwell time is observed to have a similar effect as pressure possibly due to increasing compaction of the fiber bed as discussed earlier. In the case of larger flakes, due to the difficulties in flowing, the architecture of flakes might have got disturbed and hence the observed results show a large scatter in the radii at the entrance, unlike the case of smaller flakes.

## 4.4 Results and discussion: Small rib

The results of the experimental study on molding of small ribs with different aspect ratio are discussed in this section. The filling process described in Section 4.3 can be assumed to hold in this case as well, except for the possible additional effects caused by the flashing of the material at the mold boundaries and the multiple ribs present in the part. Experimental observations show a significant difference in the consolidation quality of the chopped woven semi-preg material, compared to observations from the deep rib, when the material is allowed to flash-out. However, both the test cases show changes in the distribution of flakes and matrix as a function of the experimental variables.

Figure 4.14 shows a molded plate and a typical section of a 4 mm wide rib molded with flakes of size 5 mm with a consolidation pressure of 5 bar. Three types of regions can be observed to occur in all the test cases, namely voids (V) in the matrix phase, matrix rich regions (MR) or matrix pockets and non-impregnated regions in the fiber bundles (NI). This is substantially different from the observations in the case of deep rib (refer to Section 4.3). Therefore, in this part of the study the filling quality is quantified with the following three parameters, namely V, NI and MR. Information from both dark field and bright field micrographs are used to obtain the data by image analysis procedure, especially for the non-impregnated regions in the fiber bundles.

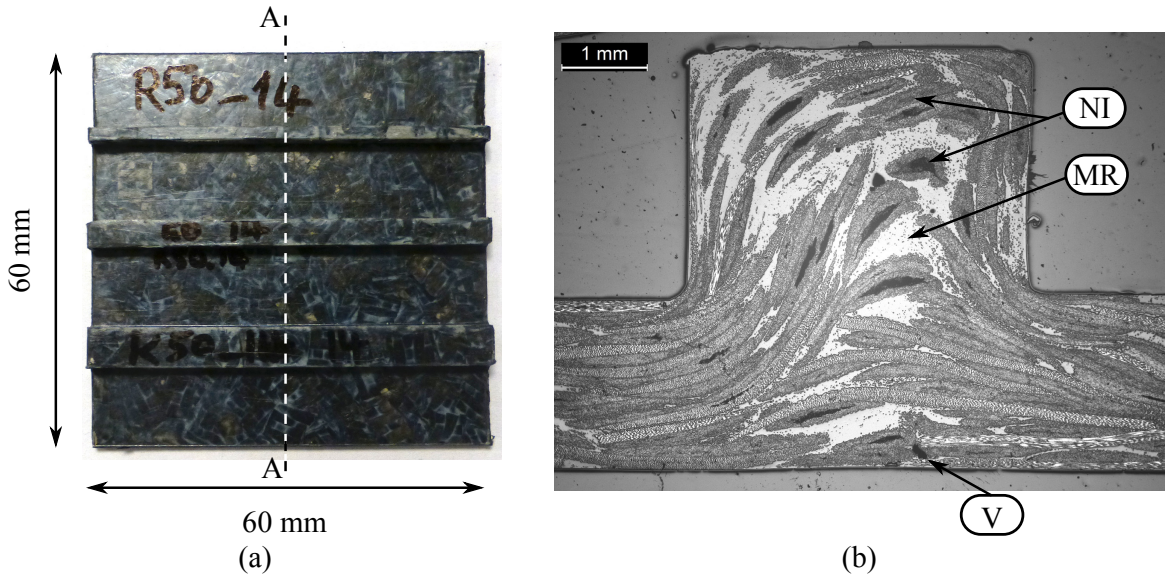


**Figure 4.14** *(a) Rib side view of the molded plate with ribs of width 2, 4 and 6 mm using 5 mm flakes and 5 bar pressure. (b) A typical cross-sectional (dark field) micrograph at section A-A of a 4 mm wide rib showing impregnated fiber bundles, matrix pockets, partially impregnated fiber bundles. Some of the non-impregnated regions are not visible in the dark field image.*

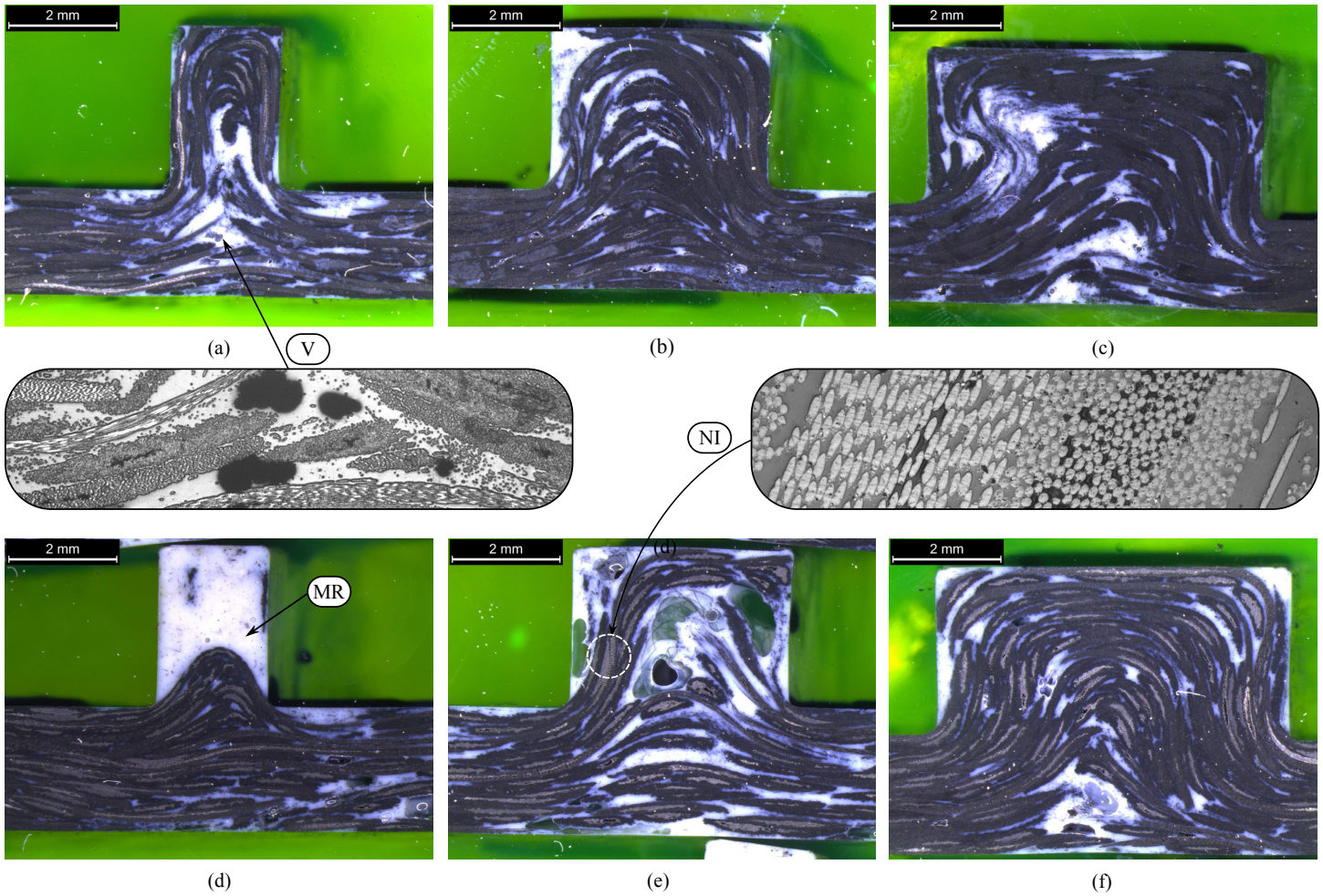


**Figure 4.15** *Micrograph of rib sections with different parameter combinations. (a-f) bright field images showing white matrix rich regions (MR), voids (V) and non-impregnated bundles (NI). The insets are dark field images showing the V, NI regions at a larger magnification. The regions adjacent to the NI places are well impregnated.*

### 4.4.1 Rib filling

The specimens in the first row of Figure 4.15 were molded with flakes of size 5 mm (see Table 4.1 for other process settings) and the second row with 12.5 mm flakes. The columns correspond to different consolidation pressures of 5, 10 and 15 bar. It can be observed from (a), that 5 bar pressure is sufficient to fill the 2 mm wide rib with 5 mm flakes. However, the non-uniformities such as matrix pockets at the junction of the rib and base, the presence of voids and non-impregnated core of the fiber bundles suggest a poor consolidation quality. When larger flakes were used for molding the 2 mm wide rib (d), severe fiber-matrix separation was observed. As mentioned earlier, the larger the flake size, the larger is the required deformation of the flake, which requires a larger force for filling a thin rib or for a large ratio of flake size to rib width. With insufficient pressure, the flakes bridge the rib entry region without flowing inside. Adversely, the bridging flakes at the rib opening act as a filter and allow the matrix to percolate into the rib under the applied consolidation pressure, until the pressure difference between the base plate and the rib cavity becomes negligible.

Similarly, in the other cases shown in Figure 4.15, such as (e), the filling of the rib is mostly disturbed by the formation of voids at the entrance and in the corners (bottom of rib) due to the insufficient pressure available to push the flakes inside the rib. These consolidation defects also show that the pressure at the rib section is below the average applied pressure. Apart from bridging of flakes at the rib entrance and the flash boundaries, another possible cause for insufficient consolidation pressure might be due to the formation of mechanically jammed regions (see Section 4.3.5) next to the ribs, which causes an uneven local pressure distribution. Moreover, the base plate in most of the cases seems to be impregnated well compared to the ribs and the rib-entry region. Therefore, in this part of the study only the rib section is analyzed and the definition of the rib section is extended to the base plate including the junction at rib entrance.

### 4.4.2 Effect of flake size and consolidation pressure

Figure 4.16 shows the fractional void content present in the matrix phase for different rib sections molded with different flake sizes as a function of the consolidation pressure. Due to the stochastic nature of the material, only a qualitative trend can be obtained from the results. In general, as the consolidation pressure increases, the void content reduces for all the investigated rib aspect ratios and flake sizes. However, at the maximum pressure tested, the void fraction tends to increase, especially for the medium size rib (4 mm) and a large flake size combination. A possible reason is the larger non-uniformity of flow at the entrance region due to high pressure, compared to experiments with lower applied pressure. A large pressure creates a non-uniform flow at the rib entrance where the flow from the sides merge and enter the rib.

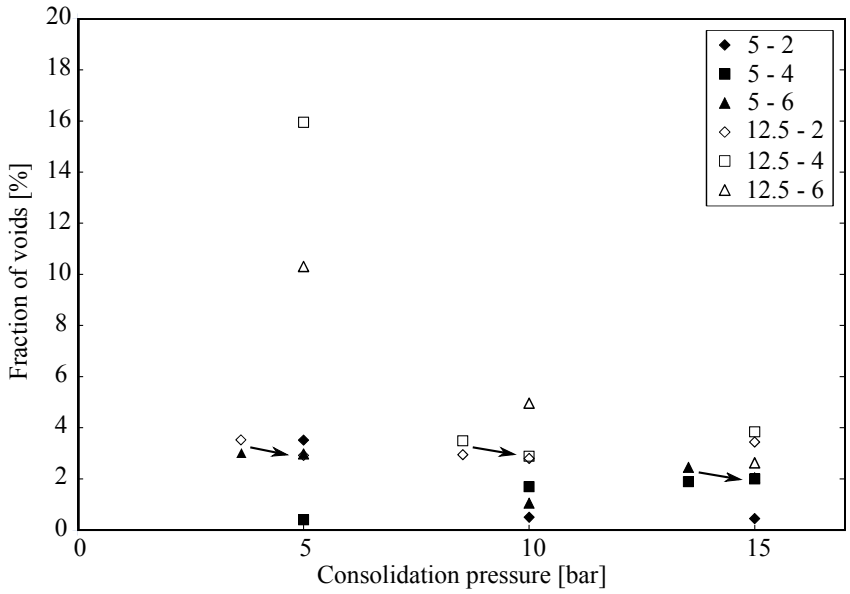


**Figure 4.16** *Area fraction of voids in the matrix phase as a function of consolidation pressure. Data is presented for flake sizes of 5 and 12.5 mm and rib widths of 2, 4, 6 mm. Legend entries: flake size - rib width in mm.*

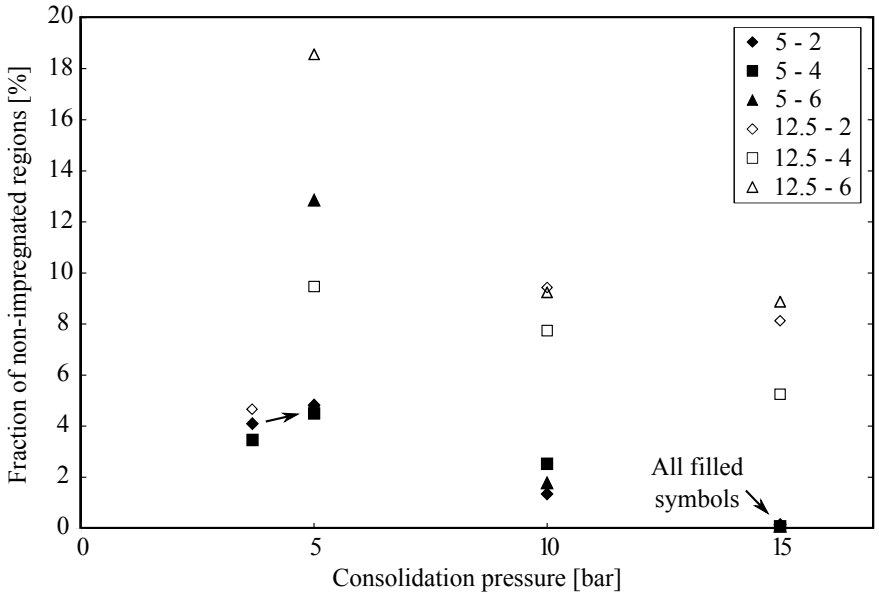


**Figure 4.17** *Area fraction of non-impregnated regions in the fiber bundles as a function of the consolidation pressure, flake size and width of rib. Legend entries: flake size - rib width in mm.*

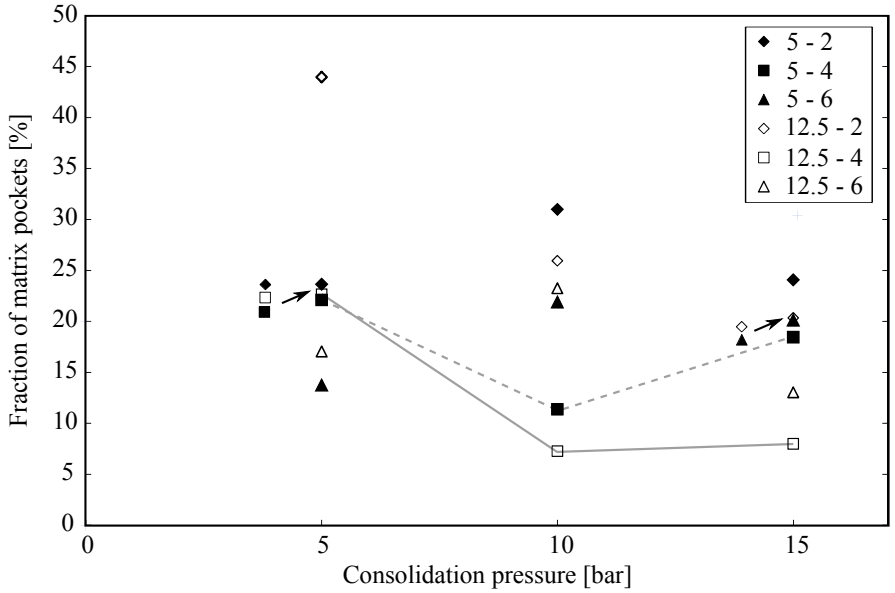


**Figure 4.18** *Area fraction of matrix pockets in the rib section as a function of the consolidation pressure, flake size and width of rib. The trend of the medium sized rib is shown with a dashed (5 mm) and a solid line (12.5 mm flake). Legend entries: flake size - rib width in mm.*

Figure 4.17 shows the fraction of non-impregnated regions present in the rib sections. The fraction of non-impregnated regions tend to reduce consistently with increasing consolidation pressure for both flake sizes. However, the absolute values are much smaller in the case of 5 mm flakes. As the flake size gets smaller the material gets more homogeneous compared to larger flakes, which correlates with the reduced amount of voids and non-impregnated regions observed in the case of smaller flakes.

Fiber-matrix separation as mentioned in the previous section manifests itself as pockets of matrix between the fiber bundles visible in the rib sections. As it can be seen in Figure 4.18 that for thinner rib sections and large flake sizes, test case 12.5 - 2, the matrix pockets reduce consistently. Whereas, increasing the width makes the ribs more fillable with less matrix pockets for a certain pressure.

However, as the pressure increases the non-uniformity of the flow at the rib entrance increases and the matrix starts getting accumulated in regions with less pressure and corners. This can be observed in the case of medium size ribs indicated as dashed and solid lines. Initially, a decreasing matrix pocket fraction can be observed and as the pressure is increased further, the matrix rich regions also increase due to the above mentioned entrance effect. This suggests that an optimum consolidation pressure might exist so as to obtain a minimal separation of the matrix. However, more quantitative data is required to prove this hypothesis.

In summary, for a fixed flake size and a rib opening, the filling quality can be observed to improve with the increase in consolidation pressure, however, beyond a limiting pressure the fiber-matrix separation tends to have a non-monotonic behavior,

as seen in the dashed and solid lines in Figure 4.18. Consequently, the difference in fiber volume fraction between the rib and base section becomes large which in turn affects the mechanical performance of the part.

## 4.5 General discussion: Practical applicability

The experimental observations show the need for a proper combination of design, material and process parameters to obtain a certain filling quality in the ribbed region. This section of the article summarizes the results with a view to transferring them to a real life application.

Table 4.2 shows a summary of parameters grouped into different categories which play a role in the compression molding of chopped woven fabric materials. The design parameters and the material parameter such as flake length ($l$) or the probability density function (pdf) of the distribution of flake length pdf($l$), can be modified independently to obtain the required part properties. However, the interconnection between the different groups as discussed earlier, and between parameters of the same group, such as $\eta = \eta(l, v_f, \text{pdf}(l))$, gives rise to a rather complicated behavior of the material. This study provides a preliminary overview of the behavior, nonetheless, it can be used as a starting point for a more thorough study by non dimensionalizing groups of parameters and using them as variables for the experiments.

| Design parameters |
|---|
| Part design: base thickness ($t_b$), rib width ($w_r$), rib depth ($d_r$), entry radius ($r_e$); Tool design: flash edges, draft angle |
| **Material parameters** |
| Viscosity of polymer ($\eta$), fiber volume fraction ($v_f$), stiffness of fabric ($E$), flake length ($l$), flake length distribution (pdf($l$)), flake thickness ($t_f$) |
| **Process parameters** |
| Processing temperature ($T$), consolidation pressure ($P$), mold closing speed ($\dot{h}$), consolidation dwell time ($\tau_{\text{dwell}}$), filling pattern of flakes |

**Table 4.2** *Important parameters involved in compression molding of discontinuous composites.*

### 4.5.1 Aspect ratio of rib

This subsection illustrates the interconnection between the rib aspect ratio, anomalies in flake or matrix distribution and the location of the rib in the plate. A suggestion for the design of a deep rib with tapered depth at the lengthwise edges is proposed.

From the experimental observations made in this study, for a small aspect ratio rib (relatively large depth), a high pressure is required to reduce the matrix rich junction at the rib entrance and to obtain a better distribution of flakes along the entire depth of the rib. Therefore, a deep rib located at the far edge of a large part consequently would tend to have a large non-uniformity at the rib entrance and thus reduced fiber content at the bottom of the rib. This is due to the lower pressure at the edge of the large part and due to the presence of flash edges. Furthermore, a homogeneous distribution of flakes/fiber bundles with a small matrix pocket at the entrance would reduce the possibility of cracks due to reduced differential shrinkage. Additionally, the choice of a smaller flake size when molding parts with deep and thin ribs would reduce the flow resistance and a large deformation of the flakes. Therefore, a better distribution of the matrix and flakes can be attained at lower consolidation pressures.

As discussed earlier, material flowing into the rib has to overcome a resistance at the rib entrance. Figure 4.19 shows an illustration of the material flowing from two land faces into the rib. Considering a section of the rib, the material from the two sides of the base plate flows in to the rib, which can be assumed to be a two dimensional flow along the length of the rib. However, at the lengthwise edges an additional face (land) of the base plate exists. In such places the flakes can have more resistance to flow inside, or have a higher chance of bridging the opening of the rib cavity. Consequently, a large pressure is needed to push the flakes to the entire depth. Therefore, introducing a taper in the depth direction towards the lengthwise edge provides a better filling of the rib with fibers at edges.

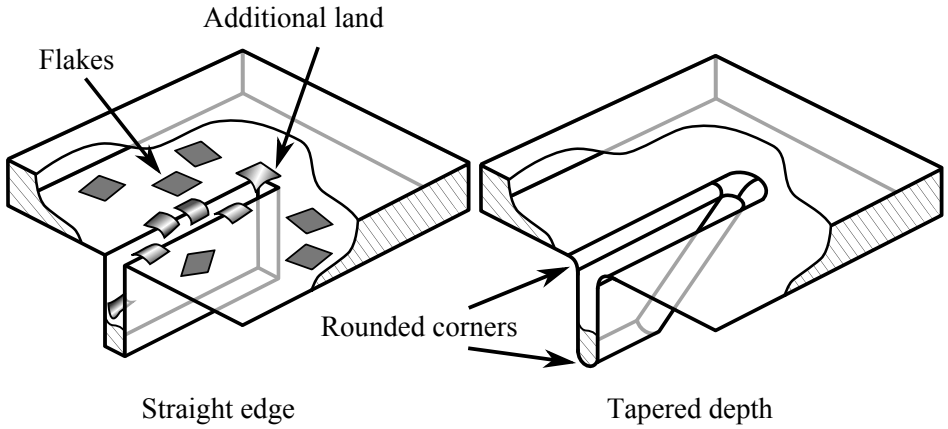


**Figure 4.19** *Illustration of a deep rib with a straight vertical edge and a tapered depth at the end of the rib. Rounded corners are also illustrated. Only a few flakes are shown for clarity.*

Furthermore, smaller ribs (less deep ribs) can be added where consolidation pressures are expected to be lower than the nominal applied pressure, since small ribs tend to have lesser anomalies at the entrance compared to deep ribs.

### 4.5.2 Entry radius and corner radius

From the experimental observations, it can be observed that the flakes do not conform to sharp corners and hence cause matrix pockets close to the entrance, and the corner of the rib near the blind end. Therefore, a small radius can be included, as illustrated in Figure 4.19, to reduce the matrix regions at the sharp corners which are prone to initiate failure due to the stress concentration. The choice of the minimum radius can be based on the flexural rigidity of the flakes which is a function of the fabric architecture for thin flakes. Moreover, the entry radius is found to reduce the flow resistance of the material into the ribs, however, it also tends to increase the sink mark due to the creation of a large region of disturbed flow near the rib entrance [19]. Hence, a minimal radius can be used such that the flakes can conform to the shape and avoid using larger radius to avoid sink marks.

## 4.6 Conclusions

The compression molding process of rib stiffened plates with chopped woven reinforcements has been experimentally investigated in this study. Semi-preg material based on thermoplastic matrix and fabric reinforcement was chopped into smaller flakes to be used as the molding compound. The filling behavior with different combinations of design, material and process parameters has been analyzed and discussed qualitatively and quantitatively. The results show that for high quality parts with a specific flake size and rib opening combination, the choice of the consolidation pressure is essential for obtaining proper impregnation and low void content. At the same time, the consolidation pressure should be bounded for limiting excessive fiber-matrix separation. A similar trend is observed with the consolidation dwell time due to the percolation flow of matrix towards low pressure regions. Moreover, in the presence of flash edges, a larger pressure is required for proper impregnation due to matrix seeping through the least resistant path of flash. Therefore, the consolidation process window should be selected such as to provide adequate time for filling and void suppression, but should be limited to avoid intensification of jammed regions and matrix rich rib sections. Moreover, an entry radius at the rib entrance and a corner radius at the end of the rib could reduce the unevenly distributed matrix rich regions adjacent to these places. Thereby, this can potentially avoid failure initiation by reducing the contrast in properties near sharp corners. Furthermore, a depth taper is suggested at the lengthwise edges of deep ribs

so as to attain better distribution of fibers in the entire depth at the lengthwise edges. The choice of flake size depends on other factors, such as part property requirements, however, for obtaining a better distribution of flakes in deep and thin ribs a smaller flake size should be considered or a higher consolidation pressure. In the future, the knowledge gained from this experimental investigation can be used as a basis for the development of semi-analytical process models considering a meso-scale flow and a pseudo random arrangement of flakes for ribbed sections. Further study is required to quantify the closing rate dependency in filling of deep ribs.

# References

[1] L. Orgéas, P. J. J. Dumont, T. . Le, and D. Favier. Lubricated compression of bmc, a concentrated and fibre-reinforced granular polymer suspension. *Rheologica Acta*, 47(5-6):677–688, 2008.

[2] Olivier Guiraud, Pierre J. J. Dumont, Laurent Orgéas, Jean-Pierre Vassal, Thai-Hung Le, and Denis Favier. Towards the simulation of mould filling with polymer composites reinforced with mineral fillers and short fibres. *International Journal of Material Forming*, 3(2):1313–1326, October 2009.

[3] Roberto J. Silva-Nieto. *Prediction and characterization of compression mould flow for unsaturated polyester resin sheet moulding compound*. Thesis, Loughborough University, 1980.

[4] M. R. Barone and D. A. Caulk. A model for the flow of a chopped fiber reinforced polymer compound in compression molding. *Journal of Applied Mechanics*, 53(2):361–371, June 1986.

[5] G. Kotsikos and A. G. Gibson. Investigation of the squeeze flow behaviour of sheet moulding compounds (smc). *Composites Part A: Applied Science and Manufacturing*, 29(12):1569–1577, December 1998.

[6] P. Dumont, L. Orgéas, S. Le Corre, and D. Favier. Anisotropic viscous behavior of sheet molding compounds (smc) during compression molding. *International Journal of Plasticity*, 19(5):625–646, May 2003.

[7] J. Fudge. "HexMC - Composites in 3D" a new high performance molding compound. In *SAMPE Technical conference proceedings*, 2001.

[8] G. Kotsikos, J. H. Bland, and A. G. Gibson. Rheological characterization of commercial glass mat thermoplastics (GMTs) by squeeze flow testing. *Polymer Composites*, 20(1):114–123, February 1999.

[9] Ronnie Tornqvist, Paul Sunderland, and Jan-Anders E. Månson. Determination of the rheological properties of thermoplastic composites for compression flow molding. *Polymer Composites*, 21(5):779–788, October 2000.

[10] M. A. Dweib and C. M. ÓBrádaigh. Extensional and shearing flow of a glass-mat-reinforced thermoplastics (GMT) material as a non-newtonian viscous fluid. *Composites Science and Technology*, 59(9):1399–1410, July 1999.

[11] Gilles-Philippe Picher-Martel. *Compression moulding of randomly-oriented strands thermoplastic composites: A study of the flow and deformation mechanisms*. PhD thesis, McGill University, Quebec, Canada, 2015.

[12] M. I. Abdul Rasheed, B. Rietman, H. A. Visser, and R. Akkerman. Rheological behavior of chopped fabric reinforced thermoplastic prepreg: Squeeze flow. *In preparation for submission in Composites Part A*, 2016.

[13] M. I. Abdul Rasheed, B. Rietman, H. A. Visser, and R. Akkerman. Experimental investigation of a flow phenomenon in processing woven composite flakes: Jamming. *In preparation for submission in Composites Part A*, 2016.

[14] S.K. Christensen, B. Hutchinson, E.M. Sun, T.A. Osswald, and B.A. Davis. Fiber-matrix separation in ribbed SMC and BMC parts. In *Proceedings of the SPE-ANTEC*, volume 1, page 782, 1997.

[15] Alejandro Londoño-Hurtado, Juan Pablo Hernandez-Ortiz, and T.A. Osswald. Mechanism of fiber-matrix separation in ribbed compression molded parts. *Polymer Composites*, 28(4):451–457, 2007.

[16] P. Dumont, L. Orgéas, D. Favier, P. Pizette, and C. Venet. Compression moulding of smc: In situ experiments, modelling and simulation. *Composites Part A: Applied Science and Manufacturing*, 38(2):353–368, February 2007.

[17] Laurent Orgéas, Pierre J. J. Dumont, Veronique Michaud, and Denis Favier. Separation of the polymer matrix and the fibrous reinforcement during compression moulding of glass mat thermoplastics (GMT). *International Journal of Material Forming*, 1(1):929–932, April 2008.

[18] W.S. Rasband. ImageJ, U. S. National Institutes of Health, Bethesda, Maryland, USA. http://imagej.nih.gov/ij/, 1997-2015.

[19] Kenneth L. Smith and Nam P. Suh. An approach towards the reduction of sink marks in sheet molding compound. *Polymer Engineering & Science*, 19(12):829–834, September 1979.

# Chapter 5

# Effect of meso-scale morphology on the scatter of mechanical properties of woven-flake reinforced composites*


### *Abstract*

Thermoplastic composites made of chopped woven prepregs are investigated in this study. The stochastic nature of discontinuous molding compounds leads to a large variability in strength. However, at present there is little means of quantifying the variability that plays a crucial role in estimating the design allowable. The aim of this study is to widen the knowledge base and answer basic questions like: how much scatter can be expected? And does variability in strength saturate with increasing reinforcement size? A systematic approach for estimating a statistically based design allowable for tensile strength is proposed based on the principles of mechanics and extreme value statistics. Intuitive insights are quantified, such as increase of variance in strength with larger sized reinforcements and decrease in strength with a longer specimen. Finally, some preliminary guidelines for narrowing down the choice of flake size based on design, manufacturing and strength aspects are briefly touched upon.


*Reproduced from: M.I. Abdul Rasheed, B. Rietman, H.A. Visser, R. Akkerman. Effect of meso-scale morphology on the scatter of mechanical properties of woven-flake reinforced composites. Submitted to *Journal of Composite Materials*, **2016**.

## 5.1 Introduction

The increasing popularity of high performance thermoplastic composites (TPC) in the aerospace and automotive sectors stems from the need for lightweight materials with cost effective manufacturing and recycling processes. However, limitations in the processing of complex parts with continuous fiber reinforced materials, such as limits in formability and formation of wrinkles, remain intact. Introducing discontinuities in the highly stiff reinforcing phase such as micro perforations [1], array of slits [2] or breaking at natural break points by stretching [3] enables a higher degree of formability. Manufacturing of 3D geometries with a high fiber volume content requires more frequent discontinuities in the continuous fiber material. One such case of having frequent discontinuities is the use of chopped prepreg materials. One of the downsides of having discontinuities in the materials is the introduction of stress concentrations, which lead to reduced macroscopic mechanical properties compared to continuously reinforced composites. In this investigation, tensile strength of composites with chopped prepreg material with a woven architecture is studied experimentally and a statistical framework is developed.

The theory for 1D discontinuous reinforcements (chopped fibers) at dilute concentrations can be extended to composites with planar reinforcements (PRC) by applying the theory to the in-plane directions of the planar reinforcement. The former is studied [4] and used widely in many engineering applications owing to manufacturability of parts at lower fiber concentrations compared to continuous fiber composites. Whereas, the latter has been studied mostly theoretically assuming highly ordered structures with few model experiments [5, 6]. Hence, in the case of PRC, further development is required for maturing towards real world application. In this study a randomized structure with a fiber concentration comparable to continuously reinforced composites is investigated.

Recently, engineering applications for chopped materials based on both thermoplastics (TenCate BMC®) and thermosets (Hexcel HexMC®) are being developed owing to their formability, manufacturability of near net-shaped complex geometries with compression molding processes, without losing the possibility of retaining larger reinforcements. Several experimental studies have been carried out on the basic mechanical properties of such materials with unidirectional (UD) flakes of different sizes e.g. [7, 8] and very few in the case of woven flakes [9, 10]. It is worth noting that in the case of woven fabrics, the crimps in the fabric provide a local structural integrity to the flake, unlike UD flakes. Even though flake failure is theoretically plausible, the observed failure is mostly matrix dominated with flake pull out [7, 10]. A similar failure mode was observed in this study with randomly positioned and oriented flake systems. Furthermore, the crack usually tends to avoid the agglomeration of flakes and progresses through the lesser resistant matrix [10]. From the above observations it can be noted that the failure almost always occurs

at the flake-matrix interface and avoids the reinforcements leading to a meandering crack path.

Literature on the mechanical properties of PRC in the case of biological materials, like nacre, is vastly available unlike engineering materials. Nacre efficiently achieves mechanical properties with a mostly regular staggered pattern of mineral platelets (95 % by volume) bonded by bio-polymer [11]. The optimum strength was found to be a function of critical overlap length and the properties of the constituents [11]. Besides overlap, the local structural arrangement of the platelets has a major role in the failure mechanism [12, 13]. Precise control of the arrangement of reinforcements is not feasible in engineering applications with a potential for high volume production. In a typical compression molding process, the mold cavity is filled with chopped prepreg material uniformly spread in all places, leading to a random positioning of reinforcements. The material flows to fill the cavity, thereby relocating and re-orienting the reinforcements, depending on the process settings. Consequently, with random size, positions and orientations the local structural arrangement of the platelets (and thus of the flake-matrix interfaces) is also random leading to stochastic failure and a large scatter in material properties. Understanding of the stochasticity in failure is still missing, despite the fact that it is vital when such materials are applied for structural applications.

The aim of this study is to generate a fundamental understanding of the scatter in the tensile strength due to the randomness in the structure, size of the prepreg flakes and length of the specimen. Design values for the tensile strength of such stochastic materials with random structural arrangement is obtained with a systematic approach as shown in Figure 5.1. A Metropolis Monte-Carlo packing algorithm is used to generate representative volumes containing randomly overlapping flakes of fixed length and thickness. The meandering crack path in the random structure is described by a non-dimensional measure, tortuosity. The tortuosity values are translated in to strength, based on phenomenological approximation. The statistics of shortest tortuous path followed by the hypothetical cracks is estimated from the generated volumes with extreme value theory and inferential statistics [14]. Experiments are performed on model (woven) flake systems molded with different overlap lengths to provide an insight on the effect of overlap. Plates molded with different flake sizes, random position and orientation are tested to observe the scatter and to validate the theory.

## 5.2 Methodology

In this section the terms used throughout the article are defined and the different methods used to analyze the problem are briefly explained.

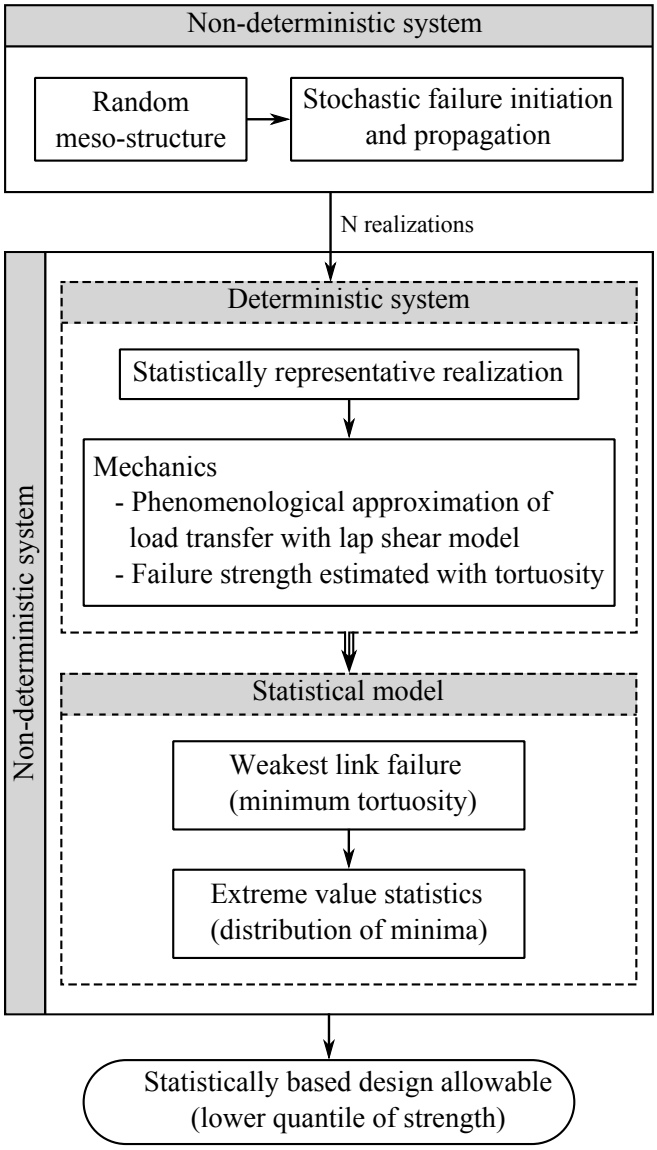


**Figure 5.1** *The approach followed in this research to study the problem of planar reinforced composites.*

### 5.2.1 Material definitions

Fiber reinforced composites have a hierarchical structure spanning multiple scales. The smallest of all is in the order of the filament diameter (6-8 $\mu$m for carbon fibers) referred to as micro-scale. Groups of filaments (yarns) are woven with a repeating pattern to form a reinforcing fabric. The basic repeating pattern is referred to as a unit cell and is shown in Figure 5.2 (a) for a 5 harness satin weave with 3000 filaments per yarn. The prepreg fabric is chopped in to flakes in the order of the size of a unit cell. A local structural arrangement is generated by the overlapping flakes as illustrated in Figure 5.2 (b,c) and is referred to as the meso-structure. The meso-structure spans

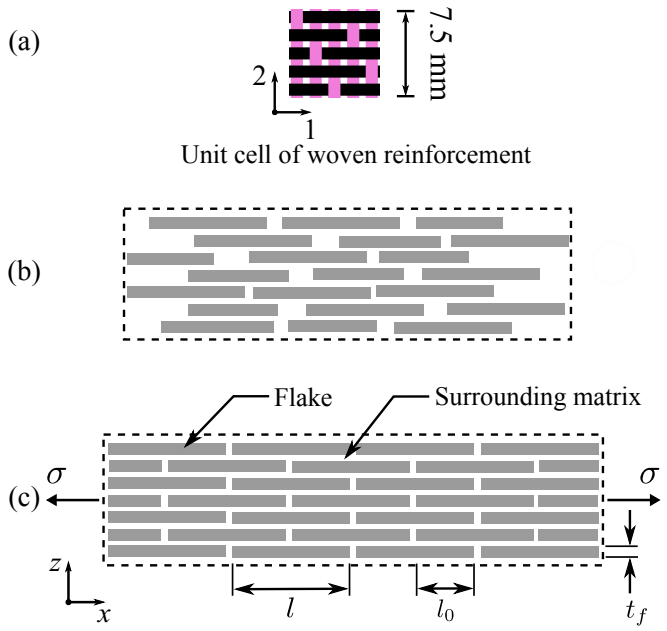


**Figure 5.2** *(a) Unit cell of a typical 5 harness satin weave. (b) Random in-plane arrangement of flakes through the thickness of a plate. The flakes are shown as rectangles. (c) An idealized brick and mortar arrangement showing the loading axis and typical variables.*

the entire specimen creating the macroscopic PRC shown in Figure 5.3. Furthermore, a representative volume is defined in the order of the size of a standard tensile test specimen ASTM D3039 for the purpose of statistical analysis of failure.

### 5.2.2 Chopped prepregs: process and properties

Flakes chopped from the prepreg materials have a uniform thickness and fiber content. Flakes are shaped as regular quadrilaterals for the feasibility of the study. However, in practice all shapes and thicknesses might be used based on the prepreg material. The size of the unit cell is considered as a geometrical limit for the flake size, below which weave pattern is not stable and a complete disentanglement of the weave can occur during processing. Additionally, for flake sizes larger than the unit cell size, the edges of the flake might get disentangled depending on the flow leading to a flake with reduced effective size.

A compression molding process with a closed picture frame mold is used to consolidate chopped prepreg composite without addition of extra (polymeric) matrix material. As mentioned earlier, initial filling and the amount of flow during the process influences the final positioning of the flakes in the molded part. Macroscopic flow of flakes is assumed to be negligible since the mold is filled completely and is closed on all sides. Furthermore, an in-plane random orientation of flakes and negligible out-of-plane orientation is assumed in the consolidated part.

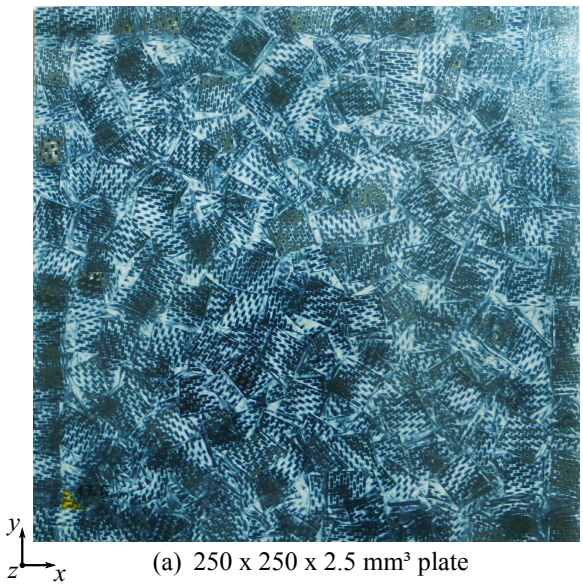


**Figure 5.3** *Chopped flake reinforced plate made of 15 mm square prepreg flakes.*

In the meso-scale, flakes are composites themselves and therefore, they inherit the mechanical properties of the parent prepreg based composite unless they get disentangled. The anisotropy of the flakes is not considered in this analysis, thus each flake is assumed to be isotropic. The interface between the flakes consists of the polymer in the prepreg flakes since no extra polymer is added during the process. The polymer at the interface is assumed to be an incompressible and linear elastic material. Hence, the von-Mises yield criterion is used to describe the failure envelope of the interface. The yield strength is given by $\tau_m^y = \sigma_m^{ult}/\sqrt{3}$, where $\sigma_m^{ult}$ is the ultimate uniaxial tensile strength of the polymer matrix.

### 5.2.3 Mechanics of load transfer and failure

**Load transfer between flakes**

Figure 5.2 (c) shows an idealized brick and mortar-like structure with the important meso-structural parameters namely, the flake length $l$, flake thickness $t_f$ and the overlap length $l_0$. The applied uni-axial tensile stress $\sigma$ is assumed to be parallel to the alignment plane.

In the classical sense, the applied load on the composite is transferred to the reinforcements via shearing of the polymer surrounding it, assuming the reinforcements are sufficiently separated [15, 16]. A similar approach is followed for platelets [5, 6]. In the case of PRC at higher fiber volume content, the closer packing of flakes leads to a thin interface compared to the thickness of the flake. Hence, a uniform shear stress at the inter-reinforcement region (thickness direction) [17] can be assumed unlike

the Cox's shear-lag theory. Therefore, a generalized form of stress transfer between overlapping adherends in a lap joint configuration with a thin interface layer is used in this study.

Simplified closed form solutions for adhesive bonds in single lap and double lap configurations have been developed in [18] for deterministic overlap lengths. The solutions are based on the assumptions of uniform or non-uniform state of shear stress along the length of the interface and the joint configuration. Figure 5.4 (a,b) shows an idealized cross section of the overlapping region of two flakes with a relatively thin interface and the forces acting on an infinitesimal section. The flakes are assumed to be disbonded at the ends.

The load transfer efficiency of the bonded flakes depends on the shear stress profile at the interface assuming elastic behavior. Figure 5.4 (c) shows the normalized shear stress profile relative to the average shear stress across the interface, for different overlap lengths [18]. Since the flakes (are assumed to) have identical elastic modulus and thickness, the obtained shear stress profile is symmetric about the center.

As the overlap length increases the relative peak at the boundaries increases, whereas it decreases further to very low values in the mid span. This indicates that most of the shear stress is transferred near the edges [11, 18]. Therefore, an optimum overlap length exists beyond which the overlapping flakes do not transfer any further load under a quasi-static load case [11]. A force balance between the flake rupture load and

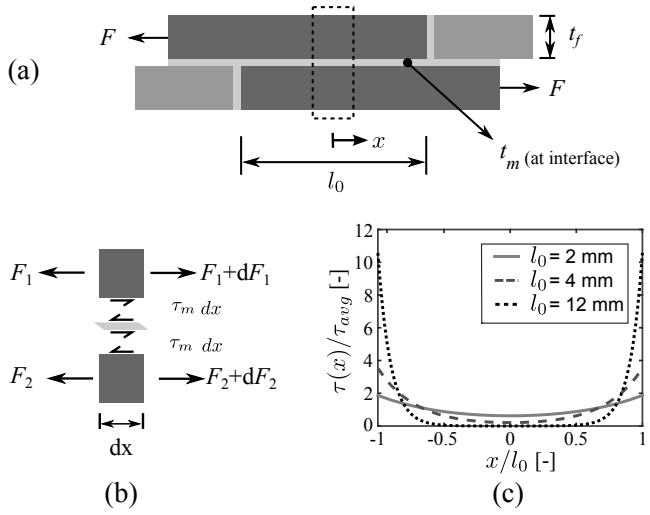


**Figure 5.4** *(a) An idealized cross section of the overlapping flakes in the molded plate with overlap length $l_0$. The adjacent flakes are shown in light gray. (b) Free body diagram of the configuration. (c) Normalized shear stress profile at the flake-matrix interface.*

failure load of interface results in a critical overlap length given by (see Figure 5.2 (c)),

$$L_c = \sqrt{\frac{\sigma_f^{ult} t_s}{(n-1)\tau_m^y}}, \tag{5.1}$$

where $\sigma_f^{ult}$ is the rupture stress of the flake, $\tau_m^y$ is the yield stress of matrix, $n$ is the number of adherends in the cross section and $t_s$ is the thickness of the specimen which is equal to $n \cdot t_f$. For overlap lengths ($l_0$) below $L_c$, the flakes are not loaded fully and a pull-out mode of failure can be expected. On the other hand, for $l_0 > L_c$ a higher load is transferred to the flakes, however, a rather poor interface might initiate a premature interface failure instead of failure of the flake itself.

The spatial distribution of flakes in the through-thickness direction is non-deterministic as illustrated in Figure 5.5. The random meso-structure can be considered to be a parallel connection of lap joints in a section and multiple such sections joined in series providing a macroscopic response. The strength of the link is based on the parallel connections and is denoted by $\sigma_{link}$.

Therefore, a closed form analytical solution for the load transfer considering both overlap distribution and random local meso-structure is non-trivial. Solving with finite element simulations is another possible option. However, a large number of repetitive computations for obtaining statistical significance lead to prohibitive computational cost. Hence, based on the experimental observations of failure, a phenomenological parameter is defined as explained below in Section 5.2.3.

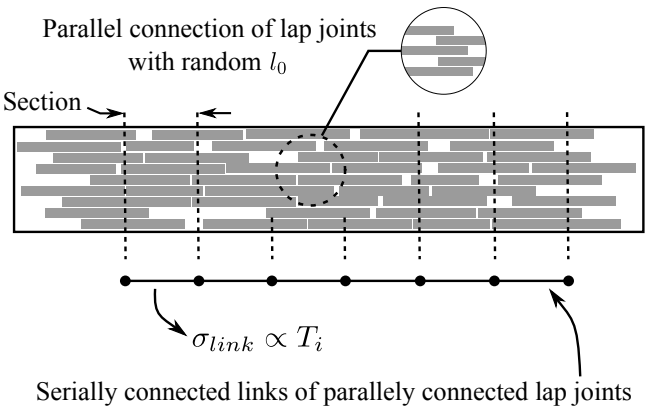


**Figure 5.5** *Hypothesized parallel-series connection of lap joints in a typical PRC with chopped prepreg flakes.*

### Tortuous path of failure

If the average shear stress in the interface reaches the shear strength of the interface material, the joint fails at the interface that acts as a crack initiator, as was discussed in Section 5.2.3. The crack further grows through the matrix rich regions, traveling through the path with least resistance. As mentioned earlier, the tensile failures observed in the specimens with randomly oriented and positioned flakes in this study were mostly adhesive failure between the polymer matrix and the flakes (see Figure 5.6 (b,d)). For a comparison, the failure in the case of aligned flakes is shown in Figure 5.6 (c). With a highly disordered microstructure, a similar adhesive failure has been observed in chopped carbon fiber reinforced PPS [19] as shown in Figure 5.6 (a). This effect was attributed to a weak adhesion between carbon and PPS matrix causing interface failure and thus fiber debonding. It is further intensified by the brittle nature of PPS interface leading to crack coalescence and a catastrophic failure of the material.

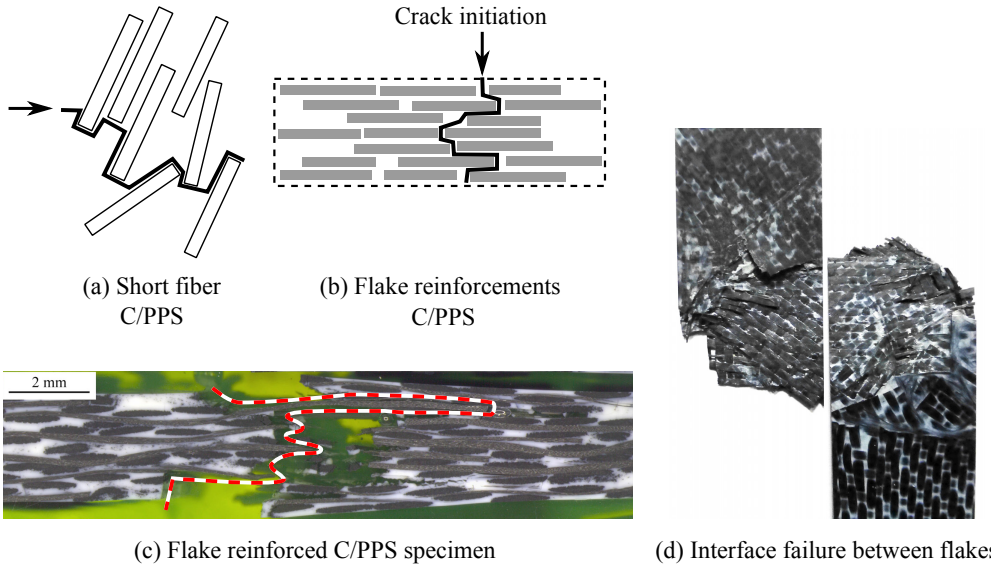


**Figure 5.6** *(a) Adapted from [19], the failure of short fiber C/PPS system with debonding failure rather than fiber failure. (b) The failure pattern in the flake reinforced system where the crack tends to avoid agglomerated regions. (c) Cross-sectional micrograph of a failed specimen with aligned flakes. (d) Failed interface between large flakes in a randomly filled flake composite.*

On the basis of the assumption that the crack avoids the reinforcements, a tortuosity measure is defined to characterize the meandering crack path. In [20] the strain field pattern in a spatially random morphology of circular inclusions was compared between a purely geometric method of calculation to a finite elements solution assuming an elasto-plastic composite. The resulting strain pattern was found to match closely and was attributed to the stiffness difference between the polymer and inclusions causing the strain to localize in the polymer. Analogously, in the present case the large localized strain developed at the interface potentially initiates failure.

In the case of PRC, a geometrically derived shortest path (see Figure 5.6 (b)) includes information of both the random overlaps and the local meso-structure in the through-thickness direction. Furthermore, it can be normalized with respect to the thickness of the specimen which is the shortest path a hypothetical crack could travel in the material through the matrix in between the flakes. Formally, a non-dimensional tortuosity $T$ is defined as,

$$T = \frac{L}{t_s}, \tag{5.2}$$

where $t_s$ is the thickness of the specimen, $L$ is the total length of the crack and is given by,

$$L = (n-1)l_0, \quad \text{for } l_0 = \text{constant (case in Figure 5.2 (c))} \tag{5.3}$$

$$L = \sum_k l_{0,k}, \qquad \text{for } l_{0,k} = \text{random (case in Figure 5.2 (b))}. \tag{5.4}$$

The total length $L$ of the crack is the sum of the overlap lengths of the adherends for both cases, a brick and mortar structure with constant $l_0$ and a structure with random overlaps $l_{0,k}$, apart from the limits of the summation. It should be noted that the thickness of the specimen is neglected in the calculation of $L$. Therefore, $T = 0$ is the minimum value of tortuousness of the crack path for a region in the specimen with polymer matrix and no flake interface through the thickness. This limit case could occur around a stack of flakes through thickness, especially under low flow conditions, forming a mechanically jammed region. Mechanical jamming leads to a matrix rich region around the jammed location due to the squeeze-out of polymer from the flakes. In such a case failure is initiated by the matrix rich region leading to a strength less than or equal to the matrix tensile strength. The limitation of this formulation is that the calculated lower value of the strength does not hold for this lower limit in tortuosity.

The effective stress, $\sigma_{eff}$, that the unit joint, with an overlap length of $l_0$, can withstand per unit width assuming no hardening of the matrix material, is given by,

$$\sigma_{eff} = \frac{l_0 \tau_m^y}{t_s}, \tag{5.5}$$

where $\tau_m^y$ is the yield strength of the interface matrix and $t_s$ is the total thickness of the representative volume, in this case the specimen thickness. The overlap length $l_0$ is assumed to be smaller than the critical overlap length for the failure to occur in the matrix which is also observed experimentally. Assuming a constant overlap between two adherends ($k = 2$), Eq. (5.2) is substituted in Eq. (5.5) resulting in,

$$\sigma_{eff} = T\tau_m^y, \quad \text{for } T\tau_m^y > \sigma_m^{ult} \tag{5.6}$$

where $\sigma_{eff}$ is the effective strength of a cross section of the specimen with a tortuosity $T$. For the limit case of $T = 0$, due to the absence of the flake at the failure section, the failure strength of the section reduces to the matrix tensile strength $\sigma_m^{ult}$ or even lower due to the stress concentration at the transition from the flakes to the matrix. In practice, strengths that are half of the matrix tensile strengths are observed.

**Phenomenological failure criterion**

It can be observed that the integrity of the structure depends on the minimum value of strength in the assumed chain of finite links as shown in Figure 5.5. Therefore, a simple phenomenological failure criterion for flake reinforced materials is given by,

$$\frac{\sigma_i}{\sigma_{eff}} \geq 1, \tag{5.7}$$

where $\sigma_i$, ($i \in [1, 2]$) is the applied uniaxial tensile stress along the principal axis of the laminate. It is worth noting that the strengths of the links are proportional to the tortuosity $T$ of a section as shown in Eq. (5.6) and the problem reduces to finding the minimum of $T$ across a specimen.

### 5.2.4 Extreme (minimum) value of strength

Unlike evolution optimized biological composites like nacre, in man-made flake reinforced composites the choice of the manufacturing process and its constraints defines the structural arrangement. As mentioned earlier, the meso-structure has a significant influence on the variability of the material response leading to a large scatter. The conventional way of characterizing the central tendency of the experimental response (e.g. ultimate strength) by its mean does not provide enough information in the presence of outliers unless a very large number of specimens are tested. A large scatter is evidence of the occurrence of extreme events [13], which in this case is the failure event such as interface failure in a weakest section (minimum strength) within the specimen. Therefore, studying the lower tail of strength distribution, especially for non-homogeneous materials, is indispensable and aids in characterizing its variability.

Analogous to the central limit theorem which describes the asymptotic convergence of the mean value to a normal distribution, the extreme values of an ordered set of random variables also have a universal behavior, leading to a set of specified asymptotic distributions [21]. Extreme value statistics (EVS) is widely used to study the extreme events in statistical processes such as strength of brittle materials, catastrophic events in weather, finance and in many other fields [14].

Let us consider tortuosity $T_i$, $i \in [1, n]$ as a random variable indicating failure strengths of $n$ sections in the specimen under tensile loading conditions. As mentioned earlier the $n$ sections are connected in series hence, the strength of the chain is the minimum strength of the elements of the chain, $\min(T_i)$. Considering a sample of $m$ specimens from a population, each represented by an ordered array $T_i^j$, where $i \in [1, n]$, $j \in [1, m]$, the problem boils down to finding the distribution of minimum tortuosity values $\min_j(T_i^j)$ consisting of $m$ values. This is equivalent to the well-established theory of $k^{\text{th}}$ order statistics for $T_{(k)}$ ($k = 1$ and $k = n$ for obtaining the distribution of minima and maxima respectively) referred to as extreme value statistics [14, 22]. Provided $m$ is large and the values are independently and identically distributed, the distribution of the extreme values asymptotically converges to one of the following three types of distributions [22]. The converged distribution is based on the tail of the parent distribution from which the values were sampled from, leading to Type I: Gumbel, Type II: Fréchet, Type III: reverse Weibull distribution. For a detailed proof for these limiting distributions, interested readers are referred to [14].

The choice of the EV distribution for a set of data is non-trivial without the assumption of the type of the parent distribution and the boundedness requirements [22]. Hence, a Generalized Extreme Value distribution (GEV) is used in this study which essentially unifies all the three types of EV distributions.

The GEV cumulative distribution function (CDF) is given as [14],

$$F(x; k, \mu, \sigma) = \begin{cases} \exp\left\{-\left[1 + k\left(\frac{x-\mu}{\sigma}\right)\right]^{\frac{-1}{k}}\right\}, & \text{for } k \neq 0 \\ \exp\{-\exp\left[-\frac{x-\mu}{\sigma}\right]\}, & \text{for } k = 0 \end{cases} \tag{5.8}$$

where $k$, $\mu$, $\sigma$ are shape, location and scale parameters of the GEV distribution respectively and $\sigma > 0$.

For $k \neq 0$, $1 + k\left(\frac{x-\mu}{\sigma}\right) > 0$ and for $k = 0$, $-\infty < x < \infty$. Based on the value the shape parameter $k$ being $= 0$, $> 0$ or $< 0$ the type of EV distribution is identified as Type I, II, III respectively.

The maximum likelihood function is found to perform better in estimating the GEV distribution parameters due to its asymptotic properties [14, 23]. In this study the maximum likelihood estimators (MLE) $\hat{k}$, $\hat{\mu}$, $\hat{\sigma}$ are found for the distribution of minimum $T$ values. The test for goodness of fit is performed with a modified Anderson-Darling (AD) test statistic [24]. The modifications account for the parameter dependency of the test statistic and small sample error.

**Statistically based design value**

Intrinsic material variability is of primary interest in the design of parts for structural applications. The strength values which can be used to design a part to render very low failure probabilities are referred to as design values [23]. For deciding on a rational design value, from the observed measurements with limited sample size, inferences have to be made from the estimated distributions. The distributions defined in the previous section help to model the population from the sample observations. In general, the parameters of the fitted distribution are not of interest whereas, the estimated quantiles (or percentiles) are used as design values in structural applications [23]. For aerospace applications A-basis and B-basis values are defined in [25] corresponding to the $0.01^{\text{th}}$ and $0.1^{\text{th}}$ quantile values of strength covering the upper 99 % and 90 % of the strength values respectively. Since the estimated quantiles are themselves random numbers with respect to different sets of experiments, a 95 % lower confidence bound for the quantiles is used as a statistically based design values (or material allowable [25]).

The quantile function of a distribution is the inverse cumulative distribution function given by,

$$X_p = F^{-1}(p; \hat{k}, \hat{\mu}, \hat{\sigma}), \quad 0 < p < 1 \tag{5.9}$$

where $X_p$ is the required $p^{\text{th}}$ quantile, $F^{-1}$ is the inverse distribution function and $\hat{k}$, $\hat{\mu}$, $\hat{\sigma}$ are the MLE for the parameters. Once the MLE for the parameters of the distribution are known, the point estimate of the $p^{\text{th}}$ quantile is obtained from Eq. (5.9). A robust confidence interval (CI) for the estimated quantile $X_p$ is obtained with the profile likelihood method [14, 26]. It takes into account the skewed nature of the likelihood surface for three parameter distributions. The critical value for the log-likelihood ratio test statistic is obtained from the $\chi^2_1$ distribution with one degree of freedom at $(1-\alpha)100^{\text{th}}$ percentile where, $\alpha$ is the required significance level. In this study $\alpha$ is set to 0.05 based on [25]. For a detailed analysis and approach for the profile likelihood method the reader is referred to [14, 26].

### 5.2.5 Generation of random overlaps and tortuosity estimation

**Generation of representative volume**

Random meso-structures with geometrical and statistical similarity are required to perform statistical analysis of the extreme (lower or higher tail) properties of PRC material. Statistically representative volume elements (RVE) in two dimensions are generated with a specified target fiber volume fraction of 50 %. The number of flakes in the RVE can be calculated from $N_f = (v_f A_s)/(A_f m_p)$, where $v_f$ is the fiber volume fraction, $m_p$ is the areal mass of prepreg, $A_s$, $A_f$ are the cross-sectional area of the

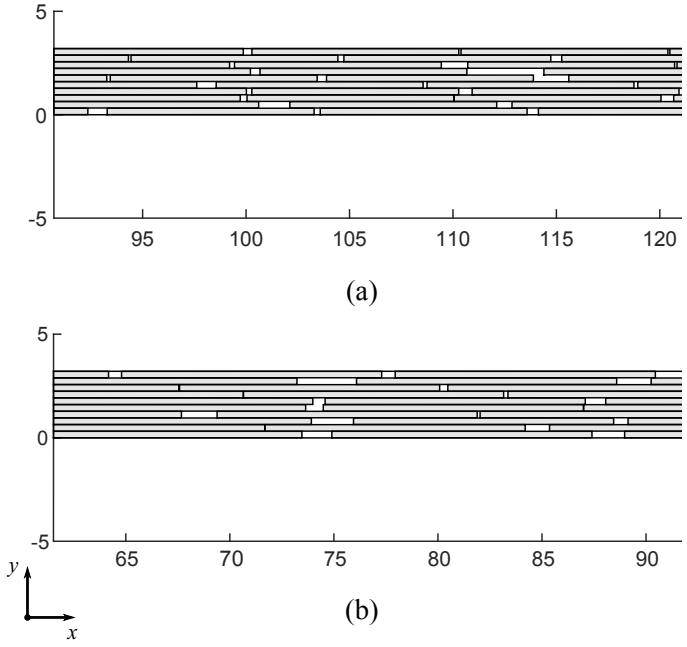


**Figure 5.7** *Realizations of RVE with overlapping flakes using Metropolis Monte-Carlo algorithm. (a) $l = 10$ mm, (b) $l = 12.5$ mm.*

RVE and flake respectively. The size of the RVE is chosen in the same order of the cross-sectional dimensions of a standard tensile specimen (ASTM D3039) of 250 mm in length and 3 mm in thickness.

The RVE is assumed to be entirely composed of flakes. Therefore, the usual method of generating spatial distribution of particles with Random Sequential Adsorption (RSA) process is not successful due to jamming[†] effect near coverage saturation [27].

In this study a Metropolis Monte-Carlo (MMC) algorithm [27] is used to generate the randomly overlapping meso-structure with a periodic boundary condition in the $x$-axis and no out-of-plane oriented flakes. Figure 5.7 shows a typical RVE generated with the MMC algorithm. The flakes are assumed to retain their ply thickness and hence, a fixed number of layers are assumed to accommodate the thickness of the specimen. The choice of initial configuration of the RVE has significant influence in generating random meso-structure with a higher volume fraction of particles [27]. Therefore, a space filling Latin hyper cube method is used to generate the initial configuration with fixed $y$ values and random $x$ values. Subsequently, each flake in the initial configuration is randomly perturbed for a large number of iterations (25000) by the MMC algorithm in the in-plane direction. After a sufficient number of iterations without allowing any excluded volume interactions and periodicity violation, the resulting structure is assumed to be statistically representative [27]. MMC algorithm attempts to randomly position a constant number of flakes in an

[†]Not to be confused with the mechanical jamming in Section 5.2.3. Jamming in RSA algorithm is caused by having fixed adsorbed particles and subsequent sequential addition of new particles.

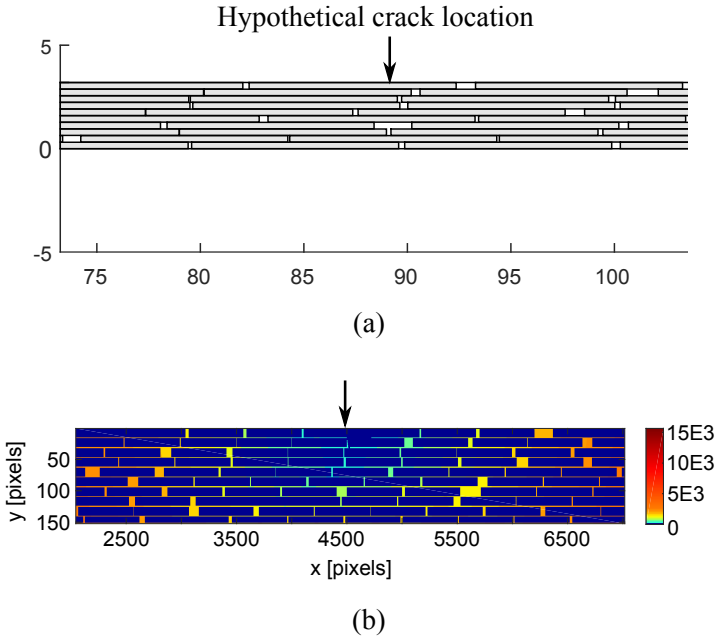


**Figure 5.8** *(a) The cross section of a 12.5 mm flake specimen. The arrows indicate the hypothetical crack location fed to the geodesic transformation algorithm. (b) The computed values of shortest path in pixels, the colors indicate the shortest distance from the starting point.*

RVE with the above mentioned constraints in a finite number of attempts. The limited number of attempts causes a very small fraction of flakes to remain overlapping either completely or partially with its neighbor on the same layer. Such random overlapping regions are regarded as having a negligible effect when taking a large number of specimens into consideration.

### Estimation of tortuosity

As mentioned earlier (see Figure 5.6 (b)) the crack is hypothesized to progress through the least resistance path along the interface. Therefore, the shortest path, namely a geodesic path from the assumed location of crack initiation (top plane) to the bottom of the specimen, is computed with geodesic distance transformation. The geodesic distance transformation function in the Image Processing toolbox of MATLAB® is used to calculate the geodesic distance on a binary image of the RVE scaled to pixel dimensions. Figure 5.8 (b) shows the computed distance metric in pixel dimensions for the cross section shown in Figure 5.8 (a). The color shows the shortest distance from the starting point, indicated with an arrow on the top surface, to all the other points in the image. Subsequently, the computed minimum value is transformed back to length dimensions. The difference between the geodesic length and the thickness of the specimen is equal to the value of $L$ defined in Eq. (5.4), since the geodesic path inherently includes the thickness of the specimen.

## 5.3 Experimental work

### 5.3.1 Materials and methods

The experimental work was performed on CETEX® Carbon/poly(phenylene sulphide) (C/PPS) semi-pregs from TenCate Advanced Composites. The reinforcing fabric is made from a 5 harness satin weave and accounts for a fiber volume fraction $v_f$ of 50 %. The thickness of the consolidated prepreg lamina is 0.31 mm. The laminates were manufactured at a nominal processing temperature of 320 °C and a consolidation pressure of 10 bar. Specimens for tensile tests were extracted and tested according to ASTM D3039.

### 5.3.2 Manufacturing of flake reinforced laminates

Two types of flake reinforced laminates were manufactured, (A) a model overlap laminate and (B) randomly filled laminate with well-defined flakes. The former has flakes with defined overlaps and in-plane alignment. The latter is closer to reality with random overlaps, in-plane orientations and possible out-of-plane orientations of the flakes. A picture frame mold of 250 x 250 mm$^2$ was used to press consolidate the composite plates.

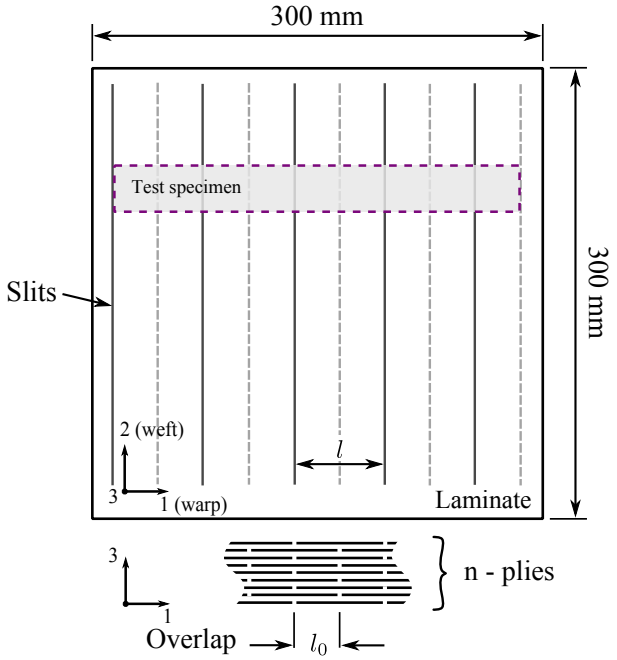


**Figure 5.9** *(a) n-ply laminate with staggered slits in the plies to realize flake reinforced specimens with constant overlap, after cutting the specimen. Inset: Cross section of the n-ply specimen with overlaps of length $l_0$ and flake length $l = 25$ mm.*

Figure 5.9 shows plate (A) with slits at an interval of $l = 25$ mm and a staggering interval of $l_0$ (3 mm and 12 mm) in the alternating plies, where the staggering interval defines a constant overlap length. Solid and dashed vertical lines indicate slits in the top ply (visible) and subsequent inner plies respectively. The length of the flake $l$ is set equal to the specimen width. The configuration of the laminate is $[(0,90)_4/(90,0)_5]$. Flake reinforced specimens were obtained by cutting the plate transverse to the slit direction. In the case of plate (B), 2.5 mm thick plates with two different flake sizes: $L_f$ =17.5 x 17.5 mm$^2$ and 26.5 x 26.5 mm$^2$ were molded with randomly filled mold cavity. The specimens from plate (B) differ from plate (A) in the random distribution of the position and orientation of the flakes.

## 5.4 Results and discussion

### 5.4.1 Experimental results

The ultimate strength values obtained from the uniaxial tensile tests of plates (A) and (B) are shown in Figure 5.10. The failure stress was calculated with the total cross-sectional area of the specimens. The failure stress of aligned flake specimens with $l_0 = 12$ mm are larger than the 3 mm overlap specimens. It can be explained from the failure mechanism observed in the specimens. At lower overlap lengths the failure was due to pull-out of the flakes and at larger overlaps the failure was due to rupture of the flakes. The critical overlap length $L_c$ can be calculated by Eq. (5.1) with the properties of C/PPS: $\sigma_f^{ult} = 735$ MPa along the principal fiber directions, $\tau_m^y = 90/\sqrt{3} = 51$ MPa and $t_f = 0.31$ mm leading to a $L_c = 4.93$ mm. Hence, the observation of pull-out failure in the specimens with $l_0 = 3$ mm $< L_c$ is expected.

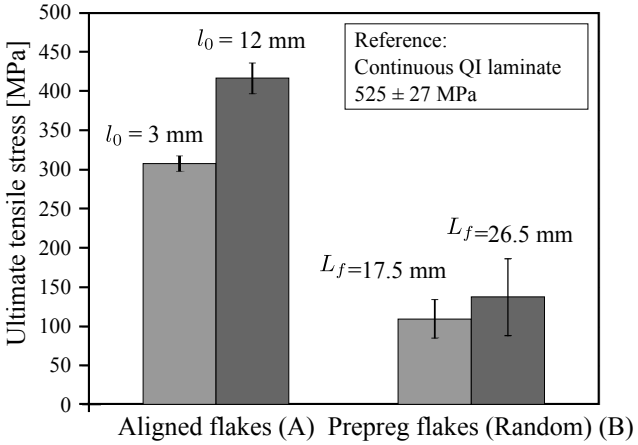


**Figure 5.10** *The ultimate failure stress of plate (A) with aligned flakes and consistent overlap $l_0$, and for plate (B) with random flake locations and orientations.*

Furthermore, for the pulled-out specimens the calculated average interface shear stress at failure resulted in 45.96 MPa. It is found to be moderately lower than the approximated yield stress of (PPS) $\tau_m^y = 51$ MPa with von-Mises criterion, possibly due to the stress concentrations at the discontinuities. This has an adverse effect of increasing critical overlap length needed for efficient stress transfer.

Beyond the critical overlap length a saturation of maximum load carrying capacity occurs very soon, above which the increase in flake overlap does not provide any further benefit. This can be observed (see Figure 5.4) from the reducing shear stress profile at the interface, away from the edges of the overlap. Comparing the aligned flake specimens (A) to the random flake specimens (B), the latter behaves poorly due to the stochastic overlaps and randomly oriented flakes and possibly due to some out-of-plane alignment of flakes. Moreover, the strength of the rotated flakes reduces strongly due to a change in the failure mode of the woven flake with increasing rotation angle relative to the loading direction. In general, a completely random meso-structure with random orientations is advantageous in the sense of process insensitiveness (variation in manufacturing) and for isotropic strength properties. However, other flaws such as out-of-plane alignment of flakes and mechanically jammed regions tend to deteriorate the strength.

### 5.4.2 Extreme values of tortuosity

MMC algorithm was used to generate 60 specimens for each flake size and length of the specimens shown in Table 5.1. The geometric tortuosity was estimated at an equal number of random sampling locations in the mid span of every specimen. Longer specimens were sampled at 600 locations and the smaller specimens at 300 locations. An exclusion zone was considered equivalent to two specimen widths (50 mm) near the clamping edges to avoid any possible edge effect in the generated structure. The minimum value of $T$ was extracted from each of the specimens and was sorted. An empirical cumulative probability value $F_e(T^j_{(1)}) = (j - 0.5)/m$, $j = [1, m], m = 60$ was assigned to each $T$ based on its position. The obtained empirical CDF $F_e(T^j_{(1)})$ was used to find the MLE for the GEV distribution as stated in Section 5.2.4. The fitted distributions passed the modified AD goodness of fit test performed according to Section 5.2.4. Figures 5.11 and 5.12 show the fitted GEV distributions for the respective empirical distributions corresponding to the different flake sizes and specimen lengths $L_{sp}$. Table 5.1 shows the MLE for the shape, location and scale parameters for the three cases.

It can be observed that the shape parameter $k$ for all the three distributions are negative, denoting that the estimated distribution is asymptotic to a reverse Weibull distribution. An important property of a reverse Weibull distribution is the boundedness from the upper side. Therefore, the obtained minimum tortuosity

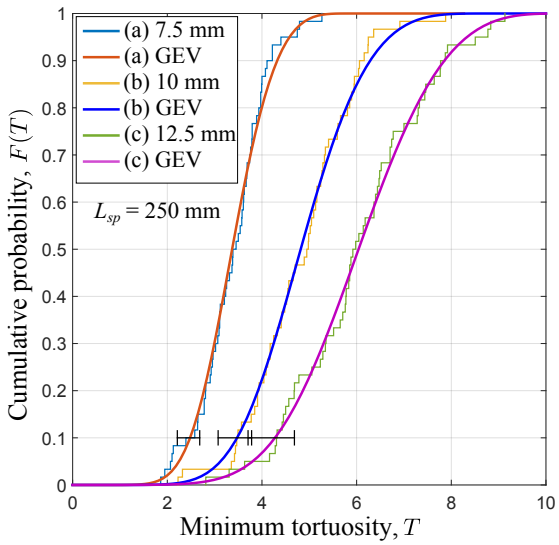


**Figure 5.11** *Empirical cumulative distribution (stepped lines) of minimum tortuosity values $T^j_{(1)}$ for $m = 60$ specimens consisting of randomly distributed flakes with corresponding size shown in the legend. The specimen of length ($L_{sp}$) 250 mm is sampled at (n) 300 locations. CDF of the fitted GEV distribution are shown as smooth lines. 95 % confidence interval is plotted for the $0.1^{th}$ quantile.*

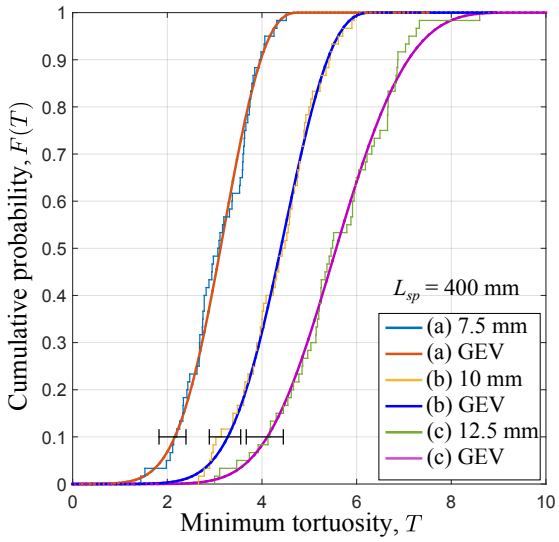


**Figure 5.12** *Empirical cumulative distribution (stepped lines) of minimum tortuosity values $T^j_{(1)}$ for $m = 60$ specimens consisting of randomly distributed flakes with corresponding size shown in the legend. The specimen of length ($L_{sp}$) 400 mm is sampled at (n) 600 locations. CDF of the fitted GEV distribution are shown as smooth lines. 95 % confidence interval is plotted for the $0.1^{th}$ quantile.*

| Flake size [mm] | $\hat{k}$ | $\hat{\mu}$ | $\hat{\sigma}$ | Mean | Variance |
|---|---|---|---|---|---|
| | | $L_{sp}$ = 250 mm | | | |
| 7.5 | -0.250 | 3.126 | 0.695 | 3.386 | 0.499 |
| 10 | -0.237 | 4.448 | 1.055 | 4.851 | 1.169 |
| 12.5 | -0.279 | 5.563 | 1.371 | 6.049 | 1.880 |
| | | $L_{sp}$ = 400 mm | | | |
| 7.5 | -0.383 | 2.875 | 0.728 | 3.087 | 0.482 |
| 10 | -0.383 | 4.108 | 0.844 | 4.355 | 0.650 |
| 12.5 | -0.267 | 5.174 | 1.133 | 5.585 | 1.302 |

**Table 5.1** *The MLE for the GEV distribution of $T^{j}_{(1)}$ for different flake sizes and specimen lengths $L_{sp}$.*

values tend to have an upper bound, whereas the lower tail extends to very low values. However, the probability of achieving a zero tortuosity is less than $10^{-5}$.

### Effect of flake size and resulting scatter

The effect of flake size can be observed in Figure 5.11 and 5.12 for the two different specimen lengths. As the flake size increases the distribution translates towards larger tortuosity values. Based on the estimated mean of the minimum $T$ values, it can be observed that for every increasing step of flake size the relative increase in the mean is progressively getting smaller. Whereas, the variance of the minimum value of $T$ shows an increasing trend. These effects are more pronounced in the case of longer specimens, since in a statistical sense longer specimens are far more likely to fail. However, in the simulated case, the possibility of out-of-plane orientation and the formation of mechanical jamming are not considered. These defects have a detrimental effect on the strength and the risk of their presence increases with the poor processability of larger flakes. Furthermore, the experimental results of plate (B) (with random flakes shown in Figure 5.10) also indicate large variability where the mean strength values are within the scatter of the each other. Therefore, increasing the size of the reinforcement does not necessarily provide better strength properties; it might actually be detrimental owing to the variability it creates in the property values.

### Effect of specimen length

In this study, the length of the sampled region is increased twofold from 150 mm to 300 mm (not including the exclusion zones) with a fixed density of sampling

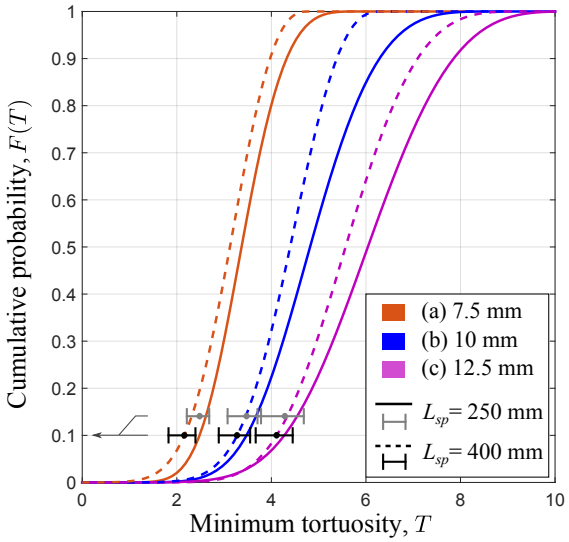


**Figure 5.13** *CDF of $T^j_{(1)}$ for two different lengths of specimen composed of different flake sizes 7.5, 10 and 12.5 mm. 95 % CI for the $0.1^{th}$ quantile is shown for all the distributions. For brevity, the CI for the 250 mm specimens are shifted vertically to show the overlap with the 400 mm specimens. The dot in the interval indicates the location of the point estimate of the quantile.*

points. The distributions become steeper in the upper tail with the increase in specimen length as shown in Figure 5.13. When compared to the previous case of change in flake length, a small amount of translation can be seen in the case of smaller flake size (7.5 mm), but in the direction of smaller tortuosity. The increase in steepness illustrates an adverse effect whereby the probability of attaining at least a certain minimum tortuosity decreases. Formally, $P(T \geq T_{req})$ becomes smaller where, $T_{req}$ is a required minimum tortuosity and $T$ is the tortuosity random variable. In other words the failure probability increases with the increase in specimen length. Interestingly, the lower quantiles which form the design values are not affected greatly as shown in Figure 5.13. Even though the specimen is twice as long, the lower bounds of the CI are closer to each other for the larger flake sizes.

### Experimental scatter vs EVS estimation

An increased scatter can be observed as the flake size increases (see Figure 5.10) in the case of random flakes. This effect can be attributed to the smaller flake number density (number of flakes per unit volume) and poor in-plane arrangement. Furthermore, flakes get aligned near the edges of the specimen creating a short range order. Nevertheless, the trend in experimental scatter is reflected in the estimated variance of the distribution of minimum tortuosities obtained with EV theory (see Table 5.1). Simulating a larger number of specimens with a more realistic flake packing algorithm close to the real molding process provides a more conservative

estimation of the population. Additionally, more realistic failure scenarios can be obtained by considering the flow, out-of-plane alignment and agglomeration of flakes.

### 5.4.3 Statistically based design value

The lower confidence bound (design value) for the point estimate of the $0.1^{\text{th}}$ quantile ($T_{0.1}$) at 5 % significance level, obtained with the profile likelihood method (Section 5.2.4) is shown in Table 5.2. The values $T_{0.1}$ have an increasing trend with flake size for both the lengths. Whereas, the change in length has a smaller influence in the lower confidence bound value as the flake size gets larger.

| Flake size [mm] | 95 % Lower confidence for $T_{0.1}$ [-] | |
|---|---|---|
| | $L_{sp}$=250 mm | $L_{sp}$=400 mm |
| 7.5 | 2.212 | 1.825 |
| 10 | 3.074 | 2.887 |
| 12.5 | 3.706 | 3.668 |

**Table 5.2** *B-Basis material allowable for different flake sizes and specimen lengths, where $T_p$ is the $p^{th}$ quantile of T.*

#### Applicability and insight on design guidelines

The choice of flake size is one of the primary questions which arises when designing with a discontinuous PRC material. Figure 5.14 shows the typical range of flake size. A theoretical minimum reinforcement size can be identified based on the efficient stress transfer with an assumption of isolated reinforcements. However, the idea of a 2D flake emerges from the local structural integrity provided by the fabric architecture. Hence, a lower bound for the flake size can be defined, irrespective of this study, as the unit cell size of the fabric.

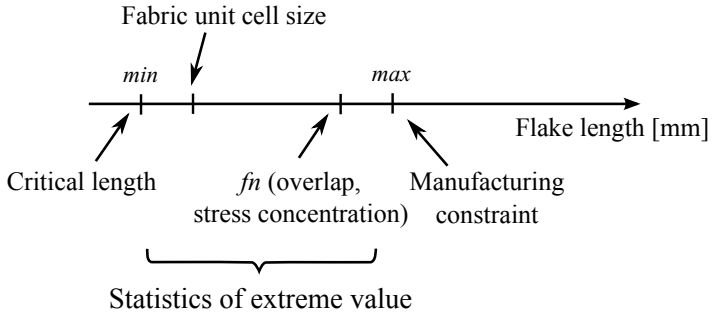


**Figure 5.14** *Typical range of flake size and the constraints in its choice.*

The probability for longer overlaps increases with increasing flake size. However, beyond the critical overlap length the increased stress concentrations near the ends of the overlap lead to premature failure initiation. Meanwhile, the material should be able to flow into narrow ribs and fill intricate locations of the part giving rise to manufacturing constraints with respect to flake size. Consequently, a balance has to be found between a flake size which provides an average overlap length larger than the critical overlap length ($L_c$) and a flake size which is suitable for filling the part. Therefore, within the limits of the assumptions, the statistical approach from this study can be used to choose a flake size between the minimum and the maximum processable flake size, and to quantify the design strength and expected variability.

## 5.5 Conclusions

The variability in the mechanical properties of planar reinforced composites, especially manufactured with chopped woven prepregs, was addressed in this study. High reinforcement volume fraction and inherent stochasticity of the material provides better isotropic elastic properties on the one hand, but leads to a largely variable strength property resulting only in a marginal increase in the lower bound strength. Existing literature on PRC does not cater to the non-determinism involved in the analysis. A systematic approach to handle the non-deterministic nature of the flake system is proposed in this study, by combining the phenomenology of failure and concepts of statistics. A tortuosity based approach is proposed to handle the random overlaps and local meso-structure simultaneously, which has a large influence on the failure. Statistically representative specimens were generated and analyzed with rather less computationally expensive geometric algorithms. Extreme value statistics was used to characterize the lower tail of the tortuosity distribution leading to the probability distribution of minimum attainable strength. Furthermore, the estimated variances in the tortuosity values were found to show a similar trend to the experimentally observed scatter in strength with respect to the flake size. Statistically significant design values were obtained with the help of simulated specimens. This approach has a potential to be used in efficiently characterizing such stochastic materials with greatly reduced experimental characterization and in developing design guidelines for the choice of material form.

## References

[1] R. A Ford. Thermo-ductile composites: new materials for 21st Century manufacturing of micro-perforated thermoplastic composites. *Materials & Design*, 22(3):177–183, May 2001.

[2] I. Taketa, T. Okabe, and A. Kitano. A new compression-molding approach using unidirectionally arrayed chopped strands. *Composites Part A: Applied Science and Manufacturing*, 39(12):1884–1890, December 2008.

[3] C. Stephen, Dustin L. Levin, Dequine, and John P. Crocco. Formability of thermoplastic stretch-broken carbon fiber vs. thermoplastic continuous carbon fiber. In *SAMPE Technical conference proceedings*, 2013.

[4] Robert F. Landel and Lawrence E. Nielsen. *Mechanical Properties of Polymers and Composites, Second Edition*. CRC Press, December 1993.

[5] G. E. Padawer and N. Beecher. On the strength and stiffness of planar reinforced plastic resins. *Polymer Engineering & Science*, 10(3):185–192, May 1970.

[6] B. Glavinchevski and M. Piggott. Steel disc reinforced polycarbonate. *Journal of Materials Science*, 8(10):1373–1382, October 1973.

[7] Paolo Feraboli, Elof Peitso, Francesco Deleo, Tyler Cleveland, and Patrick B. Stickler. Characterization of Prepreg-Based Discontinuous Carbon Fiber/Epoxy Systems. *Journal of Reinforced Plastics and Composites*, 28(10):1191–1214, May 2009.

[8] M. Selezneva, K. Kouwonou, L. Lessard, and P. Hubert. Mechanical properties of randomly oriented strands thermoplastic composites. In *Proceedings of the International Conference on Composite Materials (ICCM19)*, Montreal, CA,, 2013.

[9] Kelsi Marie Hurley. The Effect of Recyclate Geometry on the Properties of Recycled Flake Reinforced Thermoset Composites. Thesis, University of Washington, September 2012.

[10] M. I. Abdul Rasheed, B. Rietman, H. A. Visser, and R. Akkerman. Experimental characterisation of recycled (glass/tpu woven fabric) flake reinforced thermoplastic composites. In *Proceedings of the International Conference on Composite Materials (ICCM19)*, pages 3999 – 4010, 2013.

[11] B. Chen, P. D. Wu, and H. Gao. A characteristic length for stress transfer in the nanostructure of biological composites. *Composites Science and Technology*, 69:1160–1164, June 2009.

[12] J. Rexer and E. Anderson. Composites with planar reinforcements (flakes, ribbons)-A review. *Polymer Engineering & Science*, 19(1):1–11, January 1979.

[13] Dusan Krajcinovic. Chapter 2 statistical models. In Dusan Krajcinovic, editor, *Damage Mechanics*, volume 41 of *North-Holland Series in Applied Mathematics and Mechanics*, pages 33 – 220. North-Holland, 1996.

[14] Stuart Coles. *An Introduction to Statistical Modeling of Extreme Values*. Springer Series in Statistics. Springer London, London, 2001.

[15] H. L. Cox. The elasticity and strength of paper and other fibrous materials. *British Journal of Applied Physics*, 3(3):72, March 1952.

[16] A. Kelly and W. R. Tyson. Tensile properties of fibre-reinforced metals: Copper/tungsten and copper/molybdenum. *Journal of the Mechanics and Physics of Solids*, 13(6):329–350, December 1965.

[17] L. B. Greszczuk. Theroretical studies of the mechanics of the fiber-matrix interface in composites. In *Interfaces in composites ASTM STP 452, American Society for Testing and Materials*, pages 42–58, 1969.

[18] M. Y. Tsai, D. W. Oplinger, and J. Morton. Improved theoretical solutions for adhesive lap joints. *International Journal of Solids and Structures*, 35(12):1163–1185, April 1998.

[19] B. A. Sanders, editor. *Short Fiber Reinforced Composite Materials*. ASTM International, January 1982.

[20] Dominique Jeulin, Wei Li, and Martin Ostoja-Starzewski. On the geodesic property of strain field patterns in elastoplastic composites. *Proceedings of the Royal Society of London A: Mathematical, Physical and Engineering Sciences*, 464(2093):1217–1227, May 2008.

[21] R. A. Fisher and L. H. C. Tippett. Limiting forms of the frequency distribution of the largest or smallest member of a sample. *Mathematical Proceedings of the Cambridge Philosophical Society*, 24(02):180, April 1928.

[22] A. Hansen and S. Roux. Statistics Toolbox for Damage and Fracture. In Dusan Krajcinovic and Jan Van Mier, editors, *Damage and Fracture of Disordered Materials*, number 410 in International Centre for Mechanical Sciences, pages 17–101. Springer Vienna, 2000.

[23] Enrique Castillo. Extremes in Engineering Applications. In Janos Galambos, James Lechner, and Emil Simiu, editors, *Extreme Value Theory and Applications*, pages 15–42. Springer US, 1994.

[24] Francesco Laio. Cramer-von Mises and Anderson-Darling goodness of fit tests for extreme value distributions with unknown parameters. *Water Resources Research*, 40, 2004.

[25] *Military Handbook - MIL-HDBK-17-1F: Composite Materials Handbook, Volume 1 - Polymer Matrix Composites Guidelines for Characterization of Structural Materials*. Number Chapter 8. U.S. Department of Defense, 2002.

[26] Manfred Gilli and Evis Kellezi. An Application of Extreme Value Theory for Measuring Financial Risk. *Computational Economics*, 27(2-3):207–228, May 2006.

[27] Salvatore Torquato. *Random Heterogeneous Materials*, volume 16 of *Interdisciplinary Applied Mathematics*. Springer New York, New York, NY, 2002.

# Chapter 6

# Discussion

*The previous chapters discussed the aspects of processing and mechanical performance of discontinuous composite materials having a woven architecture. This chapter elaborates on this in a broader perspective towards the global objectives of this research. Firstly, an overview of the multidisciplinary problem is provided. Secondly, the different components of the framework are discussed in the perspective of a practical application. Thirdly, a strategy for selecting the relevant parameters is proposed. Finally, as a means of demonstrating the theories presented, a full scale part is manufactured and the obtained part quality is briefly discussed.*

## 6.1 Overview of the problem

The work performed in this thesis concerns the compression molding process of discontinuous molding compound consisting of planar reinforcements with a woven architecture. The sequence of a typical compression molding process and the involved variables are illustrated in Figure 6.1 along with the chapter numbers that contain additional information on the specific topic.

The main objective of the study was to develop a strategy for the manufacturing of parts with good quality and consistent mechanical properties. In that aspect, designing a reliable and repeatable industrial process requires proper material characterization data. Additionally, in the case of a random discontinuous material, the process designers need to understand the behavior of the material during the molding process in relation to the part design. They could benefit from the knowledge of whether the material will have a macroscopic flow during the process leading to re-orientation of flakes or the presence of only local mesoscopic flow, whether the material can jam at a certain mold closure rate $(\dot{h})$ and optimal consolidation time $(\tau)$ for a consistent part quality. In addition to that, the complexity of the part determines the flow stress required to be generated to fill the part

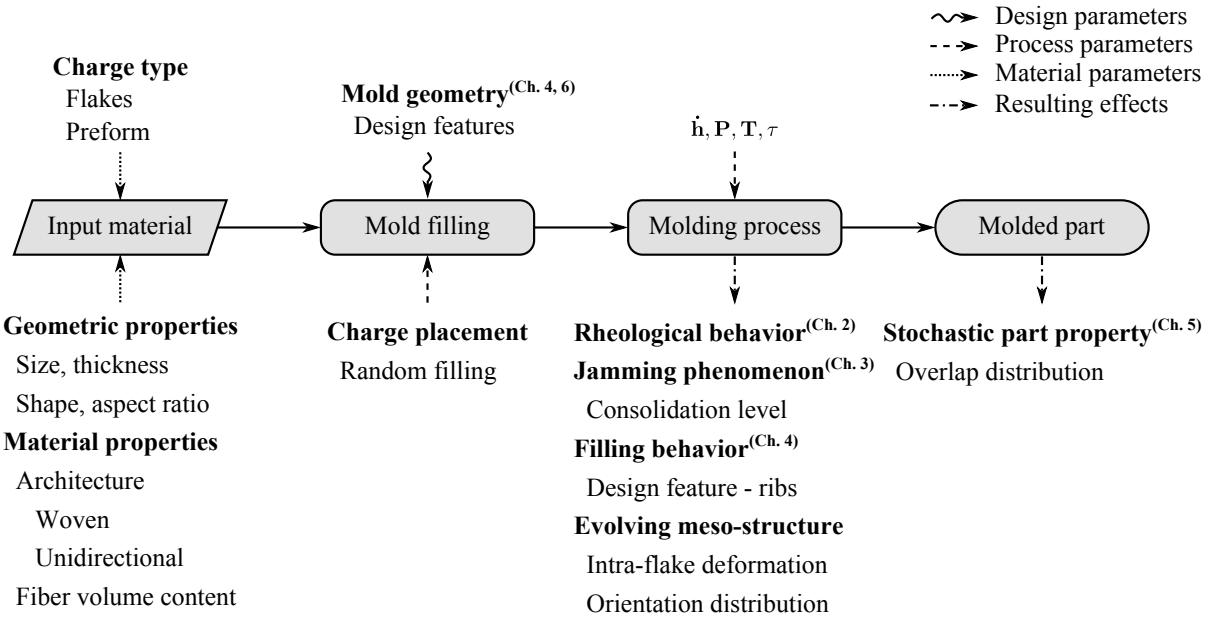


**Figure 6.1** *A typical process flow for compression molding of discontinuous composite material, where $\dot{h}, P, T, \tau$ are the process parameters, namely the mold closing rate, consolidation pressure, temperature and dwell time respectively.*

completely and the consolidation pressure $(P)$ required for filling the intricate details in the part and to obtain a certain quality. Furthermore, the flow stresses are also a function of flake size $(l)$, the bulk nature of the material, as well as temperature $(T)$. Therefore, an appropriate combination of these parameters within the processing window and knowledge of the material behavior is required to exploit the advantages of the material and to reach the goal.

Furthermore, generating a robust process window requires mathematical models representing the actual deformation process to predict the behavior of the material inside the mold. Since the architecture of the flake has a significant influence on the flow behavior, for example in terms of jamming, a multi-scale model accounting for bundle interactions and flake-flake interactions might be required. It is neither practical nor straightforward to create such general models for different materials without understanding the fundamental behavior of the material at hand. Therefore, this thesis generates a qualitative understanding of the material behavior in different processing scenarios to form a foundation for future studies.

## 6.2 Multidisciplinary framework

Figure 6.2 shows the interconnection between the design of the part, the process and the material used for molding. The final properties of the part depend on the characteristics of these components and their interrelations.

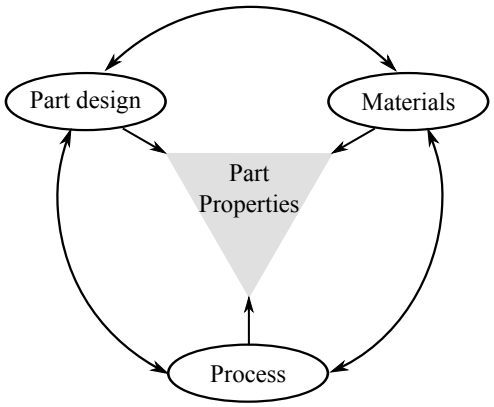


**Figure 6.2** *Multidisciplinary framework.*

The following subsections concerning each component elucidate the connection with the adjacent components.

### 6.2.1 Part design

The discontinuous nature of the material allows complex shapes to be manufactured in one shot with net-shaped edges and thereby reduces the need for sub-assemblies in the part design. Moreover, the design process can be focused to achieve large stiffness or to meet higher strength requirements or a balance of both properties.

Preliminary experiments showed that the tensile stiffness of the woven flake reinforced laminates scales with the fiber volume fraction and is a weak function of the flake size. The tensile stiffness was found to be around 70-80 % of a quasi-isotropic (QI) continuously reinforced laminate made from the same parent material. Additionally, the stiffness of the part can be increased by adding integrated design features. The ability of the chopped material to fill intricate design features such as ribs, thickness transitions and joggles can be utilized to its full extent without the formation of typical processing defects such as wrinkles.

In terms of part strength, an un-notched tensile strength was considered as a basic strength property in this study. Even though the random and discrete nature of the material facilitates the processing of complex shapes, it increases the number of local stress concentrations, which reduces the tensile strength. The un-notched tensile strength of the flake reinforced laminates was found to be considerably lower, in the range of 20-25 % of the QI laminates (Figure 5.10). However, experiments with aligned flakes and with a large overlap between the flakes resulted in a strength value of around 80 % of the QI reference. (Chapter 5). Large overlaps in randomly filled material are statistically plausible with larger flakes. However, in the context of the process, the choice of flake size is also restricted by the design features which need to be filled (Chapter 4). Furthermore, the structural arrangement and orientation of the

flakes, as a result of the process, influence the overlapping area between the flakes where the stress transfer occurs. The amount of overlaps with a random arrangement of the flakes and a fixed orientation show increasing uncertainties as the flake size increases (Chapter 5). However, these uncertainties can be reduced by controlling the distribution of position as well as the orientation of the flakes or by increasing the part thickness. One of the methods to obtain and control the desired range of overlaps between the flakes is to make a preform, or a mat-like structure, similar to the manufacturing process of Oriented Strand Boards (OSB) [1, 2] or HexMC [3] mats. The production of such preform is carried out by dropping the flakes onto a conveyor belt through guiding vanes and spraying of a suitable binding material. The position of the guiding vanes can be changed to obtain a change in the orientation of the flakes and the speed of the belt can influence the position of the deposited flakes. Such an automated process can provide a statistically consistent material form as a starting point for the molding process. However, adapting the process to thermoplastic materials requires further study in terms of preserving the structure of the mat, since there can be no binder involved with thermoplastic composite flakes. Furthermore, the process induced re-orientation of the flakes needs to be studied to obtain a suitable correction factor to determine the resulting amount of overlap in the molded part. Subsequently, this could be used as an indicator for the strength.

As a general guideline, for a strength based design, a thicker part will be beneficial since the probability of having a large amount of overlap is higher and hence the load carrying capacity also increases. Moreover, the larger the part volume, the larger the chance of failure, hence, smaller is the average strength. Whereas, the variability can reduce with the increase in part volume. In the case of a stiffness based design, the chopped material can be put to use to its best by utilizing various design features mentioned earlier, which augments the inherent material stiffness.

### 6.2.2 Material

This section concerns the material parameters such as variable flake size and flake thickness, and its connection with part design, properties, and the manufacturing process.

#### Flake size

Figure 6.1 illustrates a typical set of material parameters. For a given type of material, for example a 0.31 mm thick, C/PPS woven prepreg with a fiber volume content of 50 %, flake size is one of the few material parameters which can be tailored to meet the part property requirements. However, the flake size has a strong influence on the filling ability of the material in intricate design features (Chapter 4). In all the previously discussed chapters and in Section 6.2.1 a constant flake size was

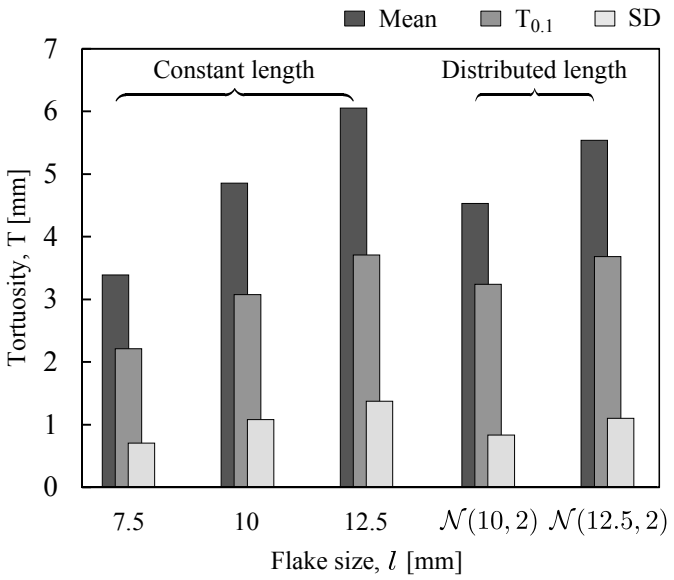


**Figure 6.3** *Comparison of tortuosity (T) values for constant flake lengths and flake lengths distributed around a mean value. $T_{0.1}$ is the lower confidence interval for the $10^{th}$ percentile of the T distribution, SD is the standard deviation of the T distribution.*

considered, although different fixed flake sizes were investigated. However, the flake sizes can be mixed together to achieve flexibility in manufacturing as well as to maintain the properties. Moreover, in the scenario of recycling, the size of the flakes is not likely to be the same after the size reduction process. The question is, what is the benefit of using a distribution of flake sizes with respect to processing as well as mechanical performance?

In terms of processing, smaller flakes can be more useful in the filling of intricate design features whereas the larger ones might bridge the gaps in between the smaller flakes in other uniform sections. The mixture in size might help to avoid the formation of persistent stacks of flakes leading to reduced jamming effects while maintaining the mechanical performance of the part.

As far as the properties are concerned, a larger mean length provides a better opportunity for relatively higher strength compared to flakes with shorter lengths. Moreover, the distribution of sizes also influences the strength distribution. The influence of flake size distribution on the tortuous path (strength) distribution is shown in Figure 6.3, a constant flake length of 7 mm, 10 mm and 12.5 mm and a normally distributed flake length, $l \sim \mathcal{N}(l_m, 2)$, around a mean of $l_m$ and a standard deviation of 2 mm. The resulting shortest path to failure, tortuosity values ($T$), are shown in the $y$-axis. As discussed in Chapter 5, the tortuosity values can be scaled to approximate the maximum stress value the material section can bear, with the use of the shear strength of the matrix. The different bars show the mean of the

obtained distribution of tortuosity values for 60 specimens with a length of 250 mm and thickness of 3 mm. The $T_{0.1}$ bar shows the lower confidence interval for the $10^{th}$ percentile tortuosity value, b-basis value in terms of strength, used for design purposes in aerospace industry. The SD bars show the standard deviation for the obtained probability distribution for each class of flake length. It can be observed that as the flake length increases the variance also increases for specimens with a constant flake length. However, if a distribution of flake lengths is used, the variance for the same mean flake length (group 2 and 4 from left or group 3 and 5) reduces moderately and hence there is a small increase in the $T_{0.1}$, despite the expected reduction in mean value of tortuosity. Therefore, for a moderate loss in the mean value or a small gain in the $T_{0.1}$, a significant advantage in processability can be attained with the introduction of a distribution in the flake length. This is however hypothesized based on the effects observed in the filling behavior with smaller flake sizes. Further research is required to quantify the increase in processability, and to judge whether the increased processability makes it possible to increase the mean flake size such that a similar higher mean value of tortuosity can be achieved along with an increase in $T_{0.1}$. Hence, as stated in the introduction and in terms of recycling, a controlled size reduction process or controlling the flake size after the size reduction with a sieving process seems to be a viable solution. However, further in-depth study is required for a quantitative argument.

**Flake thickness**

A constant flake thickness of 0.31 mm was used in this thesis, which is a nominal ply thickness for a consolidated woven C/PPS semi-preg. However, materials consisting of flakes with varying thickness is possible, for example, flakes obtained from shredding consolidated laminate scrap. Based on the shredding process and the variations in the thickness of the scrap laminates, the shredded material will have a distribution in the thickness of the flakes. Preliminary molding experiments with shredded consolidated scrap showed that a large variability in thickness of the shredded flakes renders it un-processable with the molding procedure followed in this thesis. This is primarily due to lack of flow because of early jamming of the thick flakes during the compression process (Chapter 3). Consequently, the consolidation process is hindered and the material is poorly consolidated, as shown in Figure 6.4 (a) with holes and unfilled regions. However, flakes with lower thickness variations can be consolidated properly as seen in Figure 6.4 (b).

Therefore, an intermediate process can be added prior to compression molding of non-uniformly thick consolidated scrap flakes such as to convert the flakes to a melt blob of fibers and molten polymer using an extruder or a blender. Such a blended material can improve the processability in the subsequent compression molding process. However, depending on the blending process, the structure of the flakes

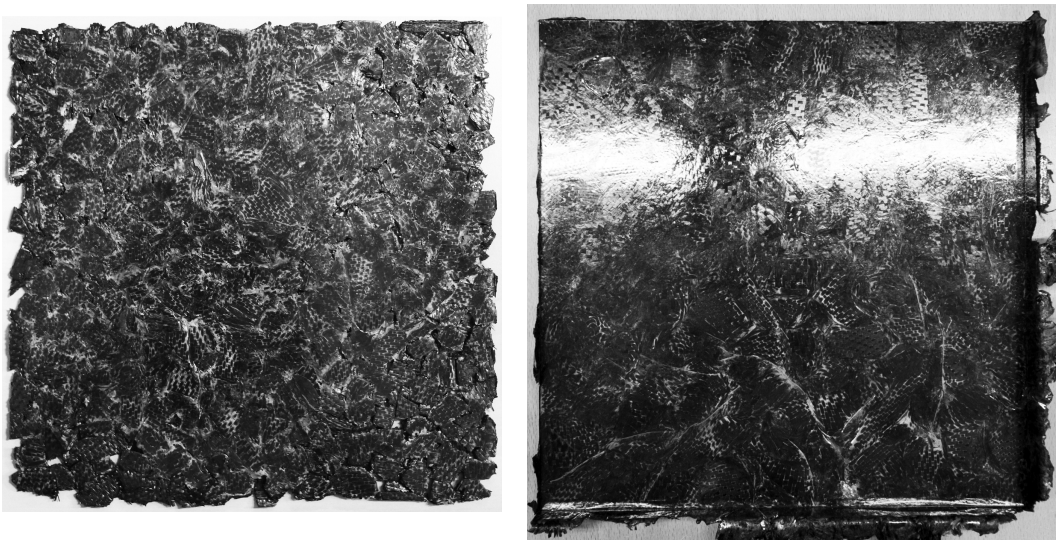

(a) (b)

**Figure 6.4** *Laminates manufactured from shredded consolidated scrap consisting of (a) flakes with large thickness variation, (b) flakes with a small thickness variation. Laminate (a) is poorly consolidated with visible unfilled regions at top right, bottom left and right regions. Laminate (b) is fully consolidated. The process parameters for both cases: a consolidation pressure of 10 bar and consolidation dwell of 15 minutes at 320 °C.*

is not likely to be preserved in the extruded blob and hence the material is closer to a long fiber reinforced polymer.

In addition to the absolute thickness of the flakes playing a role, the ratio of the flake thickness to the part thickness can also play a role. For instance, the processing window for a large value of such ratio can exist in the region of a very large closing rate, which might not be practically feasible. Further study is required to characterize this parameter.

### 6.2.3 Process

This subsection describes the important aspects of the process and its connection to the other components shown in Figure 6.2.

#### Filling stage

The filling stage of the process, studied in Chapter 2 and Chapter 3, was found to have significant influence on the processing of chopped woven flakes. In this stage the mold is closed at a constant rate of displacement to make the material flow and fill the mold cavity until the consolidation pressure is reached. With lower closing rates the mobility of the flakes is hindered by the development of

frictional contacts and reduced boundary lubrication leading to jamming of the material (Chapter 3). As mentioned earlier, the randomly jammed stacks form highly stiff fiber rich regions and as more polymer is driven out they become severe. Further compression may lead to local deformation of the mold due to the incompressibility of fibers. Furthermore, upon severe jamming, the fiber rich jammed spots and the resin rich region around those jammed spots can act as stress raisers in the molded part. Therefore, these jammed regions are detrimental to both mold life and part properties.

The jamming of flakes can be reduced by suitably modifying the design, material and processing aspects. For example, it could be beneficial to promote a macroscopic flow by modifying the design of the part, such as material flow from thick sections to thin sections rather than opting for the opposite scenario. Similarly, use of relatively thick sections, compared to the flake thickness, will reduce the occurrence and severity of the jamming. Furthermore, when the part consists of uniformly thick flat sections it could be beneficial to design the mold in such a way that the flat section is inclined to the axis of the press. This is because of the reduced normal component of the consolidation load acting on the stack of flakes, which thereby reduces the severity of jamming. In terms of the material, choosing a flake size smaller by comparison to the size of the part, or the features in the part, can reduce jamming. However, flake size is closely connected to the mold closing rate. With a larger closing rate, relatively larger flakes can be processed with less jamming or delayed jamming as discussed in Chapter 3. Additionally, the charge placement can also be used to reduce the jamming effect. Regions of the mold with thin part sections can be filled with small amounts of material to reduce the chance of forming stacks of flakes leading to jammed regions. One of the process stages which was not studied in this thesis is the debulking stage, which comes prior to the filling stage. The debulking process is the application and subsequent release of pressure in a cyclic manner. This tends to make the material more flowable but also causes disentangling of the weave, and thereby could potentially reduce jammed regions. However, an in-depth study is required to quantitatively describe the debulking process and its advantages.

**Consolidation stage**

The filling stage is directly followed by the consolidation stage and serves two main purposes. The first purpose being, to provide enough pressure and time to fill the entire mold cavity with the material, which was not filled while closing the mold. The second purpose is to maintain a residual resin pressure to suppress voids and to create a good fiber-matrix interface. Proper choice of consolidation pressure is necessary to obtain good consolidation quality. Design features such as deep ribs require a larger pressure for complete consolidation (Chapter 4) than uniform sections. Furthermore, geometrical factors such as steepness of uniform sections like

a spherical cap and location of the ribs should be considered for obtaining a proper consolidation pressure. For instance, with steeply inclined surfaces relative to the compression axis, the normal component of the consolidation load is smaller. This can lead to loss of contact between the polymer at the material surface and the mold, causing surface porosities or blisters [4]. A similar phenomenon can be observed on the side faces of deep ribs. Furthermore, ribs at the edges of the mold can experience a reduced pressure due to the pressure gradient in the mold from the center to the edge of the mold. Therefore, the applied pressure should be compensated for such losses in these scenarios to obtain a consistent consolidation quality throughout the part. Further research is required to devise appropriate weighing factors for each scenario which can be added to compensate for the loss in pressure.

The consolidation dwell time is equally important to maintain a balance between proper consolidation and high throughput. If the consolidation dwell is prolonged, in the presence of jammed regions and flash boundary condition, the consolidation quality tends to drop marginally due to the seepage of matrix and reduction in average resin pressure (Chapter 3). The jammed regions tend to bear part of the consolidation load and hence the consolidation pressure in the part is locally non-uniform causing reduced suppression of voids near jammed regions. However, it can be inferred from a volume conservation viewpoint, that for a large part with a large area to perimeter ratio and a positively closed mold with negligible flash, such effects should not be significant. It can, however, be hypothesized that if regions that can create a pressure drop, such as ribs, exist around the jammed regions, they can act as a local flashing boundary condition. Further research is required to substantiate the above hypothesis. Hence, based on the boundary condition of the mold, size of the part, the applied consolidation pressure and the length of the flakes (larger flakes have large chance of jamming), the dwell time has to be adjusted or selected to be within a certain bandwidth for obtaining a maximum quality.

### 6.2.4 Other factors

In all the above cases, extraneous factors which affect the materials and the experimental results were not considered. For example, the effects of contamination in the reclaimed material from consolidated scrap, the batch-to-batch variation in the material properties, or the number of specimens required to obtain statistically significant results.

A typical source of contamination in trimming scrap can be from the additional materials added in the laminates during production, such as glass scrims for electrical insulation and copper meshes for lightning protection. The oxidated edges of the thermoformed laminates could also pose as a contaminant, since the polymer would have cross linked or degraded significantly. The effect of these contaminants is to reduce the mechanical properties of the part by premature failure initiation and

to some extent reduce the processability. However, further study is required to reduce the contamination and to quantify their effects on the molded part. The other extraneous factor such as batch-to-batch variation in properties might occur due to operator influence leading to a biased or less random filling process. In such cases automation of the process could reduce the variation, which requires further research as well. In the case of the number of required test specimens, a considerable scatter is observed in the experiments with small sample sizes. A minimum of 5 specimens is advised for filling experiments and 30 specimens for tensile tests. The latter is for obtaining a parametrized statistical distribution as stated in the composites material handbook used in the field of aerospace design [5].

## 6.3 Processing approach

This section provides a basic strategy for selecting some of the important parameters (Table 4.2), for manufacturing a part with chopped woven semi-preg materials using a compression molding process. Subsequently, the considerations required for obtaining the bounds of a feasible processing window are briefly discussed.

### 6.3.1 Proposed strategy for parameter selection

Figure 6.5 shows the strategy proposed for the selection of suitable process parameters for molding a part. The components are arranged in the same order as in Figure 6.2. The basic components and their dependencies were discussed in detail in the previous section (Section 6.2). The approach consists of four major steps, apart from the input and design considerations, in deciding the range of process parameters. Moreover, choosing the parameters is an iterative process in order to properly satisfy the links between the components.

#### Input and design considerations

The inputs for the approach are the part requirements, such as the required minimum strength for survival, expected quality of consolidation and filling, and a minimum thickness for the part. Design considerations include the design of part for stiffness or strength as discussed in Section 6.2.1. The design considerations can also be approached from a different angle, such as to design a part with a given strength of a particular material. The four major steps are described as follows:

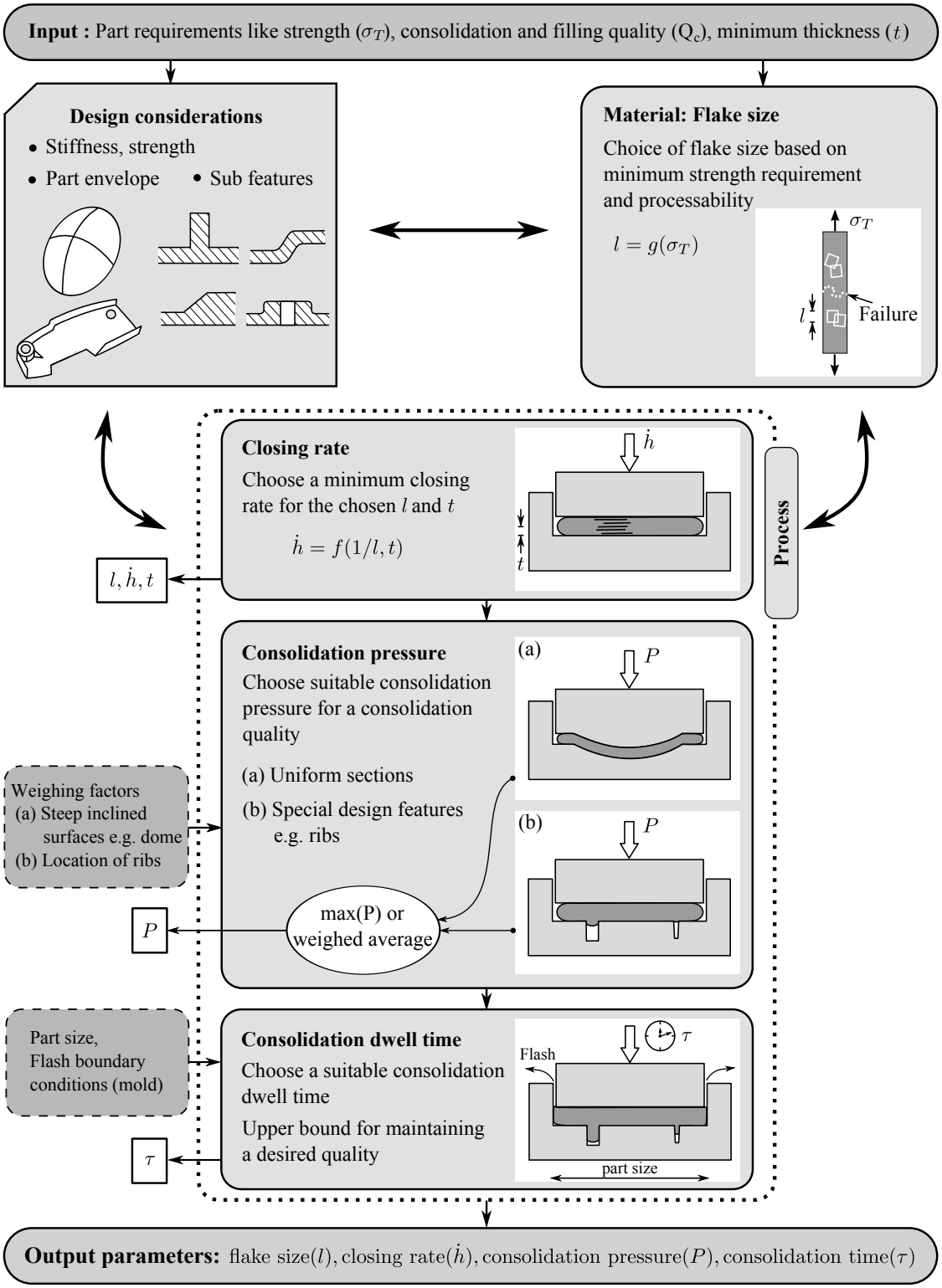


**Figure 6.5** *Proposed selection strategy based on the studied parameters.*

### 1. Choice of average flake size

The first step in this approach is to find an appropriate flake size to meet the strength requirements of the part. In the proposed approach, the use of an un-notched tensile strength is illustrated as an example. However, in a practical situation, other factors such as compressive strength, shear strength, as well as notched behavior of the material might be required for a comprehensive choice of flake size.

Moreover, while selecting the flake size, the ability to fill intricate design features such as ribs should be kept in mind. Furthermore, a distribution of flake size can be considered to strike a balance between the strength and the ability to fill.

### 2. Choice of mold closing rate

In this step of the selection process, a feasible closing rate is chosen with the flake size and the desired thickness of the part. This is crucial to avoid the jamming of flakes in the mold. This step can also be approached in such a way that an optimum part thickness is chosen based on the flake size and a known operating range of mold closing speed. Whichever route is taken, a re-iteration is required to choose a proper flake size for avoiding jamming based on the limitations in closing rate of the machine or the chosen part thickness. Finally, this step will result in obtaining a suitable flake size, mold closing rate and a minimum part thickness.

### 3. Choice of consolidation pressure

The third step is to find a suitable consolidation pressure considering proper weighing factors for obtaining the final consolidation pressure. Appropriate weights can be thought of as additional pressure required to compensate for the loss in pressure in each scenario. The final choice of consolidation pressure can be a maximum of the obtained consolidation pressures for different features in the part or a weighed average.

### 4. Choice of consolidation dwell time

The last step in the approach is to find a suitable consolidation dwell time considering the flash boundary conditions of the mold, size of the part, the applied consolidation pressure and the length of the flakes.

### 6.3.2 Process window

The preliminary insights obtained from the previous chapters on different aspects of the processing were discussed above in the form of a strategy for the selection of suitable parameters. This section gives an overview of the conceptual processing window with the important parameters.

Figure 6.6 shows the parameter space of consolidation pressure and inverse flake size. The quality of the part is shown with arrows spanning diagonally from low quality (LQ) to high quality (HQ) in terms of the consolidation quality. The polygonal region formed by the intersection of solid and dashed lines denotes a feasible window for processing of simple flat sections. For a given fiber volume fraction and material type, the physical limitations in the flake size arises from the unit cell size of the weave architecture, which maintains the integrity of the flake. Beyond the lower limit ($l < l_{min}$) on the right side, the chopped material disentangles and becomes similar to long fiber reinforced material. Moreover, a certain minimum size of the flake is required for an efficient transfer of stresses from the matrix. On the other side, the maximum flake size is based on the part size and the size of the features required to be filled. Beyond a certain maximum flake size, the frictional effects will dominate

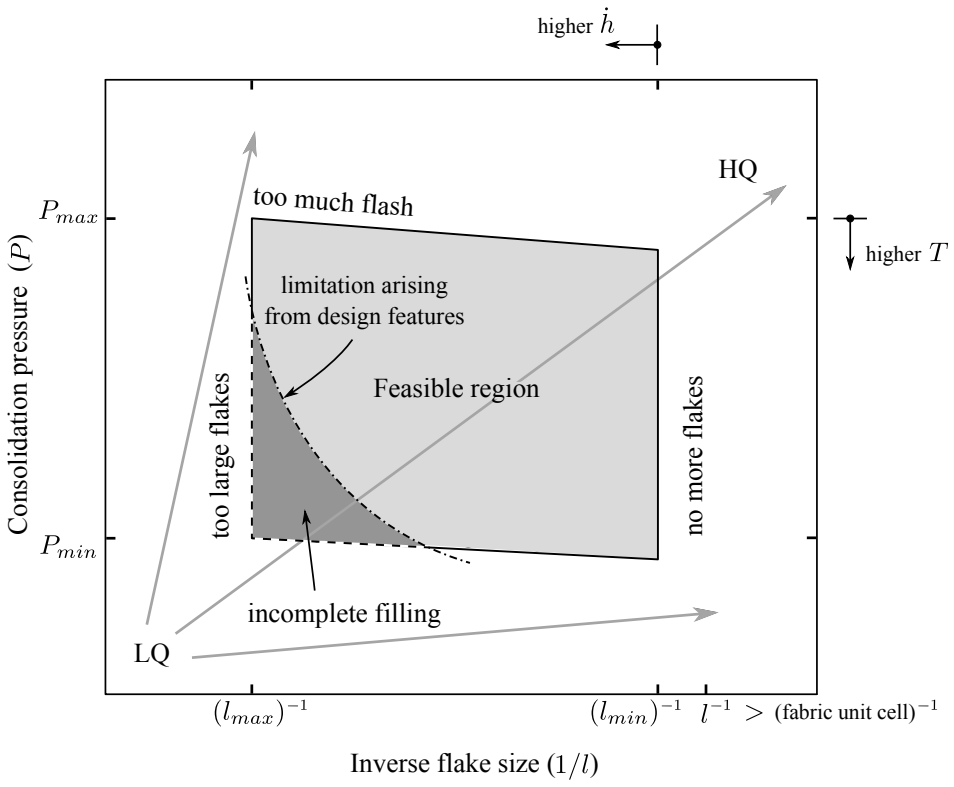


**Figure 6.6** *A conceptual process window based on the observed trends. LQ and HQ denotes low and high quality with the arrows (gray) denoting the direction of change in the quality.*

the material flow inside the mold and the material becomes un-processable. If a larger mold closing rate ($\dot{h}$) is used, the boundary of the processable flake size can be shifted towards the larger values.

In terms of pressure, for a certain fixed flake size, the quality increases with the pressure. Thus, the lower bound for pressure is based on improper consolidation. For larger flakes, a marginally higher pressure might be required to attain a certain quality. On the higher side, the upper bound for pressure is based on too much flashing out of material. Furthermore, a larger pressure can also intensify jammed regions in the presence of flash and reduce the consolidation quality as discussed earlier. Too much pressure can also cause local damage to the mold in the presence of jammed regions. However, for positively closed molds, the upper bound of pressure can be extended further since there can be no flash and thus negligible intensification of jammed regions considering volume conservation. Even though the effect of temperature was not studied in the work performed in this thesis, from a theoretical perspective the increase in temperature reduces the viscosity of the matrix polymer. As a result, a qualitatively better filling and higher part quality for a relatively lower consolidation pressure can be obtained. However, it also promotes seepage, flash and fiber-matrix separation. Therefore, further research is required for a quantitative characterization.

Furthermore, the presence of design features, such as ribs, introduces an additional constraint in the process window denoted by the dash-dotted curve. This limitation arises from the ability to fill the ribs with a certain flake size. As the flake size increases a larger pressure is required to fill the ribs. Hence, the dark shaded region corresponds to incomplete filling of the features and hence the remaining region of the polygon is the feasible window for a complex part with design features.

## 6.4 Application: Manufacturing of an access panel door

The major advantage of compression molding of discontinuous materials is the ability to manufacture near net-shaped parts with complex features. The results and observations presented in this thesis are put together to manufacture a full scale part with integrated features to demonstrate the capability of the material and the process. Figure 6.7 shows the part which is based on an access panel door used for accessing a hinge in the rudder of an aircraft*. This section provides a brief overview of the considerations that were taken into account when choosing the different parameters for manufacturing the part, following the approach presented earlier. Subsequently, the results of part quality is discussed based on cross-sectional micrographs from the demonstrator.

*Design courtesy to Fokker Aerostructures B.V.

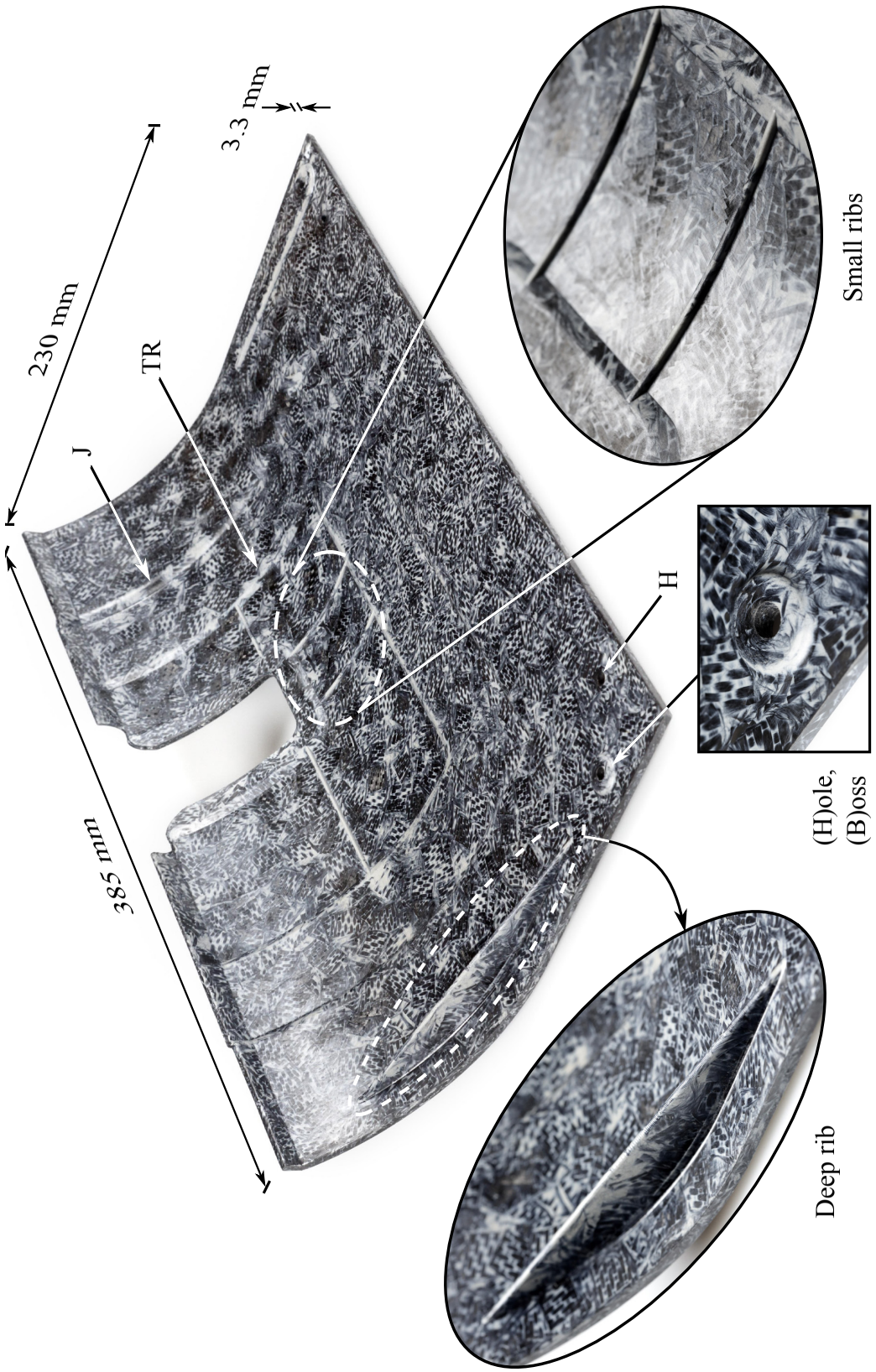


**Figure 6.7** *Demonstrator part with integrated design features like ribs, joggle (J), thickness transitions (TR) and as-molded holes (H) with boss (B). Inset shows the ribs of different width to depth ratio and an as molded hole.*

### 6.4.1 Material, design and process parameters

The main objective was to manufacture the part with reduced jamming effects and a good consolidation quality to ensure a homogeneous material property across the part. The part was designed with thick and thin sections with all the design features shown in Figure 6.5. The material used was chopped C/PPS semi-preg with a 5 harness satin weave architecture.

The first step is to choose the flake size, which in this case was chosen based on the processability. A trade-off exists between the filling ability of the material and the mechanical properties that can be obtained. Based on the study in Chapter 4 a feasible flake size of 10 mm was chosen so as to fill the thin and deep rib close to the edge of the part. A large closing rate of 5 mm/s was chosen so as to avoid any severe jamming of the material. This is larger than the closing rates studied in the previous chapters with simple features or flat sections. The consolidation pressure was chosen to be 15 bar to enable proper filling of the ribs. Results from Chapter 4 show that flat sections can get consolidated well with 10 bar pressure. Moreover, other features like the joggle is a flattenable feature which does not pose a threat for poor consolidation at high pressure. Hence, the maximum pressure was chosen among the choice of pressures. The last step is the choice of consolidation dwell time. The chosen part is relatively larger than the experimental investigations performed in previous studies and the large mold was designed to allow negligible flash with a semi-positive type of closure. Therefore, a consolidation time of 15 minutes was chosen to ensure proper consolidation of the part.

The other considerations that were implemented were the filling pattern of the flakes and the orientation of the flat surfaces in the design of the mold. The mold was filled with the flakes such that regions with thin sections were filled with less material than the remaining regions, so as to reduce the probable formation of stacks of flakes. In Chapter 3, a proposal was made to orient large flat surfaces, with uniform sections, slightly inclined to the axis of the compression instead of being perpendicular. This can potentially reduce the chance of jamming in uniform sections due to the reduced normal force on a random stack of flakes and hence it was implemented in this mold design.

### 6.4.2 Results: Part quality

The consolidation quality in the intricate features present in the molded part was assessed with cross-sectional micrography. This subsection gives a brief overview of the results with respect to the observed jamming, the extent to which the features are filled with fibers and the void content.

### Jamming of material

Figure 6.8 (a,b) shows a jammed region in a 2 mm thick section, a 3.3 mm thick flat section and in a joggle. The dark regions are consolidated carbon fiber bundles and the white regions are PPS matrix. The micrograph with higher magnification shown in the inset of Figure 6.8 (a) reveals the tightly packed fiber bundles in the jammed regions. For comparison, a 3.3 mm thick flat section with no jamming is shown in Figure 6.8 (h) which shows a rather uniform distribution of matrix pockets. The effect of jamming is observed to be severe in the thinnest section, and in the joggle where the material movement is restricted by the contours. As discussed earlier in Chapter 3, the jamming of the material can be delayed with a high mold closing rate. However, it can be inferred that the effect is prone to occur if the desired thickness is a few multiples of the flake thickness for materials with high fiber volume fraction and woven structure, such as the one used in this study. A typical matrix rich section between two jammed regions is shown in Figure 6.8 (b). Similar observations were made in Chapter 3 in which voids were found in between jammed regions, in small sized parts with flash edges. However, as hypothesized in Chapter 3, in the case of a large part with negligible-flash, voids are found to be absent.

### Filling of features and void content

Figure 6.8 (c-g) shows a joggle, thickness transition, deep rib section, a small rib section, and an as-molded hole with a boss respectively. It can be observed that the deep ribs are not completely filled with fibers at the center. One of the possible reasons is insufficient development of pressure due to the mechanical stops in the semi-positive mold. Another reason might be due to the location of the rib being at the edge of the mold unlike the centrally located ribs investigated in Chapter 4. Moreover, addition of extra material to compensate for the pressure build up, also leads to similar results. Therefore, this effect can be carefully attributed to the location of the rib. Thus, the location of the rib should be considered as one of the weighing factors in the choice of the consolidation pressure apart from the aspect ratio of the rib. Further, the addition of a small radius at the rib entry reduced the matrix rich entry-corners and allowed the flakes to conform to the corners. In the case of small ribs, similar to the observations from Chapter 4, the cavity is filled with matrix due to the percolation of matrix through the flake bridged entrance. Additionally, cracks were observed in the entrance and the deep end of the ribs due to the differential shrinkage of the matrix rich regions. As expected the small ribs were filled with matrix since the flakes are too large compared to the width of the rib.

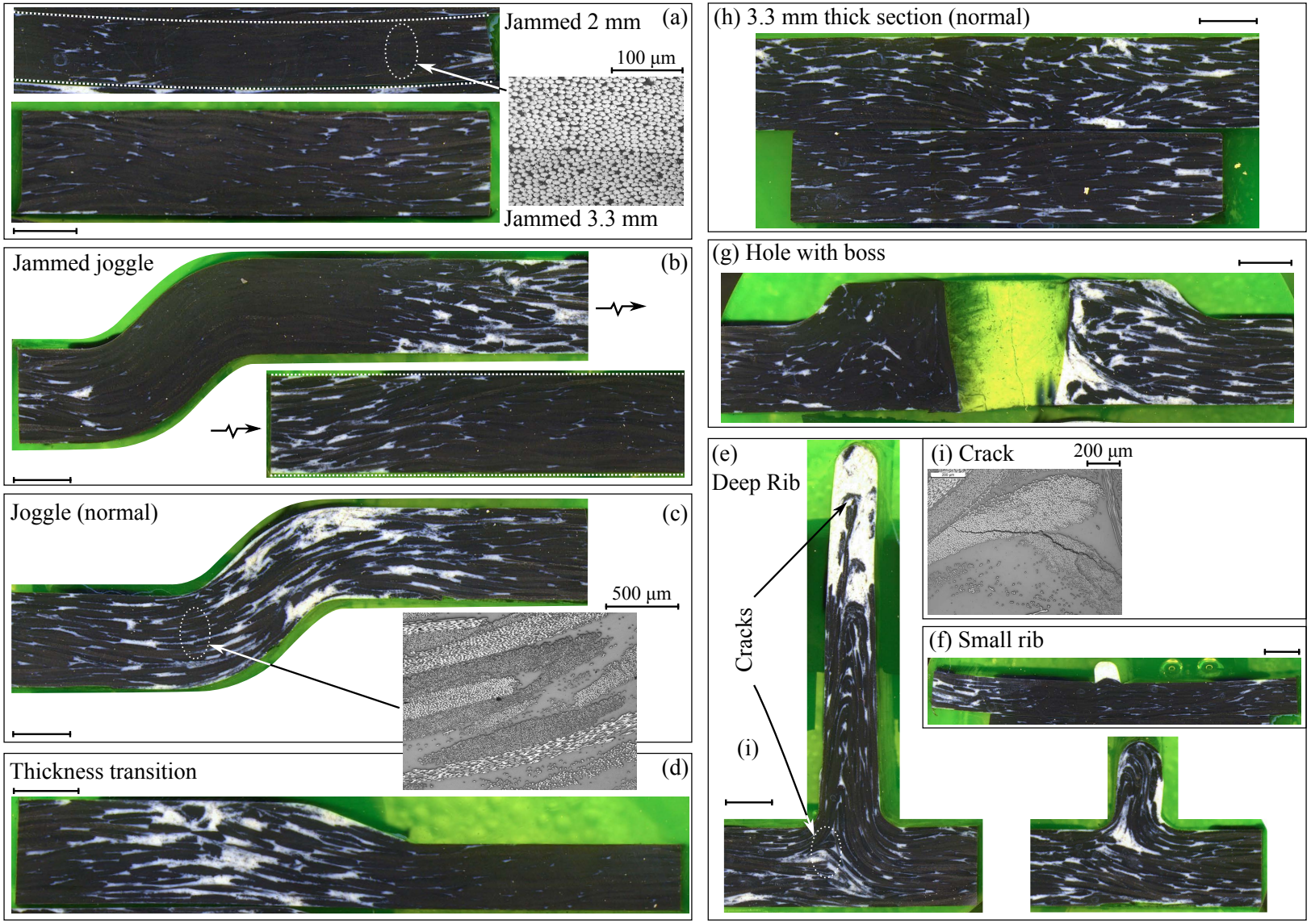


**Figure 6.8** *Cross-sectional micrographs of design features in the demonstrator part. Broken arrows in (b) indicate the direction of continuity of the section. (e) Deepest rib section and a section close to the end. Unless stated explicitly, all the scale bars are 2 mm in length.*

Overall, a more or less uniform filling of flakes with almost negligible void content was observed in the other features experimented with in this demonstrator part. A few voids were found to be present at the net edge of the part. In the case of a joggle with uniform section shown in Figure 6.8 (c), the matrix is distributed similarly along the section except for the curved region. Moreover, in the case of a thickness transition, the thinner section is always found to be dry compared to the thick section. This effect can be possibly explained with the existence of relatively lower pressure locally in the thick section and the fact that the thin section has a larger chance to jam. A combined effect of these phenomena causes the matrix to be driven to the thicker region. Figure 6.8 (g) shows a cross section of the as-molded hole and boss, where the region to the right of the image is close to the net edge of the part and the other side is towards the inner side of the part. The net-edge side is found to be rich in matrix, compared to the other side. This is possibly due to the restriction of the movement of flakes between the mold pin in the center and the net edge.

#### Other defects

Warpage of the straight edges and flat faces was observed in the molded part and was found to reduce with increasing consolidation pressure. During the cooling stage, residual stresses can arise due to the differential shrinkage of the random material and due to the differences in local arrangement of flakes, leading to differences in local stiffness. However, it was not studied explicitly in this thesis and further research is required to characterize the warpage. Blisters were not observed on the surface of the part. Even though they were not explicitly examined in this work, a few preliminary experiments with dome shaped molds revealed blisters due to loss of pressure in the steeply inclined sections.

## 6.5 Concluding remarks

This thesis presented the studies performed on the processability and performance of composite parts manufactured with chopped woven reinforcements using a compression molding process. A fundamental understanding of the material behavior was gained by idealizing the flow as a squeeze flow process, and by fixing some of the key material parameters such as the shape and size of flakes. The variability in the basic mechanical properties was studied assuming a negligible coupling between the process and the final material property. This chapter discussed the results in the perspective of transferring the idealized knowledge towards a practical application along with an actual demonstration.

# References

[1] Rubin Shmulsky and P. David Jones. *Forest Products and Wood Science An Introduction*, chapter Structural Composites, pages 321–363. Wiley-Blackwell, 2011.

[2] D. Barnes. A model of the effect of orienter design and operating variables on the mean angular deviation of oriented wood strands. *Forest products journal*, 52(7-8):63–71, 2002.

[3] J. Fudge. "HexMC - Composites in 3D" a new high performance molding compound. In *SAMPE Technical conference proceedings*, 2001.

[4] Benoit Landry and Pascal Hubert. Experimental study of defect formation during processing of randomly-oriented strand carbon/PEEK composites. *Composites Part A: Applied Science and Manufacturing*, 77:301–309, October 2015.

[5] *Military Handbook - MIL-HDBK-17-1F: Composite Materials Handbook, Volume 1 - Polymer Matrix Composites Guidelines for Characterization of Structural Materials*. Number Chapter 8. U.S. Department of Defense, 2002.

# Chapter 7

# Conclusions and recommendations

## 7.1 Conclusions

The compression molding of chopped woven thermoplastic composite flakes was investigated in this thesis. The main objective was to develop a strategy for manufacturing of parts with good quality and consistent mechanical properties. This section summarizes the important conclusions from the obtained results in the aspects of processing and performance.

### *Processing*

1. The flow behavior of the woven flake reinforced polymer melt under squeeze flow conditions is a strong function of flake size and closing rate of the mold. The material flow is found to be quasi-isotropic in the in-plane directions.

2. A power law type of material model is proposed for the flowing regime of the material. The apparent viscosity of the material is found to change as the mold closes and as the material meso-structure evolves during the flow.

3. The woven nature of the reinforcements provide a local structural integrity to the flakes. As a consequence, a combination of larger flakes and lower mold closing rates lead to jamming of the flakes through the thickness of the mold cavity. The reduced viscous drag force on the flakes compared to the force network formed between the flakes, and the lack of boundary lubrication are assumed to be the major causes for jamming. Excessive jamming may lead to local damage of the mold.

4. A processing envelope in the form of a jamming transition diagram is proposed. The jamming transition diagram can be used to characterize the jamming behavior in the parameter space of closing rate and inverse flake size. This

could be further put to use in the selection of a feasible closing rate to avoid jamming for the chosen flake size in the phase of the process design.

5. The filling behavior of the flake reinforced melt in design features, such as a rib, is a function of flake size, rib aspect ratio and the applied consolidation pressure. The mold boundary condition, in terms of flash edges, has a large significance in the consolidation quality of the part especially for small parts. For large parts, the design features might act similar to flash boundaries in terms of generating a pressure drop locally.

### *Performance*

1. The strength of the flake reinforced material is a function of the flake size and the random structural arrangement of the flakes. However, the stiffness is found to scale with the fiber volume content. Therefore, the chopped woven materials are more suitable for *design for stiffness*.

2. The randomness of the meso-structure causes a large scatter in tensile strength and the variability is found to increase with the flake size. Furthermore, flake-matrix interface failure was found to be the major mode of failure, potentially initiated by the stress concentrations along the edge of the flakes.

3. Jamming of the material promotes fiber-matrix separation giving rise to dense fiber rich region surrounded by resin rich regions. These resin rich regions are weak spots in product as these can act as stress raisers and initiate premature failure. Hence, the presence of jammed regions is detrimental to both part properties and mold life.

4. A theoretical analysis with lap shear type of stress transfer combined with statistical principles proved to be a simple but effective means to capture the trend in the scatter of tensile strength values.

## 7.2 Recommendations

The work performed in this thesis is a first step towards understanding the behavior of the molding compound with chopped semi-preg flakes having a woven architecture. Therefore, further work is absolutely necessary to improve the understanding and to make use of the advantages of the material. This section puts forward some recommendations based on the study performed in this thesis.

### Processing

1. Since the material and the methods used in this thesis for analyzing the flow behavior are explorative, the experiments were performed on a fixed size specimen for different flake sizes. However, the effect of the ratio of specimen size to the flake size should be characterized to be able to scale the results to a scenario of molding large parts. Similarly, the jamming behavior was characterized with a single initial specimen thickness to flake thickness ratio. However, tests on specimens with different initial thickness will provide a better insight on the charge placement strategy and its effects on the prevention of jamming.

2. Preliminary molding experiments with small-sized flat plates show a dependence of consolidation quality on dwell time in the presence of jammed regions and flash edges. However, further investigation with a closed mold, but with induced jamming and multiple features should be performed. Such a scenario could induce a local pressure drop which can be used to prove the significance of the time dependency of the consolidation quality, for large parts.

3. A typical set of parameters and their inter-dependencies were investigated in the case of filling behavior of the material in rib cavities. However, a more in-depth experimental study with the support of dimensional analysis should be performed in the future with a large sample size to improve the statistical significance of the results.

### Influence of material type

The type of the constituent material such as the fiber, matrix and the weave architecture of the fabric was fixed in this study. However, the influence of the material should be studied which can provide further insights such as the following. The effect of inter-fiber or inter-bundle frictional behavior on jamming, as a function of the fiber material. Additionally, the weave pattern can also influence the resistance to disentangle during the flow and therefore, increase or reduce jamming of the flakes. Furthermore, the effect of polymer viscosity on the flow behavior of the chopped material should be studied to improve the ability to fill intricate features.

### Warpage and dimensional tolerance

The filling and consolidation phases of the molding process which ensure a stable manufacturing process, were the main points of focus in this thesis. However, during the cooling phase, residual stresses can arise in the part due to the differential shrinkage of the random material. These residual stresses can deform or warp the

part which potentially reduces its mechanical performance. Therefore, the effect of processing parameters on warpage should be studied further to obtain a better dimensional tolerance.

### *Performance and process-property coupling*

As a first step a static failure situation was considered in this thesis. However, the final failure is based on a progressive failure of the material taking into account the fracture toughness of the polymer and the frozen-in thermal stresses. Furthermore, the coupling between the process and the mechanical performance was not studied in this thesis explicitly. A fully coupled solution is highly beneficial to optimize the part quality and its performance.

# Acknowledgments

Op een dag... one fine day...
four years ago I started the next phase of my life envisioning to become a responsible person and to contribute my tiny part to the scientific community.. and here I am in the verge of merely finishing the first task. Nevertheless, it has been quite an intense learning opportunity along this path. To be honest I have had a great time working in the faculty at the UT and at TPRC for the past four years. I would like to acknowledge all the people who have made it possible for me to finish this thesis. I hope I haven't missed anyone in the list, if so oops.. my sincere apologies.

First and foremost, I would like to express my gratitude to my promoter Remko Akkerman for his invaluable support and for his confidence in my abilities. Thank you for giving me this opportunity and for always encouraging my initiatives. Your simplistic approach of breaking down a problem has always inspired me to take a step back and look at the problem with simple eyes. I would like to extend my gratitude to professor Leon Govaert for his humble nature and on accepting to promote me together with Remko Akkerman. The promoters list doesn't get complete without mentioning my co-promoter Roy Visser. Thank you Roy, for your extensive support from the day one. From the TPRC side, I am grateful to our general manager Harald Heerink and all the partners of TPRC for providing me this wonderful opportunity to work within such a dynamic group of people from both industry and academia.

This thesis would not have been possible without the meticulous support from my supervisors (over the course of time) Bert Rietman, Roy Visser, Wouter Grouve and Sebastiaan Wijskamp. I sincerely thank them for their open mindedness and the freedom which they provided to me for performing this research. Their knowledge and enthusiasm has always inspired me to bring out my best effort.

This research was funded by the consortium of TPRC, and was conducted in close co-operation with the industries through the technical advisory board and the industrial reference group. I would like to express my gratitude to all the members of the technical advisory board for their immense support and enthusiasm. The discussions which arise in the group have always given me a broader perspective of the research problem. Further, I appreciate the keen involvement and the prompt technical feedback from the following industrial reference group members namely, David Manten, Sjoerd Hooning and Yuri Verbruggen from Dutch Thermoplastic

Components; Arnt Offringa, Michael Wielandt, Johan Meuzelaar, Remco Gijseman and Marc Koetsier from Fokker Aerostructures; Winand Kok, Hans Luinge, DeWayne Howell and Jason Gabriel from TenCate Advanced Composites; Jeroen de Vries and Martijn van Wijngaarden from KVE. Their industrial expertise helped me to find a direction for the project and thereby set realizable goals. A special thanks to the team at Fokker Aerostructures for designing the demonstrator part which adds a great value and tangibility to this research. I take this opportunity to thank Jeroen (Henk) Houwers and Gert-Jan Nevenzel for taking the pains to design the mold and for setting it up for production. It was a tremendous help, against the clock, for which I am greatly indebted to them.

A super special thanks to Debbie Zimmerman and Belinda Bruinink for all the organizational help you offered since I chose to come to Enschede; starting from arranging my travel for my intake interview until and further than defending my thesis. From the TPRC side, I would like to thank Iris de Klerk for her full support. They were always pleasant and willing to help which made the administrative tasks very fluid.

Research is always challenging and is partly driven by curiosity which usually creates a lot of diversions; no wonder it is said that curiosity kills. However, the discussions (sometimes extensive) with my supervisors, Bert Rietman, Roy Visser, Wouter Grouve, Sebastiaan Wijskamp and Remko Akkerman have always cleared the haze. Thank you all! for such fruitful discussions and for maintaining a very supportive and positive attitude. I would like to extend my gratitude to Laurent Warnet and Ton Bor for their highly supportive nature and for providing their critical views on the research in the periodic PT group meetings and other informal settings. Their technical and pragmatic insights have always been very useful over the course of the project. Further, Laurent's experimental tips and tricks are indispensable while working in the laboratories and I am very much grateful for his support. Also, I would like to thank Ton for involving me in providing laboratory based teaching exercises which helped to improve my personal qualities as well as learn different subjects. Further, I would like to thank Ferrie van Hattum for his enthusiastic support and insights. Next comes the lab technicians, very important people indeed. I am obliged to Gert-Jan Nevenzel, Laura Vargas Llona, Bert Vos, Ivo Vrooijink, Norbert Spikker and Martin Sprenkeler. Thank you for providing your valuable support, without which the activities in the lab would have been rather difficult.

One of the important elements of research is to record and disseminate the created knowledge. In that respect, my reading committee members, Francisco Sacchetti, Lily Shaojie Liu, Bert Rietman, Roy Visser, Wouter Grouve, Sebastiaan Wijskamp and Remko Akkerman, have been very keen on the details. Thank you all for your critical assessment which has given me an excellent opportunity to improve myself on the writing aspects. Furthermore, I would like to thank the students Ahmed Alazzawy, Guido Smits, Taha Negem and Simon Veenstra for their sincere work on their assignments and Bachelors thesis concerning different research topics. I am

very glad to have had a nice co-operation with you all. I am also greatly indebted to the students, Taha Negem, Mike Broekman, Dennis Brands, Francisco Saraiva and Maurice Koopman, who helped in chopping-up a significant amount of flakes in the nick of time. Thank you all for your support and sorry for the itchy evenings you would have had after chopping carbon fibers.

A possible funny side effect of doing a research is stress, for which a set of nice colleagues will be greatly beneficial to cope with it. Fortunately, I have had more than a handful of super nice colleagues who have been very considerate, helpful and pleasant to work with. I had the opportunity to do my work at the UT for a year and at TPRC for three years, hence, I have a huge list of friends and colleagues. From the UT side, my office mates, Bo Cornelissen, Sybren Jansma, Johan van Ravenhorst and Luca Mainini; my colleagues, Lily Shaojie Liu, Ismet Baran, Yibo Su, Jos Havinga, Jurnan Schilder, Marieke Bezemer-Krijnen and Andrea Sanchez-Ramirez; old colleagues, Arnoud van der Stelt, Emiel Drenth, Ted Ooijevaar, Andriejus Demcenko, Arjan Schutte, Vitali Koissin and Kirill Il'in. It was a pleasant experience with all of you, having nice discussions during a short Koffie session every morning in the Dynamics lab and at lunch breaks in the Canteen. It helped me greatly to adapt very quickly to the new environment; Thank you all!

From the TPRC side, I would like to thank my office mates, Francisco Sacchetti, Uli Sachs, Thijs Kok, Devi Wolthuizen, Jeroen (Henk) Houwers, Thijs Donderwinkel, (Marky) Mark Bouwman, Tjitse Slange and Guillaume Vincent, for being a wonderful group. My gratitude is further extended to Sebastiaan Haanappel and René ten Thije for sharing their knowledge and experience. It has always been a stimulating environment to work and learn from one another. Amidst that, we have had countless number of discussions from serious to funny ones and until a level where it makes zero sense. Sometimes brilliant humors pop up like the adventures of Kabouter Wesley (Op een dag, Kabouter verloren honderd miljoen miljard naar een zonnebloem, Godmiljaaar!!!), Koffiekoppen, 1 gulden! (credit to Sebastiaan Haanappel) and other silly humors alike. A special thanks to Marky Mark, Wouter, Roy and Sebastiaan W. for expressively translating my summary in Dutch. Further, I would like to thank Nick van der Vall for his support in public relations and Selma Kalee for her swift support in purchasing of tools.

I would like to thank my paranymphs Francisco Sacchetti and Uli Sachs for being my moral support during the defense.

Last but not the least, I would like to express my heartfelt gratitude to my parents, Abdul Rasheed and Jeenathunnisa Begum; and to my sister Mariamunnissa Begum; who believed in me, encouraged me, have always been with me as a moral support, and for their endless love. I dedicate this thesis to my family without whom this is beyond the bounds of possibility.

Iqbal, June 2016

37320 u later... Einde.

# Publications

## Journal articles

1. M. I. Abdul Rasheed, B. Rietman, H. A. Visser, R. Akkerman, "Rheological behavior of chopped fabric reinforced thermoplastic prepreg: Squeeze flow," *to be submitted to Composites Part A: Applied Science and Manufacturing*, **2016**. (Chapter 2 of this thesis)
2. M. I. Abdul Rasheed, W. J. B. Grouve, S. Wijskamp, H. A. Visser, R. Akkerman, "Experimental investigation of flow phenomena in processing woven composite flakes: Jamming," *to be submitted to Composites Part A: Applied Science and Manufacturing*, **2016**. (Chapter 3 of this thesis)
3. M. I. Abdul Rasheed, W. J. B. Grouve, S. Wijskamp, H. A. Visser, B. Rietman, R. Akkerman, "Compression molding of integrated ribs using chopped woven thermoplastic prepreg," *to be submitted to International Journal of Material Forming*, **2016**. (Chapter 4 of this thesis)
4. M. I. Abdul Rasheed, B. Rietman, H. A. Visser, R. Akkerman, "Effect of meso-scale morphology on the scatter of mechanical properties of woven-flake reinforced composites," *submitted to Journal of Composite Materials*, **2016**. (Chapter 5 of this thesis)

## Conference proceedings

1. M. I. Abdul Rasheed, B. Rietman, H. A. Visser, R. Akkerman, "Experimental characterization of recycled (glass/tpu woven fabric) flake reinforced thermoplastic composites," in *Proceedings of the International Conference on Composite Materials (ICCM19)*, pages 3999-4010, **2013**.
2. M. I. Abdul Rasheed, B. Rietman, H. A. Visser, R. Akkerman, "A parametric study on compression molding of reference parts with integrated features using carbon composite production waste," in *Proceedings of the 18$^{th}$ International ESAFORM conference on material forming*, pages 458-463, Graz, Austria, **2015**.
3. M. I. Abdul Rasheed, F. W. J. Van Hattum, B. Rietman, H. A. Visser, R. Akkerman, "Effect of overlap length on the mechanical properties of flake reinforced thermoplastic composites," in *CAMX conference proceedings*, pages 589-602, **2015**.

## Presentations

1. M. I. Abdul Rasheed, B. Rietman, H. A. Visser, R. Akkerman, "Experimental investigation of the flow behavior of woven composite flakes in thermoplastic resin melt," in *12$^{th}$ International Conference on Flow Processes in Composite Materials*, Enschede, The Netherlands, **2014**.

2. M. I. Abdul Rasheed, A. D. Rietman, H. A. Visser, R. Akkerman, "Characterization of recycled (glass/tpu woven fabric) flake reinforced thermoplastic composite," in *SAMPE Europe student conference*, Paris, France, **2013**.

## Awards

1. CAMX 2015 outstanding technical paper award in the ***processing track*** for the conference article on "Effect of overlap length on the mechanical properties of flake reinforced thermoplastic composites," Dallas, **2015**.

2. JEC Americas Innovation Award 2016 in the category ***aeronautics*** for the demonstrator part "Green PPS leading edge cover" manufactured as a part of this thesis, Atlanta, **2016**.

   Contribution of M. I. Abdul Rasheed in this collaborative work: a) Research on the process (chapters in this thesis); b) development of the process window and design guidelines for the mold and the part; c) manufacturing of the part and the subsequent analysis.

எப்பொருள் எத்தன்மைத் தாயினும் அப்பொருள்
மெய்ப்பொருள் காண்பது அறிவு.

— திருவள்ளுவர், திருக்குறள்

---

In any subject matter under consideration,
knowledge comes from the perception of its true nature.

— Thiruvalluvar, *Thirukkural*

Continuous fiber reinforced composites with high-performance thermoplastic polymer matrices have an enormous potential in terms of performance, production rate, cost efficiency and recyclability. The use of this relatively new class of materials by the aerospace and automotive industry has been growing steadily during the last decade. However, the use of continuous reinforcements limit the complexity of the shape of the end products, as defects such as wrinkles can form during processing. Moreover, a significant amount of process waste is generated, which lowers the efficiency of the conventional production processes involving a prepreg cutting stage and/or final trimming stages.

The overall efficiency of the manufacturing value chain of composites can be improved by adjoining a complementary manufacturing process that utilizes the process waste incurred in the primary process. The discontinuous form of reinforcements in the reclaimed material will provide a means to manufacture complex 3D geometries with near-net edges and at the same time use the raw material efficiently. However, the discontinuities in the reinforcing phase lead to a reduced mechanical performance compared to continuous reinforcements. Suitable applications include semi-structural parts and non-load bearing structures.

This thesis focuses on the processing of planar discontinuous reinforcements and the associated mechanical performance. Chopped thermoplastic semi-preg with a woven fabric reinforcement, referred to as flakes, is considered as a standalone molding compound in this study. A compression molding process is chosen to manufacture parts, as it allows for complex geometries while retaining a long fiber length. Although processing of different types of discontinuous reinforcements has been studied in the past, the processing of the specific class of planar reinforcements with a woven architecture and high fiber content has not been explored so far.

The principal objective is to develop a strategy for manufacturing woven-flake reinforced parts with good quality and consistent mechanical properties. For achieving this goal, the flow behavior of chopped woven material, process induced jamming of the material and the mechanical properties of molded plates are experimentally investigated and are explained with theoretical models.

The work presented in the thesis shows the multidisciplinary nature of the problem, with strong correlations between the material, process and the design of the part leading to the final part performance. Therefore, a processing strategy is proposed which takes into consideration the aforementioned three basic blocks to manufacture consistent parts. Finally, the proposed strategy is validated by manufacturing a full-scale part with typical design features, which successfully demonstrates the processing capabilities of the material and the developed process.

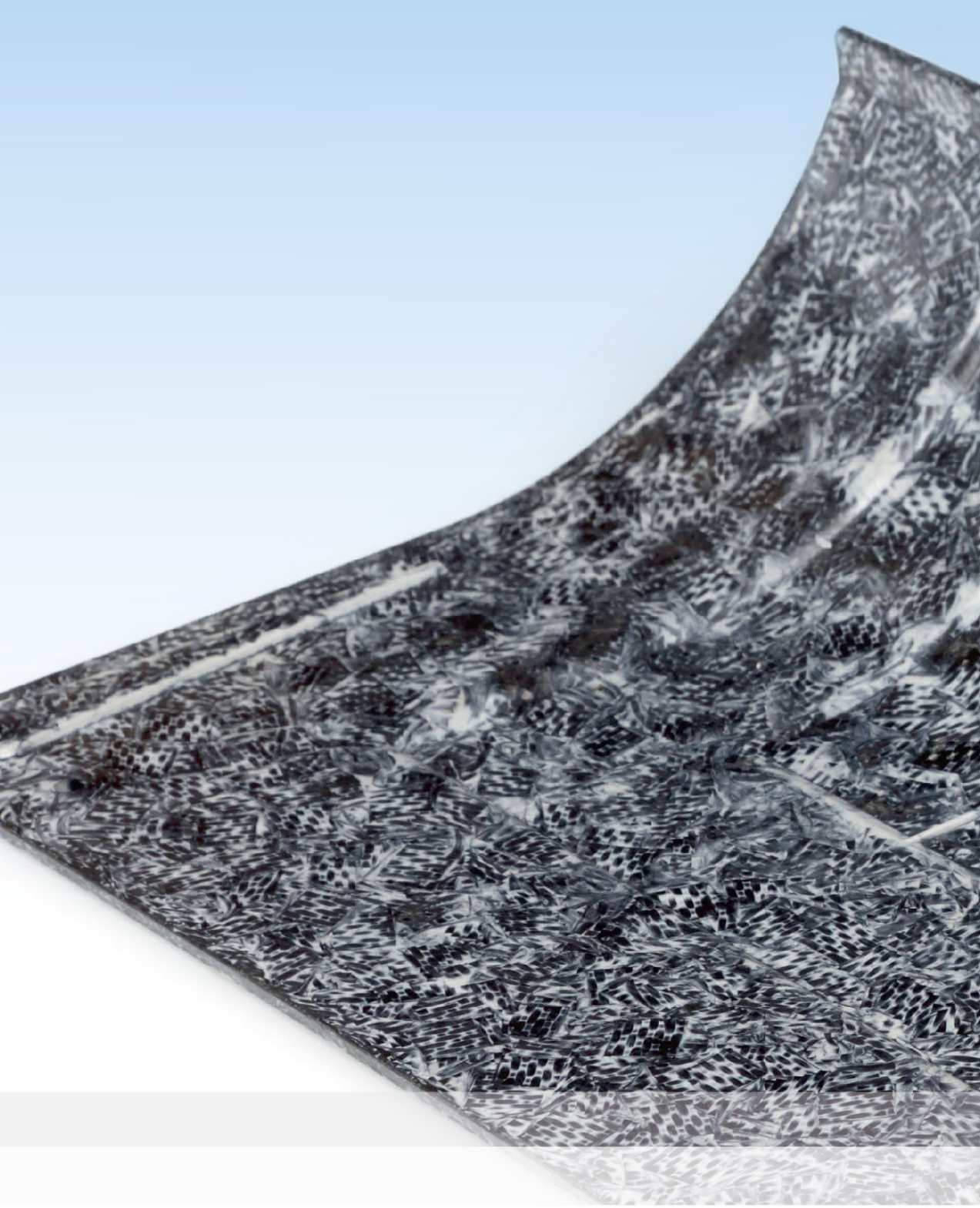

UNIVERSITY OF TWENTE.

ISBN: 978-90-365-4151-0